March 2019

Role of Oncogenic Protein Kinase C-iota in Melanoma Progression; A Study Based on Atypical Protein Kinase-C Inhibitors

Wishrawana Sarathi Bandara Ratnayake
University of South Florida, ratnayake@mail.usf.edu

Follow this and additional works at: https://scholarcommons.usf.edu/etd

Part of the Biochemistry Commons, and the Molecular Biology Commons

Role of Oncogenic Protein Kinase C-iota in Melanoma Progression; A Study Based on Atypical

Protein Kinase-C Inhibitors

by

Wishrawana Sarathi Bandara Ratnayake

A dissertation submitted in partial fulfillment
of the requirements for the degree of
Doctor of Philosophy
Department of Chemistry
College of Arts and Sciences
University of South Florida

Major Professor: Mildred Acevedo-Duncan, Ph.D.
Robert Potter, Ph.D.
Edward Turos, Ph.D.
Kirpal Bisht, Ph.D.
Meera Nanjundan, Ph.D.

Date of Approval:
March 21, 2019

Keywords: PKC-ι, Vimentin, FOXO1, c-Jun, ICAM-1, IL-6

DEDICATION

I dedicate my dissertation to my dearest parents, Mr. M.G. Ratnayake and Mrs. S.C.K. Gunaratne and my loving wife Mrs. R.C. Yatawatta. It is their love, support and values that enabled me to overcome all obstacles and achieve my goals.

A special thank goes to my doctoral supervisor, Dr. Mildred Acevedo-Duncan for standing beside me through all the challenges of the research and the graduate school and for the great support.

I would like to express my sincere gratitude to all the past teachers and faculty members who taught me since my Montessori. Their contribution have been invaluable to my success.

Finally, I would like to express my sincere gratitude to all the other family members in Sri Lanka and all of my friends for their continuous support and encouragement throughout this course.

ACKNOWLEDGEMENTS

TABLE OF CONTENTS

LIST OF FIGURES

v

vi

LIST OF ABBREVIATIONS

ACPD: 2-acetyl-1,3-cyclopentanedione

DNDA: 3,4-diaminonaphthalene-2,7-disulfonic acid

ICA-1T: [4-(5-amino-4-carbamoylimidazol-1-yl)-2,3-dihydroxycyclopentyl] methyl dihydrogen phosphate

ICA-1S: 5-amino-1-((1R,2S,3S,4R)-2,3-dihydroxy-4-methylcyclopentyl)-1H-imidazole-4-carboxamide

ζ-Stat: 8-hydroxy-1,3,6-naphthalenetrisulfonic acid

PKC: Protein kinase C

Ca^{2+}: calcium ion

DAG: diacylglycerol

PS: phosphotidylserine

(c)PKC: conventional PKC

(n)PKC: novel PKC

(a)PKC: atypical PKC

PKD: protein kinase D

PK-Ns: PKC related kinases

PB1: Phox and Bem1 domain

PKBs: Protein kinase Bs

ATP: Adenosine-5'-triphosphate

PDK-1: 3-phosphoinositide-dependent protein kinase-1

PI3K: phosphatidylinositol 3 kinase

RACKs: Receptors for activated C- kinases

STICKs: Substrates that interact with C-kinase

PP2A: protein phosphatase 2

TGF-β: transformed growth factor beta

IL-6: interleukin-6

NF-κB: nuclear factor kappa-light-chain-enhancer of activated B

IκKαβ: IκB kinase

PTEN: phosphatase and tensin homolog

NSCLC: non-small cell lung cancer

ECT2: epithelial cell-transforming Sequence 2

ATM: aurothiomalate

GLI1: homoeodomain

SEER: surveillance, epidemiology, and end results

UV: ultraviolet

CDKN2A: cyclin-dependent kinase inhibitor 2A

BRAF: proto-oncogene B-Raf

ILP: isolated limb perfusion

RT: Radiation therapy

LAK: lymphokine-activated killer

BCG: Bacillus Calmette-Guérin

PD-1: programmed cell death 1 receptor

FDA: Food and Drug Administration

CTLA-4: cluster of differentiation 152

Par6: partitioning defective 6

IC$_{50}$: Half maximal inhibitory concentration

AMPK: adenosine monophosphate-activated protein kinase

AKT2: RAC-beta serine/threonine-protein kinase

FGFR: fibroblast growth factor receptors 1/2/3/4

mTOR: mammalian target of rapamycin

JAK1/2: janus kinase

MEK1: mitogen-activated protein kinase kinase 1(FGFR)

ERK1/2: mitogen-activated protein kinase 3/6

JNK1/2: c-Jun N-terminal kinases

PKA: protein kinase A

Src: proto-oncogene tyrosine-protein kinase Src

MBP: myelin basic protein

WST1: 4-[3-(4-Iodophenyl)-2-(4-nitropheny))-2H-5-tetrazolio]-1,3-benzene disulfonate

IκB: inhibitors of NF-kB"

EGFR: epidermal growth factor receptor

HER2: human epidermal growth factor receptor 2

AID: activation-induced cytodine deaminase (AID)

APOBEC: apolipoprotein B mRNA editing enzyme, catalytic polypeptide-like

PIP_2: phosphatidylinositol 4,5-bisphosphate

PIP_3: phosphatidylinositol (3,4,5)-trisphosphate

eIF4E: eukaryotic translation initiation factor 4E complex

S6K: ribosomal protein S6 kinase

FOXO1: forkhead box protein O1

TNF-α: tumor necrosis factor alpha

PARP: Poly (ADP-ribose) polymerase

SDS-PAGE: sodium dodecyl sulfate–polyacrylamide gel electrophoresis

WB: Western blots

XIAP: X-linked inhibitor of apoptosis protein

APAF-1: apoptosis-activating factor

EMT: epithelial-mesenchymal transition

MET: mesenchymal-epithelial transition

ECM: extracellular matrix

IFs: Intermediate filaments

CDK-1: cyclin-dependent kinase 1

AKT1: RAC-alpha serine/threonine-protein kinase

SNAIL1: Zinc finger protein SNAI1

PRRX1: paired related homeobox 1

TFs: transcription factors

BME: Basement membrane extract

*si*RNA: small interference RNA

x

IP: immunoprecipitation

ZEB1: Zinc finger E-box-binding homeobox1

TWIST: Twist-related protein1

VIF: Vimentin intermediate filaments

RT- qPCR: reverse transcription-quantitative PCR

F-actin: filamentous actin

STAT: activator of transcription

ICAM-1: intercellular adhesion molecule 1

AP-1: activator protein 1

JNKs: c-Jun N-terminal kinases

ERKs: Extracellular signal-regulated kinase

ISGF3: interferon regulatory factor 9

PAX3: paired box gene 3

EGR1: Early growth response protein 1

ELISA: enzyme-linked immunosorbent assay

IPAD: Immuno paired antibody detection assay

CHOP: CCAAT/enhancer-binding protein homologous Protein

4E-BP1: eukaryotic translation initiation factor 4E-binding protein 1

IRS-1: insulin receptor substrate 1

YAP-1: yes-associated protein 1

ZAP70: zeta-chain-associated protein kinase 70

P21: cyclin-dependent kinase inhibitor 1

CXCL: C-X-C motif chemokine

GM-SCF: granulocyte-macrophage colony-stimulating factor

MIF: macrophage migration inhibitory factor

CKI: cyclin-dependent kinase inhibitor

WNV: West Nile virus

NIH: National Institutes of Health

EDTA: ethylenediaminetetraacetic acid

JHS-23: 4-methyl-N1-(3-phenylpropyl)-1,2-benzenediamine

PDB: protein data bank

MEL-2: melanocyte growth medium

EMEM: Eagle's minimum essential media

FBS: fetal bovine serum

BSA: bovine serum albumin

TBST: tris saline buffer and Tween solution

DAPI: 4′,6-diamidino-2-phenylindole

ABSTRACT

Irrespective of plentiful efforts to enhance primary prevention and early detection, the number of melanoma cases in the United States has increased steadily over the past 30 years, thus greatly affecting public health and the economy. We have investigated the effects of five novel aPKC inhibitors; 2-acetyl-1,3-cyclopentanedione (ACPD), 3,4-Diaminonaphthalene-2,7-disulfonic acid (DNDA), [4-(5-amino-4-carbamoylimidazol-1-yl)-2,3-dihydroxycyclopentyl] methyl dihydrogen phosphate (ICA-1T) along with its nucleoside analog 5-amino-1-((1R,2S,3S,4R)-2,3-dihydroxy-4-methylcyclopentyl)-1H-imidazole-4-carboxamide (ICA-1S) and 8-hydroxy-1,3,6-naphthalenetrisulfonic acid (ζ-Stat) on cell proliferation, apoptosis, migration and invasion of two malignant melanoma cell lines compared to normal melanocyte cell lines. Molecular docking data suggested that both ACPD and DNDA specifically bind to protein kinase C-zeta (PKC-ζ) and PKC-iota (PKC-ι) while both ICA-1 compounds specifically bind to PKC-ι, and ζ-Stat showed a high affinity towards PKC-ζ. Kinase activity assays were carried out to confirm these observations. Results suggest that PKC-ι is involved in melanoma malignancy than PKC-ζ. Both isoforms promote the activation of nuclear factor (NF)-κB and protein kinase B (AKT) thereby supporting survival and progression. In addition, we demonstrated that PKC-ι induced the metastasis of melanoma cells by activating Vimentin, and PKC-ι inhibition downregulated epithilial-mesencymal transition (EMT), while inducing apoptosis. Of note, PKC-i specific inhibitors downregulated the expression of both PKC-ι and phosphorylated PKC-ι, suggesting that PKC-ι plays a role in regulating its own expression in melanoma. We also report the underlaying mechanisms of the transcriptional regulation of PKC-ι (PRKCI gene) expression in melanoma. c-

Jun, interferon-stimulated gene factor 3 (ISGF3), paired box gene 3 (PAX3), early growth response protein 1 (EGR1) and forkhead box protein O1 (FOXO1), which bind on or near the promoter sequence of the PRKCI gene, were analyzed for their role in PKC-ι regulation in SK-MEL-2 and MeWo cell lines. We silenced selected transcription factors using *si*RNA, and the results revealed that the silencing of c-Jun and FOXO1 significantly altered the expression of PRKCI. The levels of both phosphorylated and total PKC-ι increased upon FOXO1 silencing and decreased upon c-Jun silencing, suggesting that c-Jun acts as an upregulator, while FOXO1 acts as a downregulator of PRKCI expression. We also used a multiplex ELISA to analyze multiple pathways other than NF-κB that were affected by treatment with PKC-ι inhibitor. The silencing of NF-κB p65 and PKC-ι by siRNA suggested that the regulation of PKC-ι expression was strongly associated with FOXO1. In addition, we observed a significant decrease in the mRNA levels of both interleukin (IL)-6 and IL-8, with a significant increase in the levels of IL-17E and intercellular adhesion molecule 1 (ICAM-1) upon the knockdown of expression of PKC-ι in both cell lines. This suggested that PKC-ι expression was affected by these cytokines in an autocrine manner. Overall, the findings of this study suggest that PKC-ι inhibition suppresses its own expression, diminishing oncogenic signaling, while upregulating anti-tumor signaling, thus rendering it an effective novel biomarker for use in the design of novel targeted therapeutics for melanoma.

CHAPTER 1

PROTEIN KINASE C

1.1 Introduction

Cells have strict regulatory mechanisms to maintain normal behavior and perform desired functions. Protein kinase C (PKC) is a superfamily of various protein kinase enzymes that are important for the phosphorylation of serine and threonine amino acid residues on other proteins and thereby play several critical roles in cellular signal transduction cascades. Yasutomi Nishizuka, a well-known biochemist, discovered the first PKC isoform in 1977 (1). During his studies of PKC function, he discovered novel intracellular signal transduction systems and elucidated the PKC regulatory mechanisms involved in many biological processes (2). Nishizuka *et al.* found that PKC can be activated by calcium ion (Ca^{2+}) dependent proteases such as Calpain, co-factors such as diacylglycerol (DAG) and phosphotidylserine (PS). Over the span of three decades numerous isoforms of PKC with different activation processes have been discovered (1– 4).

1.2 PKC isoforms and classification

The PKC superfamily currently contains sixteen isoforms in *Homo sapiens* (5). Depending on the second messenger requirements for the activation, these isoforms are classified into three main

1

subclasses with two additional related groups. They are conventional (or classical), novel, and atypical. Isoforms alpha (α), beta I (βI), beta II (βII) and gamma (γ) occupy the conventional (c)PKC class. They require Ca^{2+}, DAG, and PS for activation. Novel (n)PKCs are comprised of isoforms delta (δ), epsilon (ε), eta (η), and theta (θ). nPKCs require DAG and PS but are independent of Ca^{2+} ions for activation. The atypical (a)PKC class contains iota (ι) and zeta (ζ). aPKCs are independent of DAG and Ca^{2+} but require PS for the activation. Apart from these 3 subclasses, protein kinase D (PKD), another family of serine/threonine protein kinases, is considered as a subfamily of PKC, contains three isoforms PKD1, PKD2 and PKD3 (6). PKC related kinases (PK-Ns) are also considered as a subfamily of PKCs and contains 3 isoforms (PK-N1, PK-N2 and PK-N3) (7,8). The structural differences among subclasses are discussed in part 1.3.

1.3 Protein Kinase C structure

All the members of the PKC superfamily share a largely conserved carboxyl-terminal catalytic domain (kinase domain) (Fig. 1.1). This similarity in the kinase domains is the key factor defining the PKC family. Amino-terminal regulatory domains differ between the subclasses. The regulatory domain is crucial for secondary messenger (molecules that relay signals received at receptors on the cell surface) binding, binding to the membrane and protein-protein interactions (3).

The regulatory domain of the PKC is comprised of several common sub-regions (Fig. 1.1). The C1 domain is common in all of the isoforms of PKC and serves as the membrane binding domain. Both conventional and novel isoforms contain two tandem repetitions of cysteine rich sequences

2

called C1A and C1B. They are essential for the binding of DAG, phorbol esters and membrane lipids (9–11). However, the C1 domain in aPKCs is incapable of binding to DAG or phorbol esters.

The C2 domain serves as a Ca^{2+} detector in both cPKCs and nPKCs. Even though C2 is common to both cPKCs and nPKCs, it serves as a Ca^{2+} sensor only in cPKCs. C2-like domains in nPKCs lack essential amino acid residues that facilitate Ca^{2+} binding (12,13). Atypical PKCs do not have a C2 domain but they have an additional region called Phox and Bem1 domain (PB1), which is very important in protein-protein interaction during aPKC activation process (14).

The pseudosubstrate region, which is common in all three main subclasses of PKC, is a small sequence of amino acids that mimics a substrate and binds the substrate-binding hollow region in the kinase domain. This region lacks serine and threonine phospho-acceptor residues. Psedusubstrate binding is a critical phenomenon that keeps the enzyme in its inactive stage (13).

cPKC activation progresses once Ca^{2+} and DAG are present in optimum concentrations. Calcium ions bind into C2 and DAG binds into the C1 domain, respectively, which recruit cPKC to the cell membrane. Interaction of PKC with the membrane leads to release of the pseudosubstrate from the catalytic site and activation of the enzyme. Yet, PKC must first be properly folded prior to these allosteric interactions that are necessary for the catalytic action. PKC maturation process starts with the phosphorylation event on the activation loop with of the catalytic region.

Catalytic domains among kinases are highly conserved. Protein kinase Bs (PKBs) and PKCs demonstrate approximately 40% amino acid sequence similarity within the kinase domains. This similarity increases to approximately 70% across PKCs and even higher when comparing within classes. Selbie *et al.* reported that two aPKC isoforms, ζ and ι, share ~84% identical kinase domains (15). Kinase structure is a bilobal structure with a β sheet comprising the N-terminal lobe and an

3

α-helix constituting the C-terminal lobe. Both Adenosine-5'-triphosphate (ATP) and substrate binding sites are located in the cleft formed by these two lobes. The ATP binding C3 motif and substrate binding C4 motif sequences are highly conserved in the kinase core among other kinases (3,15).
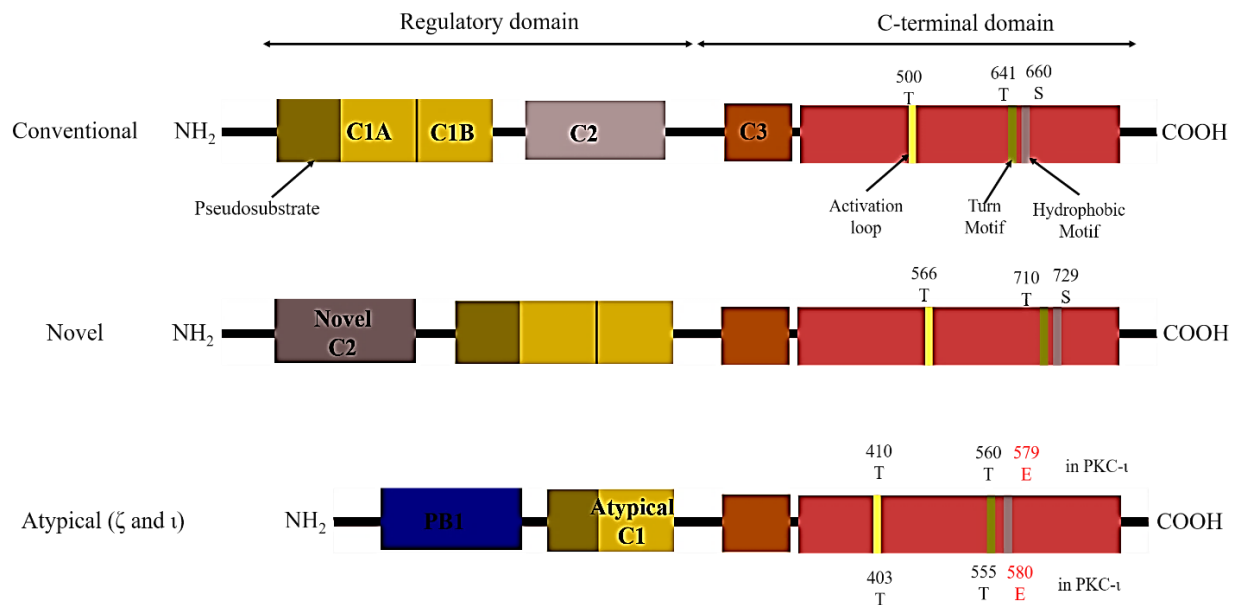
Figure 1.1 Structural differences of PKCs between subclasses. Highly conserved C-terminal catalytic domain contains three sites are essential for the activation. Activation loop, turn motif and hydrophobic motif. These sites get phosphorylated and participate for the activation except the hydrophobic motif of aPKCs which contains a glutamic acid (E) residue. The PKCs differ in the regulatory domains. Conventional PKCs have C2 (Ca^{2+} binding domain), C1A (DAG binding) domain, C1B (PS binding) domain. The novel PKCs have C domain similar to conventional PKCs. The C2 domain is altered and incompetent of binding to Ca^{2+}, thus called "novel C2" or "C2-like". The C1 domain of atypical PKCs bind to only PS. Instead of the C2 domain, they have the PB1 domain that is involved in protein-protein interaction. All PKCs have a pseudosubstrate domain within the N-terminal domain.

4

1.4 PKC regulation

Several critical post-translational and mechanistic steps are required for the complete maturation of the PKC. Among these, phosphorylation of the PKC catalytic region is essential. cPKCs and nPKCs have three phosphorylation sites, termed: the activation loop, the turn motif, and the hydrophobic motif. These phosphorylation events are essential for the activity of the enzyme, and 3-phosphoinositide-dependent protein kinase-1 (PDK1) is the upstream kinase responsible for initiating the process by phosphorylation of the activation loop (16).

The processing of cPKC and nPKC to their mature and functional form involve three sequential phosphorylations (17,18). Phosphorylation at the activation loop by PDK-1 promptly recruits a conformational change that involves autophosphorylation at the turn motif, which is very important in the maturation of PKCs. It protects the catalytically activated form of PKC from thermal degradation and from proteolysis (19,20). Autophosphorylation at hydrophobic motif takes place immediately after the autophosphorylation in turn motif (21,22). The aPKCs are phosphorylated only at the activation loop and the turn motif (Fig. 1.1). Phosphorylation of the hydrophobic motif is not required as a result of the presence of a glutamic acid in place of a serine, which provides a negative charge and acts similar in manner to a phosphorylated serine residue of cPKCs and nPKCs (3).

The pseudosubstrate remains at its substrate binding pocket even after phosphorylation. Upon extracellular stimulation, phospholipase C converts phosphatidylinositol to phosphatidylinositol 3 kinase (PI3K) and DAG. This lead to release of Ca^{2+} ions from internal stores. Ca^{2+} ions binds to the C2 domain of cPKC inducing partial interaction with anionic phospholipids at the membrane, which causes conformational changes in the protein, releasing the pseudosubstrate (23). On the

5

other hand, nPKCs do not have the Ca^{2+} binding C2 domain and therefore depend on the C1 domain to interact with the membrane.

Anchoring proteins play a critical role in the distribution and localization of PKCs which is also important for the optimum biological functioning. Receptors for activated C- kinases (RACKs) target PKCs to specific cellular localization by binding with them (24). Substrates that interact with C-kinase (STICKs), are a group of proteins that bind with immature PKCs to bring them close to processing cofactors and release them once phosphorylation events take place (25).

The open conformation of activated PKCs is sensitive to proteases like Calpain and dephosphorylation by phosphatases such as protein phosphatase 2 (PP2A) (26). PKCs are removed by degradation via ubiquitin-proteosome pathway in their regulation cycles (27,28). Therefore, protection and proper localization are essential for activated PKCs to perform their function.

1.5 Atypical PKC activation

As already discussed, aPKCs do not depend on DAG and Ca^{2+} for the activation. Chou *et al.* demonstrated that PDK-1 binds with high affinity to the PI3K lipid product phosphatidylinositol-3,4,5-trisphosphate (PIP$_3$), phosphorylates and potently activates two other PI3K targets, AKT and p70S6K. They investigated whether PDK-1 is the kinase that activates PKC-ζ. *In-vivo* results show that PI3K is both necessary and sufficient to activate PKC-ζ (29). PDK-1 phosphorylates threonine 410 (T410) in the PKC-ζ activation loop and activates PKC-ζ *in-vivo* in a PIP$_3$ enhanced manner. T403 serves as the targeted phosphorylating site for PDK-1 in PKC-ι, which is similar to T410 in PKC-ζ (29).
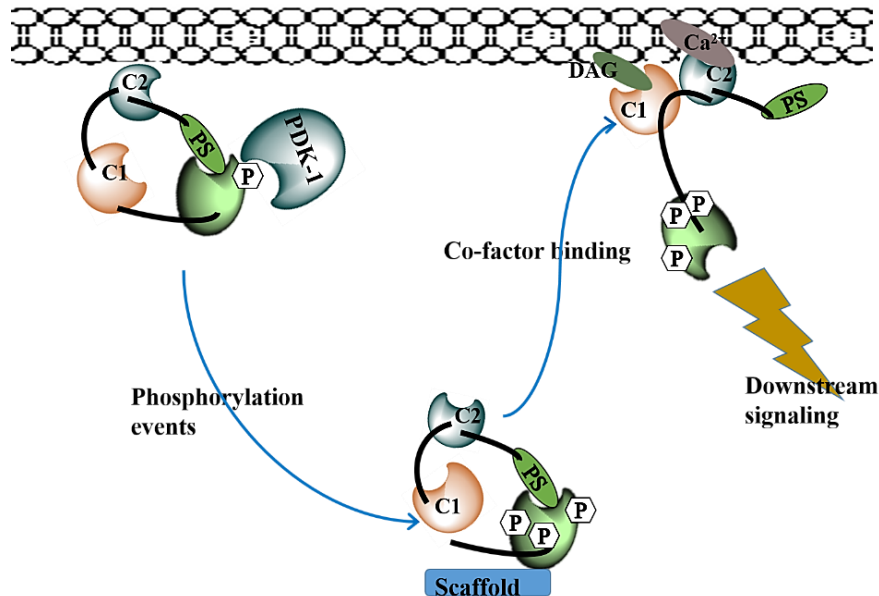
Figure 1.2 Activation process of a conventional PKC. PDK-1 initiates the activation process by phosphorylating the activation loop at the C-terminal. This stimulates two rapid auto-phosphorylation events at the turn motif and the hydrophobic motif, respectively. These phosphorylating events lead the inactive PKC into the cytosol and promote scaffold binding. The inactive status is maintained by keeping pseudosubstrate (PS) bound to the substrate binding domain. The subsequent steps in the activation are triggered by signals that promote the lipid hydrolysis from the membrane and release cofactors such as Ca^{2+} and DAG. These events promote the translocation of the PKC to the cell membrane where the co-factors bind to the complementary regions of the PKC. Ca^{2+} binds to the C2 domain and DAG binds to C1 domain. The binding of the co-factors generate the energy required to release the pseudosubstrate form the substrate binding site and completes the activation. This Figure was adapted from Newton *et al.* (22)

1.6 PKC superfamily and cancer

PKCs are specific signaling molecules that link multiple cellular processes to cancer. A large amount of work established PKCs as multifunctional regulators of cell functions such as cell proliferation, differentiation, survival, migration and invasion (30,31). PKCs have been associated with a number of diseases such as metabolic disorders, cardiovascular dysfunctions and cancer. The complexity in PKC signaling and biological functions is largely due to the fact that PKC

superfamily is a large structurally and functionally diverse group of kinases. In recent years there have been major advances in the understanding of PKC functions in tumor development, progression and metastasis. The PKC isozyme expression profile often changes in neoplastic diseases compared to normal tissues and has therefore been of interest (31).

PKC-α is well known as a regulator of multiple aspects of tumor growth, including proliferation, survival, differentiation and motility (32). Many reports have demonstrated the oncogenic properties of PKC-α that linked to enhanced proliferation and anti-apoptotic signals (32–36). As a result of that PKC-α earned attention as a potential target for cancer therapy. Some literature reports PKC-α acts as a tumor suppressor. PKC-α is found to be up-regulated in bladder, endometrial, and breast cancers and down-regulated in colorectal and renal cell carcinomas (37,38). Hill *et al.* reported that PKC-α plays a key role in K-RAS-mediated lung tumorigenesis (39). PKC-α silenced mice demonstrated enhanced K-RAS lung tumorigenesis (39).

The PRKCB gene encodes PKC-βI and PKC-βII, which are splice variants and show a distinctive involvement in cancer (40). Several reports show the involvement of PKC-β isoforms in the progression of many cancer types such as glioblastoma, breast, lymphoma, prostate, and colon cancers (40–44).

PKC-δ is a well-known pro-apoptotic and anti-proliferative PKC isoform (45,46). PKC-δ is widely used as a death mediator of chemotherapeutic agents and radiotherapy (45–48). PKC-δ involvement in DNA damage and receptor-mediated cell death has been reported in the literature (30,48,49).

PKC-ε is found to be upregulated in many cancers mainly through RAS-RAF1 pathway (50–56). PKC-ε-transformed fibroblasts produced elevated levels of transformed growth factor beta (TGF-

8

β) which indicated growth autocrine loops which may account for its oncogenic activity (57,58). PKC-ε is overexpressed in ~75% of primary tumors from invasive ductal breast cancer patients (59). PKC-η has also been shown to be up-regulated in some cancers (60,61) but down-regulated in others (62).

1.7 Atypical PKCs in cancer progression

Regardless of the debates in the literature largely due to the use of non-specific approaches such as inhibitory peptides and dominant-negative mutants, many studies suggest a tumor suppressor function of PKC-ζ. In contrast, PKC-ι solidly satisfies the criteria of an oncogenic kinase (62,63). Variations of the expression of PKC-ζ has been shown in different types of human cancer. Overexpression of PKC-ζ has been reported in lymphoma, prostate and bladder cancers (63–67). Interestingly, down-regulation of PKC-ζ has been shown in kidney, renal clear cell carcinoma, glioblastoma, lung, pancreatic, colon and ovarian cancers (68–78). As an example, PKC-ζ inhibits growth and promotes apoptosis in colorectal carcinoma demonstrating an inhibitory effect on the transformed phenotype of colorectal cancer cells. This suggests that down-regulation of PKC-ζ may contribute to colon tumorigenesis (77). Similarly PKC-ζ demonstrated pro-apoptotic behavior in ovarian cancer (78). PKC-ζ knock out *in-vivo* models demonstrated increased RAS induced lung carcinogenesis, indicating the tumor suppressor features of PKC-ζ *in-vivo*. In this study, PKC-ζ downregulates RAS induced interleukin (IL)-6 production *in-vivo*. Consistent with this finding, increased production of IL-6 was observed in PKC-ζ knock out cells, which was essential for cancer cell growth under limited nutrient conditions (73). Futhermore PKC-ζ activity demonstrated a significant correlation with phosphatase and tensin homolog (PTEN) levels in human prostate tumors. PKC-ζ knock out in mice showed PTEN deficiency which correlated with elevated

9

invasiveness (73). Loss of PKC-ζ promotes human cancer cells reprograming of their metabolism in response to glucose deprivation by augmenting the utilization of glutamine through the serine biosynthetic pathway (79).

However, in contrast to PKC-ζ activity described above, some reports show pro-survival anti-apoptotic behaviors of PKC-ζ in certain systems (80–85). Win *et al.* reported that PKC-ζ induced transformed non-malignant and malignant prostate cell survival by phosphorylating IKKαβ thereby promoting NF-κB activation (80). Filomenko *et al.* reported that PKC-ζ is activated and provides protection in tumor cells which are exposed to a cytotoxic agent (81). Bezombes *et al.* showed that PKC-ζ overexpression resulted in delayed apoptosis and provided a significant resistance to antileukemic drugs in U937 human leukemia cells (82). Cataldi *et al.* reported that PKC-ζ generates a survival response with accelerated nuclear translocation to provide a radio resistance in friend erythroleukemia cells in radiation treatments (83). Xin *et al.* showed that PKC-ζ abrogates the proapoptotic function of Bax through phosphorylation in both small cell lung cancer and non-small cell lung cancer cells (84).

Accumulating evidence recognizes that PKC-ι is an oncogenic kinase and that it contributes to the transformed phenotype (86,87). Overexpression of PKC-ι is detected in several human tumors, including lung, colon, breast, pancreas, prostate, melanoma and ovarian cancer (87). The PRKCI gene is reported to be amplified in some human cancers, even if PKC-ι overexpression does not necessarily associate with gene amplification (86–92).

PKC-ι is upregulated in non-small cell lung cancer (NSCLC) cells, which is required for the transformed phenotype of NSCLC cells harboring oncogenic K-RAS mutation (93–96). NSCLC cell lines highly depend on PKC-ι even without RAS mutation and these situations typically demonstrated PRKCI gene amplification (96). Justilien *et al.* reported Rho-GEF Ect2 as an element

10

of the PKC-ι/Par6 complex, which is required for transformed growth (97). The epithelial cell-transforming Sequence 2 (ECT2) gene was reported to be amplified with PRKCI, which indicates a coordinated mechanism for tumorigenesis. The anti-rheumatic agent aurothiomalate (ATM) was used as an inhibitor, which targets PKC-ι/Par6 interaction. ATM was tested against several PKC-ι overexpressing cell lines. ATM was effective against K-RAS mediated expansion of bronchoalveolar stem cells and lung tumor growth *in-vivo* (94,98). ATM was the first drug that targeted PKC-ι and was considered as a novel therapeutic by Stallings-Mann *et al.* in 2006. Half maximal inhibitory concentration (IC_{50}) of ATM ranged from 0.3-100 μM and indicated that some cell lines are insensitive (i.e. H460 and A549 lung cancer cells). Importantly, ATM has the potential risk of developing gold toxicity even with low levels of the inhibitor, which is a common problem with gold therapy in rheumatoid arthritis. Acevedo-Duncan *et al.* introduced ICA-1 as a PKC-ι specific inhibitor in 2009 and its nucleotide analog was tested and reported by Pillai *et al.* in neuroblastoma cells in 2011, which demonstrated an IC_{50} of 0.1 μM, which was 1000 times less than the ATM IC_{50} in BE(2)-C neuroblastoma cells (99). The study also shows that PKC-ι is critical for the survival and progression of neuroblastoma cells *in-vitro*. Desai *et al.* reported that PKC-ι is essential for the cell cycle progression of glioblastoma cells through PI3K/PKC-ι pathway (100). Acevedo-Duncan *et al.* demonstrated that PKC-ι along with PKC-βII phosphorylate cyclin dependent kinase activating kinase during the cell cycle in human glioma progression (101). Both *in-vitro* and *in-vivo* results demonstrated that PKC-ι was responsible for cell survival and progression in colon and pancreatic cancers (90,91). PKC-ι plays a critical role for hedgehog signaling in basal cell carcinomas. Elevated PKC-ι is responsible for upregulation of the homoeodomain (GLI1) transcription factor in basal carcinoma cell lines (102). PKC-ι plays a vital role in antagonistic regulation with RhoB in glioblastoma cells to increase cellular invasion (103).

11

Win *et al.* and Ishiguro *et al.* have discussed the involvement of PKC-ι in the activation of the NF-κB pathway by increasing the phosphorylation of IKKαβ (80,104). Involvement of aPKCs in different types of cancer progression increased the attention to investigate aPKC role in other cancers as well including melanoma.

CHAPTER 2

MELANOMA

2.1 Introduction

2.1.1 Epidemiology

Melanoma is a lethal malignancy that has attracted a huge attention since the beginning of the 21st century. Even though incidences of many tumor types are decreasing, malignant melanoma incidences are in a rapid rise (105). Although most patients have localized tumors at the diagnosis point, which can be effectively removed surgically, the majority of patients develop metastases later (106,107). Increasing numbers of malignant melanoma have created a worldwide socio-economic problem. A century ago, melanoma cases were very rare, but today it is one of the most frequent cancers in the Caucasian population (108,109). As of the beginning of 2019, melanoma is regarded as the fifth most common cancer in the United States (US). According to the surveillance, epidemiology, and end results (SEER) statistics of the US national cancer institute, ~92,000 new melanoma incidences were reported in the year 2018, which was approximately 5.3% of all cancers reported (105). According to the SEER data, new malignant melanoma cases increased by approximately 300% since 1975. In 1973, the US melanoma incidence rate was 6.8 per 100,000 and in 2018, the rate was reported as 23.75 per 100,000, in which the rate for men was

29.8 per 100,000 and 17.7 per 10,000 for women. This suggests that men are more susceptible than women for the disease.

Researchers believe that a major cause for this difference may lie in men's skin which differs from women's skin. Men have thicker skin with less fat beneath. A man's skin also contains more collagen and elastin, fibers that give the skin firmness and keep it tight. These differences make men's skin more likely to be damaged by the sun's ultraviolet (UV) rays (108). Mackie *et al.* shows that Australia has the highest recorded incidence of melanoma worldwide (110). The average of new melanoma incidence is 55.8 per 100,000 per annum for males and 41.1 per 100,000 per annum for females from 1983 to 2002. New Zealand comes second in the world after Australia, and Switzerland, Norway, Sweden and Denmark report the highest number of cases in European countries, respectively (110). Africans, Middle-eastern and Asians have shown much lower numbers, which is probably due to better protection against UV rays which is typical of highly pigmented skin (106). The incidence rate of melanoma for the white population has an approximately 10-fold greater risk of developing cutaneous melanoma than black, Asian or Hispanic populations. At the same time, both white and African American populations share an equal risk of developing malignant melanoma in plantar locations (bottom of the foot). Interestingly, non-cutaneous melanomas such as mucosal melanoma are more common in non-white populations (106,110,111).

According to the SEER data for 2018, the median age at diagnosis of melanoma is 64 in the US. Markovic *et al.* reported that men are approximately 50% more likely to develop melanoma than women. However, this difference increased to approximately 300% when the average age reaches 75 years where the new incidence rate for men is 145.6 per 100,000 against 47.3 per 100,000 for women (106,112). Interestingly, data also shows a difference in the distribution of the disease

between men and women. The most frequent site of occurrence for men is the back while arms and legs are the most common sites for women (113).

Melanoma is caused by many factors, usually a combination of genetic susceptibility and environmental exposure. The most important environmental risk factor for developing malignant melanoma is the exposure to genotoxic UV rays (106,108). Elwood *et al.* reported that prolonged sun exposure appears to be a major risk for melanoma (109). Artificial UV exposure also plays a role in the development of melanoma. Psoralen–UVA radiation photochemotherapy used to treat psoriasis leads to an increased risk of melanoma (114). Presence of melanocytic nevi, family history and genetic susceptibility are the most important host risk factors. Melanocytic nevi are benign accumulations of melanocytes or nevus cells that can be congenital or acquired. Approximately 25% of melanoma cases can be related to a pre-existing nevus (115). Moreover, the higher the number of nevus and the higher the size increases the risk of melanoma (116,117). Atypical nevi are frequently associated with an increased risk of melanoma.

Family history is another strong risk factor for melanoma, indicative of possible heritable genetic causes. According to Tsao *et al.*, families with inherited melanoma demonstrated a clear pattern of autosomal-dominant inheritance with numerous family members affected, in which cyclin-dependent kinase inhibitor 2A (CDKN2A) was found as the most common genetic abnormality (118,119). Patients with an underlying genetic susceptibility to develop melanoma usually demonstrate occurrence at a very young age (<40 years). Multiple primary tumors or a history of precursor lesions (e.g. dysplastic nevi) form tumors that are superficially invasive and with a better prognosis (118). Certain phenotypic characteristics such as fair skin, red hair, freckles, sun sensitivity and an inability to tan, show greater risk of developing melanoma (119).

15

There are four main types of skin melanoma. The most common type is superficial spreading melanoma. It is more commonly found on the back, arms, legs and chest. Superficial spreading melanoma grows slower at the beginning and speeds up eventually. The second most common type is nodular melanoma, which grows faster than other types. Color typically changes from red to black over the time when tumors grow. It is commonly found on the neck, chest, back and head. The third type is called lentigo maligna melanoma, which is less common compared to the previous two. It is usually found in older people in areas such as the face and neck that have had a lot of sun exposure over a long time. It develops from a slow-growing precancerous condition called a lentigo maligna or Hutchinson's freckle. This looks like a stain on the skin. They are usually slow-growing and less dangerous than the other types of melanoma. The last of the four, and the rarest type, is called acral lentiginous melanoma. It is usually found on the palms of the hands, soles of the feet, or under fingernails or toenails. It is more common in people with black or brown skin. Acral lentiginous melanoma is a dangerous melanoma form that grows at a faster rate. Apart from these four types, another rare type of melanoma is called desmoplastic melanoma. Rarely, melanoma can start in parts of the body other than the skin, such as in the eye, which is called ocular melanoma. Sometimes it can start in the tissues that line areas inside the body, such as the anus or rectum, nose, mouth, lungs and other areas.

The stage of a melanoma describes how deeply it has grown into the skin, and whether it has spread away from the primary tumor. Clark scale and Breslow scale are most frequently used systems to classify melanoma. These scales are different from each other and doctors often use both to interpret the disease with the stage numbering because Clark and Breslow scales only look at the depth of melanoma cells in the skin.

16

The Clark scale is a way of measuring how deeply the melanoma has grown into the skin and which levels of the skin are affected. The Clark scale has 5 levels: level 1 is also called melanoma *in situ* where melanoma cells are present only in the epidermis (outer layer of the skin). Level 2 means there are melanoma cells in the papillary dermis, which is the layer directly under the epidermis. In level 3, melanoma cells distribute throughout the papillary dermis and start to spread into the next layer down (the reticular dermis). Level 4 means the melanoma has spread into the reticular or deep dermis. Level 5 means the melanoma has grown into the layer of fat under the skin (subcutaneous fat). For the Breslow scale, the pathologist measures the thickness of the melanoma tumor. It measures in millimeters (mm) how far melanoma cells have reached down through the skin from the surface.

In general, melanoma can be categorized into 5 stages (116,120). In stage 0 melanoma, the tumor is confined to the upper layers of the skin and have not grown deeper. Stage I melanoma is defined as a tumor that is up to 2mm thick. A Stage I melanoma may or may not have ulceration, but there is no evidence the cancer has spread to lymph nodes or metastasized. Stage II melanoma is defined by tumor thickness with ulceration. Still there is no evidence the cancer has spread to the lymph nodes or distant sites. Stage III melanoma is defined by the level of lymph node involvement and ulceration. In Stage III melanoma, the depth of the melanoma no longer matters. There is no evidence the cancer has spread to distant sites. Stage IV melanoma occurs when the cancer spreads beyond the original site and regional lymph nodes to more distant areas of the body. The most common sites of metastasis are lungs, abdominal organs, brain, bones and soft tissues such as other parts of the skin and distant lymph nodes beyond the primary tumor region (116,120).

17

2.1.3 Melanoma diagnosis and currently available treatments

Early detection is the most important factor for lowering the malignant melanoma mortality. Timely detection and proper treatment is critical for higher survival rate. Compared to other lethal cancers malignant melanoma has the assistance of the cutaneous location, which allows its early detection through non-invasive approaches and provides a better chance to apply non-invasive treatments. Pathological examination plays one of the most important steps in the diagnosis. Skin self-examination is a simple, convenient method of screening for melanoma and precancerous lesions (116,120). The "ABCDE" criteria was developed in 1985 for the identification of melanoma. ABCDE stands for "asymmetric" mole, "border" (irregular border), "color" (changes over the time), "diameter" (>6 mm) and "evolving". This criteria is applied for differentiating common moles. Glasgow 7-point checklist is another clinical tool used to identify melanoma, which includes three major factors which are change in "size", "shape" and "color". Additionally, it considers four minor factors which are "sensory change", "diameter change", "inflammation" and "bleeding" (106). Dermoscopy is also a non-invasive diagnostic method for *in-vivo* observation of the skin; this device uses optic magnification to provide a better visualization of morphological structures that are not visible to the naked eye.

Atypical pigment network changes, appearance of irregular dots/globules, irregular streaks, irregular pigmentation are used to spot malignant lesions. Regression structures are also a characteristic of malignant lesions. During the process of regression, fibrosis and melanosis are usually found together and, thus, the regression structures appear as white scar-like areas, blue areas or a combination of both (121).

Total-body photographic images and short-term surveillance can also be used to detect minimal changes in the early stages of melanoma tumor development. This approach gives viability to assess dynamic evolution of the melanocytic nevi over time (121).

For stage IV melanoma, the National Comprehensive Cancer Network recommended first line agents are dabrafenib, ipilumumab, vemurafenib, and high-dose IL-2. Most of these drugs target proto-oncogene B-Raf (BRAF) mutation (V600E), which occurs in ~60% melanoma cases, yet melanoma has a poor prognosis and tumors acquire resistance to BRAF mutation inhibition (122). Currently available and United States Food and Drug Administration (FDA) has approved combination therapies for advanced melanoma include dabrafenib + trametinib and vemurafenib + cobimetinib. These may improve survival, but they also pose adverse toxic effects (123,124). The FDA approved only decarbazine as a chemotherapeutic drug for melanoma which has only 7-12% response rate (124). Isolated limb perfusion/infusion, interferon-α therapy, topical imiquimod therapy, cryotherapy, radiation therapy, and intratumoral interleukin-2 injections are also available as new emerging treatment methods. Another new class of treatment include anti-programmed death-ligand 1 agents, anti-programmed cell death 1 receptor agents such as nivolumab and pembrolizumab, and oncolytic vaccines. Available treatments for selected sites include adoptive T-cell therapies and dendritic cell vaccines. Patients with Stage IV melanoma continue to demonstrate a poor prognosis, with a mean survival of only 8–10 months (124).

Surgery is an effective option for early stage melanoma, since patients are quickly rendered "disease-free" as a result of removal of localized tumors. In contrast, systemically administered therapies require prolonged treatment courses to achieve relatively inferior local response rates. But surgery alone cannot identify and address microscopic metastases, and once the disease reaches later stages, the effectiveness of surgeries decreases (125).

19

More recently, isolated limb perfusion (ILP) has developed as an effective limb salvaging therapy for regional cutaneous and subcutaneous metastases. In ILP, high chemotherapy doses are delivered locally to the patient under an extracorporeal circuit that isolates the affected limb, which avoids systemic toxicity. The rationale of ILP is that there is high localized doses of cytotoxic agents applications with minimal systemic adverse events. In cryotherapy, liquid nitrogen is used as a non-invasive targeted treatment for limited cutaneous metastatic melanoma (126). Cryotherapy results in tumor antigen release through local trauma to the area and thereby providing potential to elicit a systemic anti-melanoma immune response. However, outcomes of this method was not as efficient as expected earlier (127). Radiation therapy (RT) is commonly used as an additional therapy or as palliative therapy, particularly for patients with brain metastases and is carried out as sterotactic gamma knife radiosurgery (128). In the setting of inoperable disease, RT is a rational option for palliation.

In the late 1990s, the FDA approved high-dose intravenous IL-2 as an immunotherapy for metastatic melanoma. IL-2 is a glycoprotein secreted by T helper cells. It stimulates T-cell proliferation and the development of lymphokine-activated killer (LAK) cells, which have the ability to directly lyse tumor cells (129). Intravenous delivery of IL-2 provides an overall response rate only 16% in patients with metastatic melanoma (130). Due to IL-2-induced vascular leak syndrome and other associated toxicities, intravenous IL-2 therapy is rarely used nowadays. Intralesional approach for IL-2 administration was tested to reduce systemic toxicity and increase local therapeutic effects for treatment of melanoma metastases.

Bacillus Calmette-Guérin (BCG) is an attenuated live bovine tuberculosis bacillus that is used as a vaccination for human tuberculosis. BCG is used to treat a variety of different malignancies.

20

BCG treatments for melanoma showed poor efficacy and increased the risk of death due to anaphylactic shock and development of infectious granulomas at sites of injection (125,131).

Interferon therapy is also applied against metastatic melanoma. IFN-α is a type 1 interferon endogenously produced by macrophages, T cells, and natural killer cells that have shown anti-tumor properties. However, IFN-α for the treatment of metastatic melanoma survival outcomes have been largely inconsistent between different trials. Both autologous and allogenic cancer vaccination strategies have been used in metastatic melanoma but response rates were not consistent (132,133).

The programmed cell death 1 receptor (PD-1), expressed by T cells, which has two primary ligands; PD-L1, found on cancer cells and tumor-infiltrative macrophages; and PD-L2, found on antigen-presenting cells. PD-1 acts as a negative regulator of T cells. As with anti-CTLA-4 (cluster of differentiation 152) therapy, antibodies against both PD-L1 and PD-1 have been developed to inhibit this down-regulatory pathway, allowing for unopposed T-cell activation (133,134). The purpose of this is to activate tumor-specific T cells and "bystander" T cells that may also contribute to the anti-cancer response. Recent phase I trials of nivolumab (anti-PD-1) in combination with ipilimumab (anti-CTLA4) and BMS936559 (anti-PD-L1) showed promising results in patients with advanced melanoma (134).

2.1.4 Atypical PKC expression in melanoma

PKC expression in melanocytic lineage cells has enticed a great deal of consideration because phorbol esters needed for PKC activation are also essential components for the *in-vitro* growth of normal human melanocytes. In addition, phorbol esters have been reported to promote the

21

development of skin tumors (135–137). Other evidence associated with PKC involvement in melanoma is that bryostatins are currently being evaluated in the treatment of human melanoma which can also increase PKC activity (138–141). Therefore, to obtain a proper understanding of the role of various PKC isoforms in the process of transformation of human melanocytes, it is essential to know the distribution of PKC isoforms and ultimately their levels of activation in melanoma samples. Various research groups have shown that changes in PKC isoform expression are associated with alterations in growth and differentiation of specific human melanocyte functions. Selzer *et al*. conducted a full characterization of the distribution pattern and expression differences between normal and malignant melanocyte samples. They investigated the presence of 11 PKC isozymes in eight metastatic melanoma samples, 3 normal melanocyte cell lines and 3 spontaneously transformed melanocytes and several other melanoma tumor samples. Both PKC-ι and PKC-ζ showed a distinct difference in their expression when moving from the normal status to malignant through transformation. Elevated levels of PKC-ζ and PKC-ι were found in all transformed melanocytes and melanoma metastases samples. PKC-ζ was detected in normal melanocytes in low levels. But PKC-ι were absent in normal melanocytes (135). These results suggest that transformation of normal to malignancy of melanocyte tumors demonstrate a positive relationship with the expression of aPKCs thereby indicates that melanoma progression depends on aPKCs.

2.2 Results

We tested the aPKC expression in two normal melanocyte cell lines (PCS-200-013 and MEL-F-NEO) against two melanoma cell lines (SK-MEL-2 and MeWo) at 50% and 100% confluency. Figure 2.1 demonstrates a comparison of the expression of PKC-ι and PKC-ζ in normal

22

melanocytes (PCS-200-013 and MEL-F-NEO cell lines) against SK-MEL-2 and MeWo malignant

melanoma cell lines. As shown in Figure 2.1, PKC-ι was not detected in normal melanocyte cell

lines compared to the over-expression observed in SK-MEL-2 and MeWo malignant melanoma

cell lines. Moreover, PKC-ζ expression was very low in both normal melanocyte cell lines

compared to the amplified expression in melanoma cells. These results agreed with the expression

patterns demonstrated by different cell lines and patient samples described in Selzer *et al.* (135).
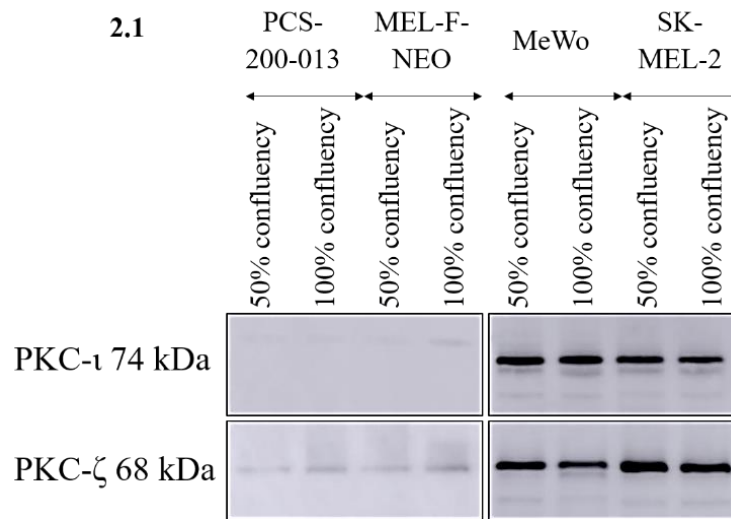
Figure 2.1: aPKC expression comparison between normal melanocytes (PCS-200-013 and MEL-F-NEO) and melanoma cell lines (SK-MEL-2 and MeWo). The expression of PKC-ι and PKC-ζ was reported at approximately 50% and 100% confluency for normal melanocytes against metastatic melanoma cells. Western blots were conducted with 50 μg of total proteins loaded in each lane. Experiments ($N = 3$) were performed.

2.3 Summary

When taken together, these results indicate a strong relationship between aPKCs and melanoma

progression. The exact roles of these aPKCs in melanoma progression were systematically studied

and findings are reported in this dissertation and in the form of full published research articles (142–145).

CHAPTER 3

NOVEL ATYPICAL PKC SPECIFIC INHIBITORS

3.1 Introduction (ACPD, DNDA, ICA-1S, ICA-1T and ζ-Stat)

We have investigated the effects of five novel aPKC specific inhibitors on various cellular aspects of melanoma such as cellular growth, differentiation, survival, migration and invasion. Figures 3.1-3.5 show 2-acetyl-1,3-cyclopentanedione (ACPD) (Fig. 3.1), 3,4-diaminonaphthalene-2,7-disulfonic acid (DNDA) (Fig. 3.2), [4-(5-amino-4-carbamoylimidazol-1-yl)-2,3-dihydroxycyclopentyl] methyl dihydrogen phosphate (ICA-1T) (Fig. 3.3) along with its nucleoside analog 5-amino-1-((1R,2S,3S,4R)-2,3-dihydroxy-4-methylcyclopentyl)-1H-imidazole-4-carboxamide (ICA-1S) (Fig. 3.4) and 8-hydroxy-1,3,6-naphthalenetrisulfonic acid (ζ-Stat) (Fig. 3.5), which were virtually screened and experimentally validated for the specificities of PKC-ι and PKC-ζ. All these five inhibitors were identified and characterized by Acevedo-Duncan *et al.* at the University of South Florida (99,142,143).

25
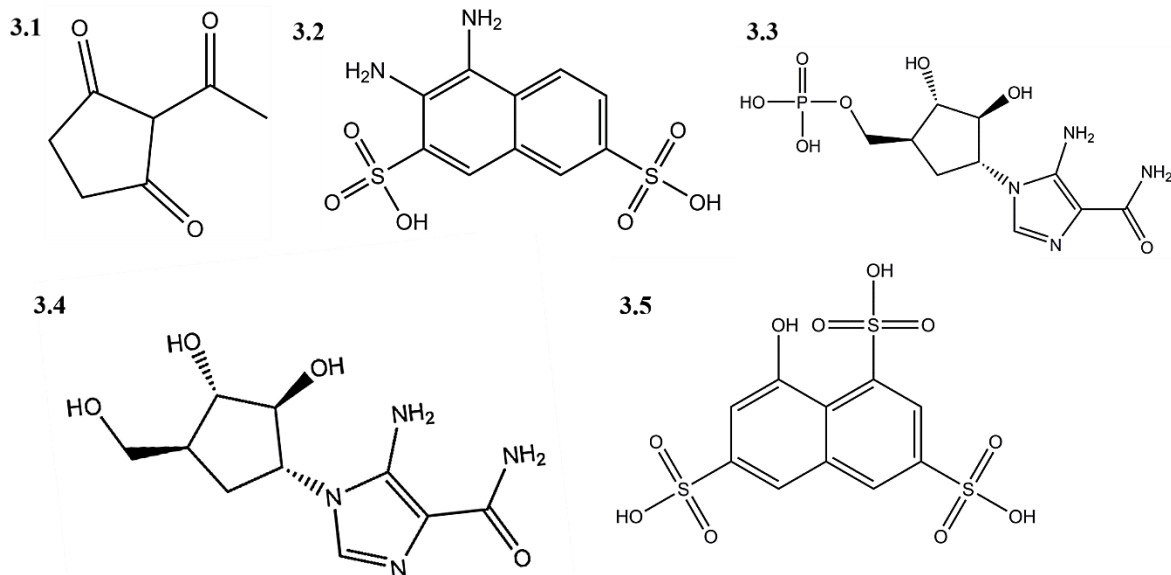
Figures 3.1-3.5: Structures of the aPKC specific inhibitors (ACPD, DNDA, ζ-Stat, ICA-1S and ICA-1T). Chemical structures of ACPD (3.1) and DNDA (3.2) are specific to both PKC-ι and PKC-ζ, ICA-1T (3.3) and ICA-1S (3.4) are specific to PKC-ι while ζ-Stat (3.5) is specific to PKC-ζ. Molecular weights of ACPD (140.14 g/mol), DNDA (318.32 g/mol), ζ-Stat (MW = 384.34 g/mol), ICA-1S (MW = 256.26 g/mol) and ICA-1T (MW = 336.24 g/mol), respectively.

Aurothiomalate (ATM) was first identified as a potent PKC-ι inhibitor, targeting the interaction between Phox and Bem1 (PB1) domain of PKC-ι and partitioning defective 6 (Par6) by Stallings-Mann *et al.* in 2006 (146). Half maximal inhibitory concentration (IC$_{50}$) of ATM ranged from 0.3-100 μM to the tested cell lines which indicated that some cell lines are insensitive (i.e. H460 and A549 lung cancer cells) to ATM (98). In addition, ATM has the potential risk of developing gold toxicity even with low concentrations, which is common in gold therapy in rheumatoid arthritis (147). The discovery of ICA-1T analog was patented in 2007 and its effects on neuroblastoma was reported by Pillai *et al.* as a novel potential inhibitor for PKC-ι in 2011. ICA-1T demonstrated IC$_{50}$ as 0.1 μM which was 1000 times less than ATM IC$_{50}$ on BE(2)-C neuroblastoma cells (99). When ICA-1T was first presented, PKC-ι crystal structure was not available, therefore a PKC homology

26

model was used for molecular docking simulations. Pillai *et al.* reported that ICA-1T is more potent compared to FDA-approved ATM (99). The inhibitory mechanism of ICA-1T was reported as competitive therefore rate of the reaction will depend on inhibitor and substrate concentrations. This suggests that the mechanism of ICA-1T may not involve adenosine triphosphate (ATP) competitive binding (99).

Sajan *et al.* reported the specificity of ACPD as it inhibits both PKC-ι and PKC-ζ without affecting other PKC isoforms in a study which investigated the effects of PKC-ζ in glucose metabolism (148). Even though the molecular simulations and specificity predictions were not reported, Sajan *et al.* reported that ACPD does not interact with other kinases such as adenosine monophosphate-activated protein kinase (AMPK), RAC-beta serine/threonine-protein kinase (Akt2), fibroblast growth factor receptors (FGFR)1/2/3/4, mammalian target of rapamycin (mTOR), glycogen synthase kinase 3 beta (GSK3β), Interleukin-1 receptor associated kinase (IRAK), janus kinase (JAK1/2), mitogen-activated protein kinase kinase 1 (MEK1), mitogen-activated protein kinase 3/6 (ERK1/2), c-Jun N-terminal kinases (JNK1/2), protein kinase A (PKA), proto-oncogene tyrosine-protein kinase Src (Src), Rho associated coiled-coil containing protein kinase 2 (ROCK2) and phosphoinositide 3-kinases (PI3K) (149,150).

3.2 Results

3.2.1 Molecular docking predictions and binding affinities

ACPD and DNDA were screened by positioning them in the structural pockets of PKC-ι and PKC-ζ homology models and then scored based on polar and non-polar interaction predictions. ACPD interacted with amino acid residues Gln 469, Ile 470, Lys 485 and Leu 488 of the PKC-ι

27

homologous structure (Fig. 3.6) and Arg 265, Pro 267, Asp 269 and Lys 290 of the PKC-ζ homologous structure (Fig. 3.7). DNDA demonstrated interactions with Asp 339, Asp 382, Leu 385 and Thr 395 of PKC-ι (Fig. 3.8) and Asp 337, Asp 380, Leu 383 and Thr 393 of PKC-ζ (Fig. 3.9). Reasonable docking scores were acquired (approximately -7 kcal/mol) for both ACPD and DNDA separately for PKC-ι and PKC-ζ homologous structures. Molecular docking predictions suggest that both ACPD and DNDA interact with both PKC-ι and PKC-ζ in a fairly similar manner. By the time molecular docking experiments of ICA-1T, ICA-1S, and ζ-Stat were performed for the PKC-ι, the complete crystal structure of PKC-ι was available. We identified an allosteric binding pocket located within the C-lobe of the kinase domain (Figures 3.10 and 3.11) which is primarily composed of residues conserved between PKC-ι and PKC-ζ. These data validated the identification of the druggable pocket as reported earlier by Pillai *et al.* using a PKC-ι homologous model with several other biochemical assays (99). In order to determine whether ATP influences the inhibitor binding, we compared molecular docking scores using ATP bound and unbound forms of PKC-ι for the affinities of inhibitors. These new molecular simulations with the solved PKC-ι structure suggested that the ICA-1S and ICA-1T have the potential to interact with PKC-ι in the presence and absence of ATP with moderate-high affinities. ICA-1T and ICA-1S showed binding scores of -7.8 and -7.3 kJ/mol in the absence of ATP for PKC-ι and the scores did not change significantly as a result of the presence of ATP as of -7.6 and -6.7, respectively. Interestingly, ζ-Stat also demonstrated a higher score for the used structure since the identified pocket has a conserved amino acid sequence between PKC-ι and PKC-ζ structures. Therefore, experimental analysis for the inhibitor specificities were essential to provide a solid support for these molecular docking predictions. Consequently, we conducted kinase activity assays for

28

aPKCs in the presence of these compounds using myelin basic protein (MBP), a known PKC substrate (151).
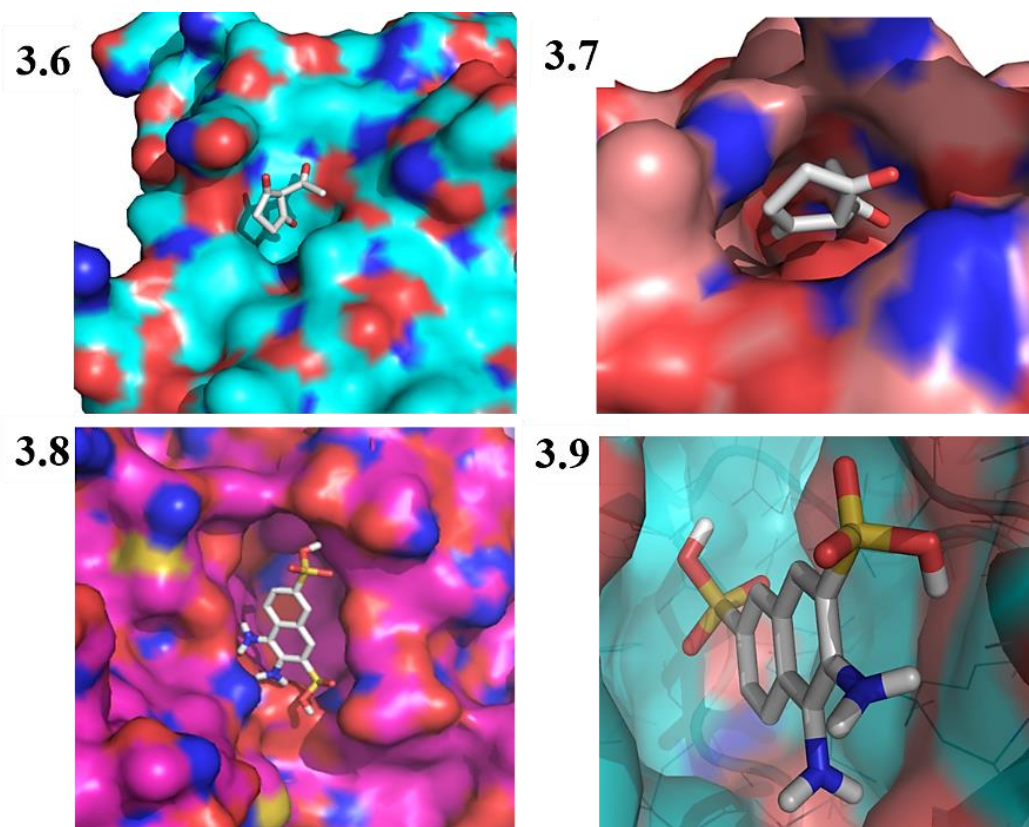
Figures 3.6-3.9. Molecular Docking of ACPD and DNDA with aPKCs. ACPD interacts with amino acid residues of 469-488 of the catalytic domain of PKC-ι (3.6) and amino acid residues of 265-290 of the catalytic domain of PKC-ζ (3.7). DNDA interacts with amino acid residues of 339-395 of the catalytic domain of PKC-ι (3.8) and amino acid residues of 337-393 of the catalytic domain of PKC-ζ (3.9).

3.10

3.11
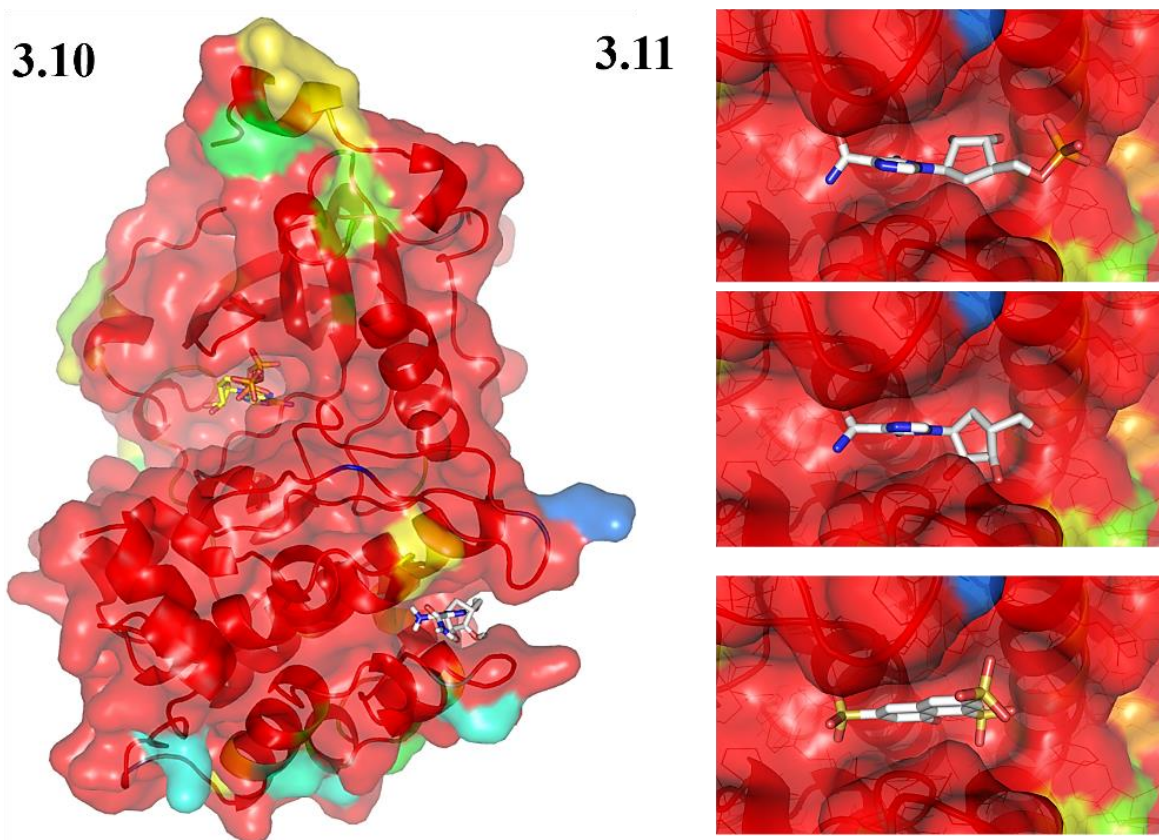
Figures 3.10-3.11: Molecular docking of ICA-1T, ICA-1S and ζ-Stat with PKC-ι. Fig. 3.10 shows the molecular surface of PKC-ι bound to ATP (3A8W) with docked ICA-1T. The molecular surface of residues that differ between PKC-ι and PKC-ζ are colored based on sequence similarity (using the Blosum62 scoring matrix). Blosum62 similarity values are: blue, 40–50, cyan, 50–60, green, 60–70, yellow, 70–90, orange and 90–100, red. Residues that are identical between PKC-ι and PKC-ζ are colored red. ATP is depicted as sticks with yellow for carbon, red for oxygen, blue for nitrogen. ICA-1T is depicted as sticks colored by element with white, red, and blue representing carbon, oxygen, and nitrogen respectively. Fig. 3.11 shows 3 enlarged pictures of lowest energy docking conformations of ICA-1T, ICA-1S, and ζ-Stat docked in the identified allosteric docking site, respectively.

3.2.2 Kinase activity assays

Experimental determination of specificities of these inhibitors was essential since PKC-ι and PKC-ζ has ~84% similarity among kinase domains (15). We conducted an *in-vitro* kinase activity assay for all five inhibitors to confirm virtual screening data. Kinase activities of ACPD, DNDA, ICA-

30

1T, ICA-1S and ζ-Stat (Figs. 3.12 and 3.13) were determined for a series of concentrations using recombinant active PKC-ι or PKC-ζ in the presence of MBP. Both ACPD and DNDA demonstrated significant inhibitions for both PKC-ι and PKC-ζ under all tested concentrations. Inhibition reached close to the maximum values approximately at 2.5 µM and did not change significantly thereafter. Nevertheless, the highest inhibitions were recorded at their 10 µM solutions; ACPD inhibited PKC-ι by 44% ($P \leq 0.05$) and PKC-ζ by 41% ($P \leq 0.05$) while DNDA inhibited PKC-ι by 38% ($P \leq 0.05$) and PKC-ζ by 29% ($P \leq 0.05$).

The specificity of ICA-1T was previously reported as inhibiting only PKC-ι without affecting other PKC isoforms (99). We tested the nucleoside analog of ICA-1T (ICA-1S) for the first time, which also shows a significant specificity towards the same allosteric site of PKC-ι. Additionally, the kinase activity shows that ζ-Stat is specific to PKC-ζ only, which agrees with the molecular docking predictions even though it used a homology model for PKC-ζ. Both ICA-1S and ICA-1T showed a significant inhibition of PKC-ι >60% ($P \leq 0.05$) at approximately 5 µM levels but resulting in only ~10% inhibition of PKC-ζ at 20 µM. On the other hand, ζ-Stat showed only 13% inhibition of PKC-ι at 20 µM, but 51% ($P \leq 0.05$) inhibition of PKC-ζ at 5 µM. This confirms the specificities we found for ICA-1T, ICA-1S and ζ-Stat through molecular docking.

3.12

3.13
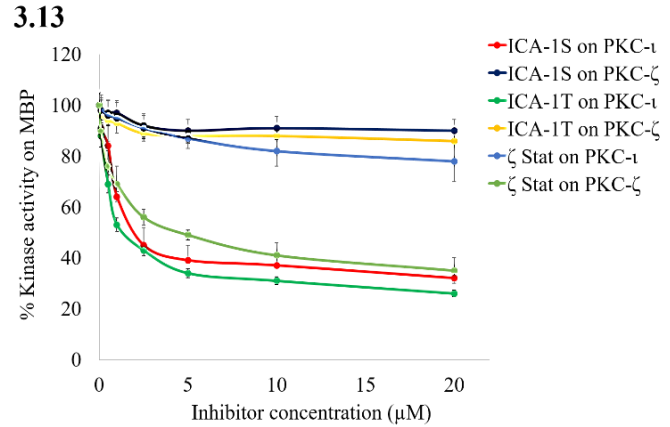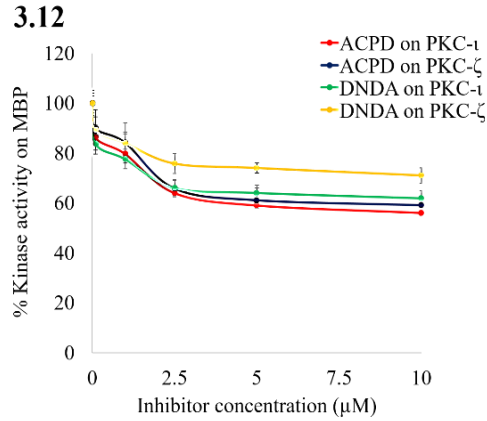
Figures 3.12-3.13: Effects of ACPD, DNDA, ICA-1T, ICA-1S and ζ-Stat on PKC-ι and PKC-ζ kinase activity. Fig. 3.12 summarizes the effects of ACPD and DNDA while Figure 3.13 summarizes the effects of ICA-1T, ICA-1S and ζ-Stat on recombinant active PKC-ζ or PKC-ι. The recombinant proteins were incubated with myelin basic protein (MBP) in the presence or absence of inhibitors (0.1- 10/20 µM) and percentage kinase activity was plotted against inhibitor concentration. Experiments (*N*=3) were performed for each experiment and mean ± SD are plotted.

3.2.3 Dose curves of ACPD, DNDA, ICA-1S, ICA-1T and ζ-Stat on normal melanocyte cell lines and melanoma cell lines

We first determined the dose curves for ACPD and DNDA since they target both aPKC isoforms. The effects of ACPD and DNDA on cell proliferation of normal and malignant cell lines over a wide range of concentration were tested. Both ACPD and DNDA did not show a significant inhibition for MEL-F-NEO normal melanocyte cells (Fig. 3.14), but significantly decreased cell proliferation of SK-MEL-2 and MeWo upon increasing the concentrations (Fig. 3.15, 3.16, 3.17 and 3.18). ACPD decreased proliferation by 48% at 2.5 µM (*P*≤0.01) (Fig. 3.15) and DNDA decreased cell proliferation by 52% at 2.5 µM (*P*≤0.01) (Fig. 3.16) in the SK-MEL-2 cell line. ACPD decreased proliferation by 54% at 2.5 µM (*P*≤0.01) (Fig. 3.17) and DNDA decreased proliferation by 46% for 2.5 µM (*P*≤0.01) (Fig. 3.18) in the MeWo cell line. These results suggest that both aPKC specific ACPD and DNDA can effectively decrease melanoma cell proliferation

32

without effecting normal melanocytes. Based on these results the IC_{50} values of ACPD and DNDA for both drugs were found to be approximately 2.5 µM, the concentration used in later experiments.

ICA-1T showed no significant effect against MEL-F-NEO (Fig. 3.19) up to 5 µM, but had maximum inhibition of 22% ($P\leq0.05$) at 10 µM. Both ICA-1S and ζ-Stat showed significant inhibitions of MEL-F-NEO cells beyond 7.5 µM ($P\leq0.05$) as 37.7% ($P\leq0.05$) and 19.3% ($P\leq0.05$) at 10 µM, respectively. All inhibitors significantly decreased cell proliferation of SK-MEL-2 and MeWo at much lower concentrations. ICA-1T decreased proliferation by 53.1% for 1 µM ($P\leq0.01$) in SK-MEL-2 cells (Fig. 3.20), and 56.1% at 1 µM ($P\leq0.01$) in MeWo cells (Fig. 3.21). ICA-1S decreased proliferation by 46% at 2.5 µM ($P\leq0.01$) in SK-MEL-2 cells (Fig. 3.20) and 50.7% at 2.5 µM ($P\leq0.01$) for MeWo cells (Fig. 3.21). ζ-Stat decreased proliferation by 47.7% at 5 µM ($P\leq0.01$) in SK-MEL-2 cells (Fig. 3.20) and by 50.6% at 5 µM ($P\leq0.01$) for MeWo cells (Fig. 3.21). These results suggest that ICA-1T, ICA-1S and ζ-Stat can effectively be used to decrease melanoma cell population at lower concentrations at which they do not significantly effect on normal melanocytes. IC_{50} values of ICA-1T, ICA-1S and ζ-Stat were found at approximately 1 µM, 2.5 µM and 5 µM, respectively, for both cell lines. Later, we used these concentrations in experiments as the testing concentrations.
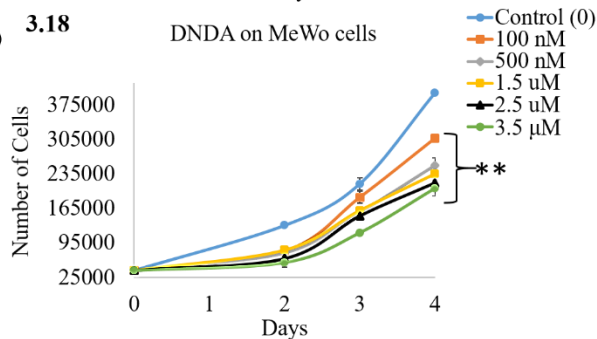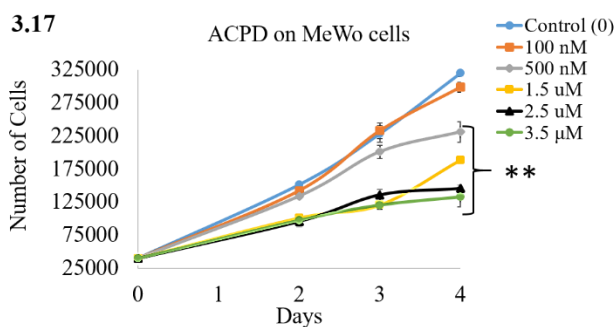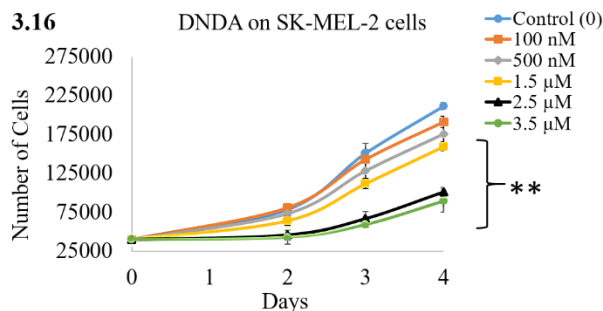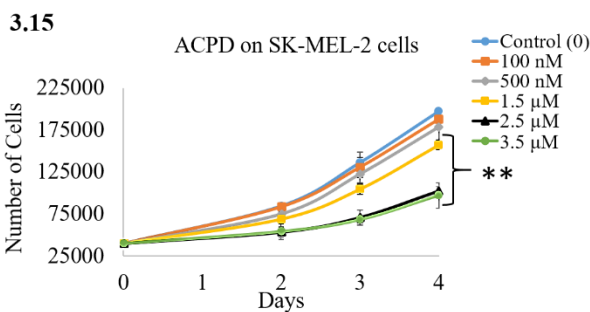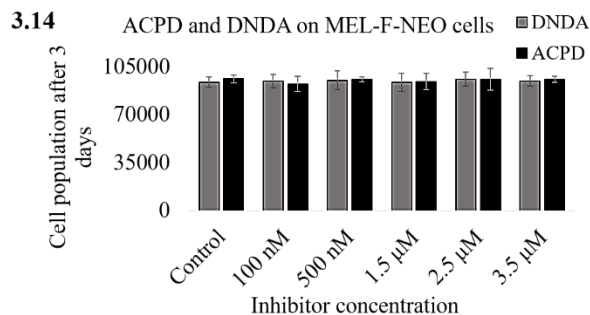
Figures 3.14-3.18. Effects of ACPD and DNDA on cell proliferation of normal melanocytes and malignant melanoma cells. Results depict the effect of ACPD and DNDA on PCS-200-013 (3.14), ACPD on SK-MEL-2 (3.15), DNDA on SK-MEL-2 (3.16), ACPD on MeWo (3.17) and DNDA on MeWo (3.18). Approximately 4×10^4 cells were cultured in T25 flasks and treated with either equal volume of sterile water (control) or ACPD or DNDA (0.1- 3.5 µM). Additional doses of sterile water or ACPD or DNDA were supplied every 24 h during a 3 day incubation period. Subsequently, cells were lifted and counted. Cell count for PCS-200-013 cells were only obtained for 3 days due to longer doubling time. The two malignant cell lines (SK-MEL-2 and MeWo) were quantified by counting the viable cells at 24 hour intervals. Experiments (N=3) were performed for each cell line and mean ± SD are plotted. Statistical significance is indicated by asterisks as *P< 0.05 and **P < 0.01.

3.19

Dose response of MEL-F-NEO cells

3.20

Dose response of SK-MEL-2 cells

3.21

Dose response of MeWo cells
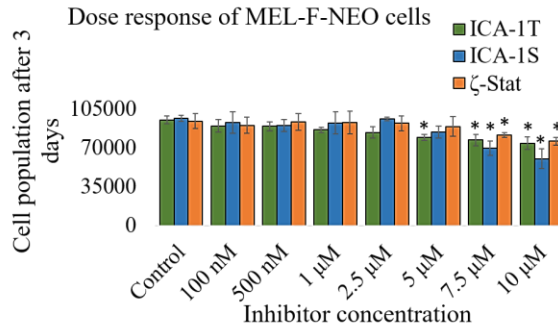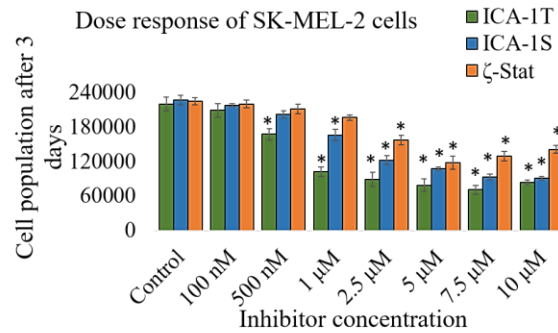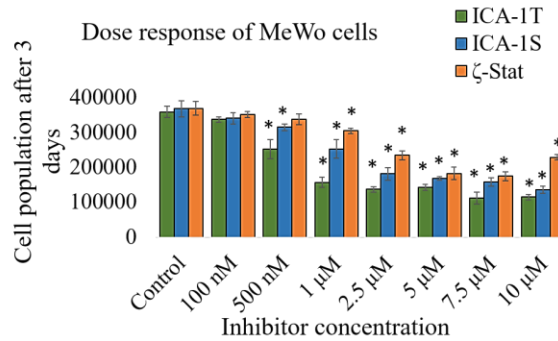
Figures 3.19-3.21: The effects of ICA-1T, ICA-1S and ζ-stat on cell proliferation and cell viability for melanoma and normal melanocyte cells. Results depict the effect of inhibitors on MEL-F-NEO (Fig. 3.19), SK-MEL-2 (Fig. 3.20) and MeWo (Fig. 3.21) cell proliferation based on cell proliferation assay. Approximately 4×10^4 cells were cultured in T25 flasks and treated with either equal volume of sterile water (control) or inhibitors (0.1- 10 µM). Additional doses of sterile water or inhibitors were supplied every 24 h during a 3 day incubation period. Subsequently, cells were lifted and counted. Experiments (*N*=3) were performed for each cell line and mean ± SD are plotted. Statistical significance is indicated by asterisks as *$P< 0.05$ and **$P < 0.01$.

35

3.2.4 WST-1 assays for cellular toxicity effects of ACPD, DNDA, ICA-1S, ICA-1T and
ζ-Stat

4-[3-(4-Iodophenyl)-2-(4-nitropheny))-2H-5-tetrazolio]-1,3-benzene disulfonate (WST-1) assay was performed to determine the *in-vitro* cytotoxicity of the inhibitors. The absorbancy at 450 nm is directly proportional to the number of viable cells present. Viable cells produce a water-soluble formazan with WST-1 as a result of their mitochondrial dehydrogenase activity.

aPKC inhibitors ACPD and DNDA did not show a significant effect on normal melanocyte cells (Fig. 3.22), but DNDA showed relatively high toxicity against both cell lines at its IC_{50} value   (Fig. 3.23 and 3.24).

In terms of PKC-ι specific ICA-1T and ICA-1S along with PKC-ζ specific ζ-Stat, none of the inhibitors showed significant cytotoxicity against normal melanocytes (Figure 3.25). ICA-1T showed a significant cytotoxicity towards both melanoma cell lines, followed by ICA-1S. ζ-Stat did not show significant cytotoxicity any of the cell lines (Fig. 3.26 and 3.27).

These results indicate that all inhibitors appeared cytostatic more than being cytotoxic during the tested time ranges, thereby retarding melanoma cell growth and proliferation. This could indicate that melanoma cells undergo a phase where their growth and differentiation stops before their apoptotic stimulation as a result of aPKC inhibition.
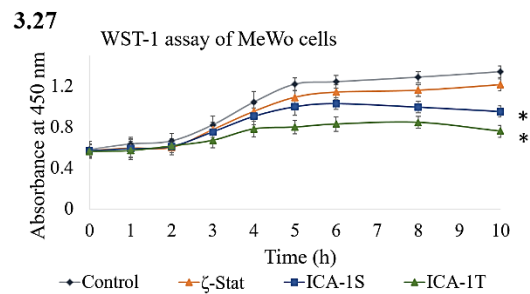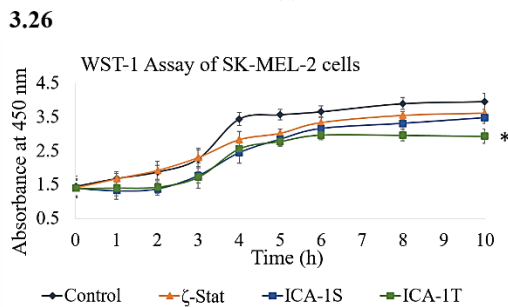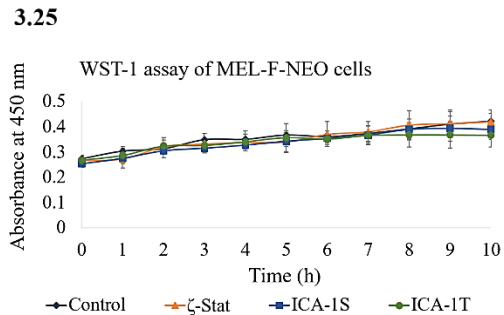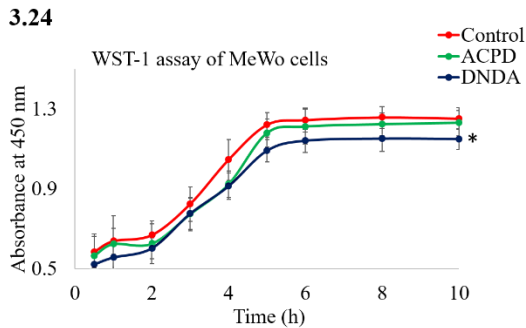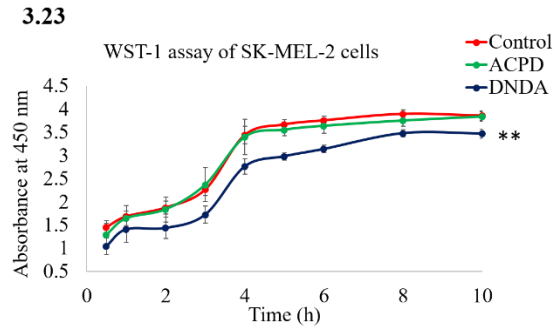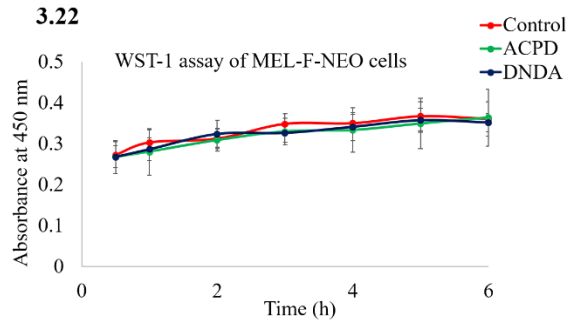
Figures 3.22-3.27: The effects of aPKC inhibitors (ACPD, DNDA, ICA-1T, ICA-1S and ζ-stat) on cytotoxicity for melanoma and normal melanocyte cells. Cytotoxicity of aPKC inhibitors was measured using WST-1 assay and the results indicate as ACPD and DNDA for MEL-F-NEO (Fig. 3.22), SK-MEL-2 (Fig. 3.23) and MeWo (Fig. 3.24) cells. Similarly, cytotoxicity of ICA-1T, ICA-1S and ζ-Stat indicates for MEL-F-NEO (Fig. 3.25), SK-MEL-2 (Fig. 3.26) and MeWo (Fig. 3.27) cells. The absorbance at 450 nm is due to production of water soluble formazan and was measured as a function of time. The absorbance is directly proportional to the number of cells. Experimental concentrations in WST-1 assay for ACPD, DNDA, ICA-1T, ICA-1S and ζ-Stat were 2.5 μM, 2.5 μM, 1 μM, 2.5 μM and 5 μM, respectively for all three cell lines. The absorbance at 450 nm against time is plotted. Experiments (N=3) were performed for each cell line and mean ± SD are plotted. Statistical significance is indicated by asterisk as *P< 0.05 and **P < 0.01.

37

3.3 Summary

The computational screening and kinase activity assay data show that ACPD and DNDA are specific inhibitors of aPKCs. ACPD showed the same effect as an inhibitor for both PKC-ζ and PKC-ι in a relative sense. DNDA showed a better action on PKC-ι over PKC-ζ.

Our virtual screening and kinase activity assays confirmed the specificity of ICA-1T and ICA-1S for PKC-ι and ζ-Stat specificity on PKC-ζ. We also were able to confirm the presence of a potentially druggable allosteric site in the structure of PKC-ι using a solved crystal structure of PKC-ι, which was initially predicted by Pillai, *et al.* using a PKC-ι homology model (99). This site, within the C-lobe of the kinase domain, is framed by solvent exposed residues of helices αF-αI and the activation segment. ICA-1T and ICA-1S were predicted to interact with this site with higher-moderate affinity based on molecular docking. Combinations of drugs targeting the ATP binding site and allosteric sites would be expected to more effectively inhibit cancer cell growth.

Assessing the cell viability and cytotoxicity of malignant and normal cells for inhibitors were crucial, considering our ultimate intent was to determine if the inhibitors had potential as therapeutic drugs. All five inhibitors were non-toxic to normal melanocytes. Overall, all five inhibitors showed more cytostatic properties on melanoma cells with a mild toxicity provided by DNDA, ICA-1T and ICA-1S at their IC_{50} values. The results show that these inhibitors are effective in arresting malignant melanoma cells in terms of their growth, differentiation and proliferation before they induce apoptosis. This confirms that malignant melanoma cells are highly dependent on aPKCs to remain viable, supporting our previous data that both melanoma cell lines overexpress aPKCs compared to the undetectable PKC-ι and low levels of PKC-ζ in normal melanocytes (Fig. 2.1).

CHAPTER 4

ATYPICAL PKCS PROMOTE CELL DIFFERENTIATION, SURVIVAL OF MELANOMA CELLS VIA NF-κB AND PI3K/AKT PATHWAYS

4.1 Introduction

Phosphatidylinositol 3-kinase and Protein Kinase B (PI3K/AKT) and nuclear factor kappa-light-chain-enhancer of activated B (NF-κB) pathways are frequently hyper-activated in various carcinomas thereby promoting cellular growth, differentiation and survival (152). As we discussed in Chapter 1, overexpression of aPKCs is often associated with anti-apoptotic effects in many cancers.

The NF-κB transcription factor family was discovered in 1986. It often plays a complex and essential role in inflammation and immune response. NF-κB is also well-known for human cancer initiation, progression and poor prognosis (153,154). The NF-κB family consists of five members; p65 (RelA), RelB, c-Rel, NF-κB1 (p105/p50) and NF-κB2 (p100/p52) (152,155–158). These subunits can form a variety of homodimers or heterodimers, which are essential for NF-κB activation, crosstalk and translocation to the nucleus. Heterodimer between p65 (RelA) and p50 NF-κB subunits is the most important complex in the NF-κB family. In many quiescent cells these dimers are bound to a family of inhibitory proteins molecules called "inhibitors of NF-kB" (IκB)

(157). IκB proteins contain ankyrin repeats, which bind with the DNA binding domains of the NF-κB transcription factors making them transcriptionally inactive (157).

Both the canonical and non-canonical NF-κB pathways are upregulated in many carcinomas. Activating mutations in NF-κB genes were first reported in B-cell lymphoid malignancies (159). Mutations of upstream signaling molecules such as RAS superfamily, epidermal growth factor receptor (EGFR) and human epidermal growth factor receptor 2 (HER2) often lead to hyperactivation of NF-κB (160). Additionally, continuous release of cytokines by macrophages in the tumor microenvironment also leads to an upregulation of NF-κB (157). Outcomes of such hyperactivations of NF-κB strictly depends on the cell type or the tumor microenvironment. The human immune system can play a dual role by being either tumor-promotive, which leads to more aggressive tumors, or host-protective. Upregulated NF-κB promotes cell survival by inhibiting apoptosis through stimulating the transcription of anti-apoptotic genes (161). This provides support to survive the physiological stress during inflammation, thereby playing an important role in the initiation of tumors (157,162). NF-κB also upregulates the transcription of proliferation regulating genes such as cyclin D1 and C-MYC (163,164). Additionally, NF-κB upregulates metastasis by altering cellular adhesion molecules and matrix metalloproteinases. NF-κB also upregulates the VEGF dependent angiogenesis (165). The tumor microenvironment of solid tumors often contain elevated levels of inflammatory cytokines and hypoxic conditions, which can elevate the activation and nuclear translocation of NF-κB (158,166). NF-κB can also induce the expression of activation-induced cytodine deaminase (AID) and APOBEC ("apolipoprotein B mRNA editing enzyme, catalytic polypeptide-like") proteins. The AID/APOBEC family is an important contributor to cancer development and clonal evolution of cancer by inducing collateral genomic damage (154).

40

On the other hand the PI3K/AKT pathway is also an actively pursued therapeutic target in oncology. Upregulation of PI3K/AKT pathway appears to be characteristic of many aggressive cancers, which activates numerous survival, growth, metabolic and metastatic functions. Once activated, PI3K catalyzes the phosphorylation of phosphatidylinositol 4,5-bisphosphate (PIP2) to produce phosphatidylinositol (3,4,5)-trisphosphate (PIP3). PIP3 activates intracellular signaling through its binding to pleckstrin homology (PH) domains of many signaling proteins, including AKT (167,168). Activated AKT phosphorylates and activates many oncogenic features within cancer cells. The mammalian target of rapamycin (mTOR) is a major downstream signaling protein, which is activated by AKT. mTOR is involved in protein translation via the eukaryotic translation initiation factor 4E (eIF4E) complex and ribosomal protein S6 kinase (S6K). Both mTOR and S6K are hyperactivated in prostate cancer due to upregulated AKT (169). AKT promotes cellular survival by inhibiting pro apoptotic Bcl-2 family members such as BAD and BAX (170). Furthermore, AKT deactivates the tumor suppressor forkhead box protein O1 (FOXO1).

PI3K/AKT pathway activates the NF-κB pathway, wherein aPKCs play a role in releasing NF-κB complex to translocate to the nucleus and promote cellular growth and survival. Win *et al*. reported that PKC-ζ actively upregulates the activation of NF-κB nuclei translocation thereby inducing cancer cell survival in prostate cancer cells (80). In addition, PI3K stimulates IκB kinase (IKKα/β) through activation of AKT by phosphorylation at S473 or S463, which ultimately stimulates translocation of NF-κB complex into the nucleus, heightening cell survival (171). Phosphatase and tensin homolog (PTEN) regulates the levels of PI3K. Phosphorylation at S380 leads to the inactivation of PTEN, thereby increasing the levels of PI3K followed by enhancement in phosphorylated AKT (S473/S463).

Here, we present our data for the analysis of PI3K/AKT and the NF-κB pathways. We have tested how NF-κB and AKT are affected by aPKC inhibition during five aPKC inhibitor applications. We tested the levels of PTEN, phosphorylated PTEN (S380), phosphorylated AKT (S473), IKBα and phosphorylated IKBα, phosphorylated IKKα/β (S176/180), NF-κB p65 in cytoplasm and in nucleus for SK-MEL-2 and MeWo melanoma cell lines. Our data indicates that inhibition of PKC-ι and PKC-ζ significantly decreased the levels of phosphorylated PTEN and phosphorylated AKT compared to control samples (142). This indicates that PKC-ζ and PKC-ι may upregulate the PI3K/AKT pathway to induce cellular survival of melanoma cells. Additionally, we tested the levels of NF-κB translocation by separating the nuclear extracts from the cell lysates to observe how NF-κB activation process alters upon aPKC inhibition in relation to the levels of inhibitor of kappa B (IκB), phosphorylated IκB (S32) and phosphorylated IKKα/β (S176/180). Our data also demonstrate the effects of tumor necrosis factor alpha (TNF-α) stimulation on the expression of aPKCs in relation to PI3K/AKT mediated NF-κB. TNF-α is a cytokine, involved in the early phase of acute inflammation by activating NF-κB pathway. This information is important for the proper understanding of the aPKC role in melanoma progression.

4.2 Results

4.2.1 Western blot analysis of AKT and the NF-κB pathways post aPKC specific inhibitor treatment

We started the analysis with a more general approach by testing ACPD and DNDA on normal melanocytes against melanoma cell lines since ACPD and DNDA specifically bind to both aPKCs and demonstrated inhibitive properties (143). Western blots were performed to investigate the

42

effects of ACPD and DNDA on the expression of aPKCs, apoptotic markers, AKT and NF-κB on malignant melanoma cell lines (Fig. 4.1 and 4.2). IC_{50} concentration of ACPD significantly reduced the PKC-ι level by 43% and by 31% of phosphorylated PKC-ι (T555) in SK-MEL-2 cell line and by 46% of PKC-ι and 26% of phospho PKC-ι (T555) in MeWo cells. DNDA significantly decreased the levels of PKC-ι by 52%, phospho PKC-ι (T555) by 33% in SK-MEL-2 and by 27% of PKC-ι and phospho PKC-ι (T555) by 20% in MeWo cells. Also, ACPD significantly reduced the PKC-ζ level by 42% and by 29% of phospho PKC-ζ (T410) in SK-MEL-2 cell line and by 42% of PKC-ζ and 23% of phospho PKC-ζ (T410) in MeWo cells. DNDA significantly reduced the levels of PKC-ζ by 33%, phospho PKC-ζ (T410) by only 17% in SK-MEL-2 and by 60% of PKC-ζ and phospho PKC-ζ (T410) by 29% in MeWo (143).

In terms of apoptotic markers, treatments of the inhibitors led to significantly increased Caspase-3 levels (26% and 17%) in ACPD treated SK-MEL-2 and MeWo cells, respectively. Caspase-3 levels significantly increased by 32% and 39% in DNDA treated SK-MEL-2 and MeWo cells, respectively. Poly (ADP-ribose) polymerase (PARP) levels significantly decreased by 33% and by 24% in ACPD treated SK-MEL-2 and MeWo cells, respectively, while cleaved-PARP levels significantly increased by 14% and 18%, respectively. In DNDA treated samples, PARP levels significantly decreased by 12% and by 9% in SK-MEL-2 and MeWo cells, respectively, while cleaved-PARP levels significantly increased by 16% and 10%, respectively. Similarly, Bcl-2 levels significantly decreased by 13% and by 25% in ACPD treated SK-MEL-2 and MeWo cells, respectively, while in DNDA treated cells Bcl-2 levels decreased by 7% and by 32% in SK-MEL-2 and MeWo cells, respectively. PTEN levels significantly increased by 44% and 55% in ACPD treated SK-MEL-2 and MeWo cells, respectively, compared to 68% and 48% increases in DNDA treated samples while respective phospho AKT (S473) levels showed a reduction. However, NF-

43

κB p65 levels were significantly heightened by 31% and 69% in ACPD treated SK-MEL-2 and MeWo cells, and there were 49% and 89% increases in DNDA treated samples. All values (percent) were calculated and compared to their respective control in WB (Fig 4.2; densitometry analysis) and significance was indicated as $P \leq 0.05$. β-actin was used as the internal control to ensure that equal amounts of proteins were loaded in each lane in the sodium dodecyl sulfate–polyacrylamide gel electrophoresis (SDS-PAGE) (143).

To establish the specific roles of both PKC-ι and PKC-ζ on melanoma progression, we subsequently used ICA-1T, ICA-1S and ζ-Stat to specifically inhibit PKC-ι and PKC-ζ in melanoma cells. A detailed analysis was conducted for aPKC expression, aPKC phosphorylation, activation of AKT and NF-κB pathway through Western blot analysis. As shown in Figure 4.3, Western blots revealed that both ICA-1T and ICA-1S significantly reduced total and phosphorylated PKC-ι while having no effect on PKC-ζ. ζ-Stat showed a significant diminution of phosphorylated and total PKC-ζ levels. Since all inhibitors significantly reduce melanoma cell proliferation, we tested the potential of the inhibitors on inducing the apoptosis. Caspase-3 and cleaved-PARP levels were significantly increased and Bcl-2 and PARP levels were significantly diminished upon inhibitor treatments. These results reconfirmed the apoptotic stimulation upon inhibition of PKC-ι and PKC-ζ using specific inhibitors. We also tested the levels of β-catenin, phosphorylated PTEN (S380), phosphorylated AKT (S473), IKBα and phosphorylated IKBα, phosphorylated IKKα/β (S176/180), NF-κB p65 in cytoplasm and in nucleus. β-catenin levels did not change significantly while phospho PTEN, phospho AKT, phospho IKBα, phospho IKKα/β and nucleic NF-κB p65 significantly decreased and levels of IKBα and cytoplasmic NF-κB p65 significantly increased as a result of the three inhibitors. Figure 4.4 shows the densitometry analysis for said markers for ICA-1T, ICA-1S and ζ-Stat treatments.

44

Additionally, we tested the effects of TNF-α and TGFβ stimulation on aPKC expression in relation to AKT and NF-κB pathways. As shown in Figure 4.5 and 4.6, we found that protein levels and the degree of phosphorylation significantly increased for both aPKCs in the presence of TNF-α, thereby significantly heightening phosphorylation on PTEN (S380), AKT (S473), IKKα/β (S176/180), IKBα (S32) and Vimentin (S39) which resulted in enhancing Bcl-2, NF-κB translocation. Furthermore, PKC-ι was upregulated as a result of TGFβ treatments and no significant change was observed for PKC-ζ levels for TGFβ treatments. This indicates that TNF-α upregulate the aPKCs in relation to NF-κB and AKT pathways which result in cellular survival and rapid growth in melanoma cells.
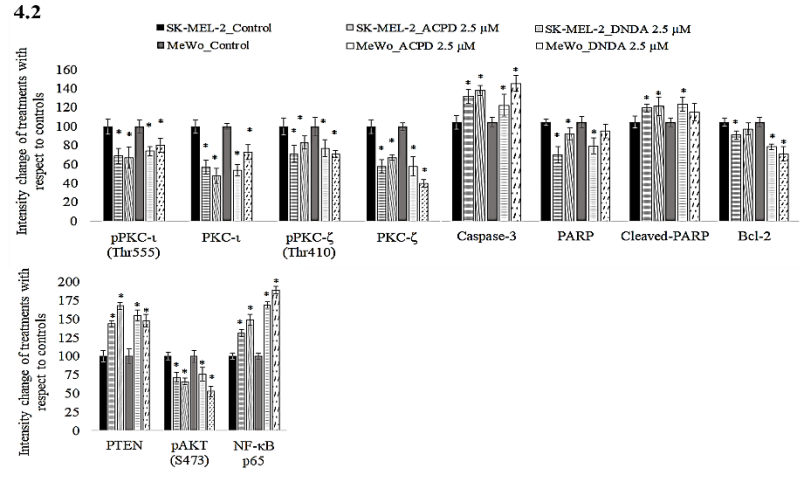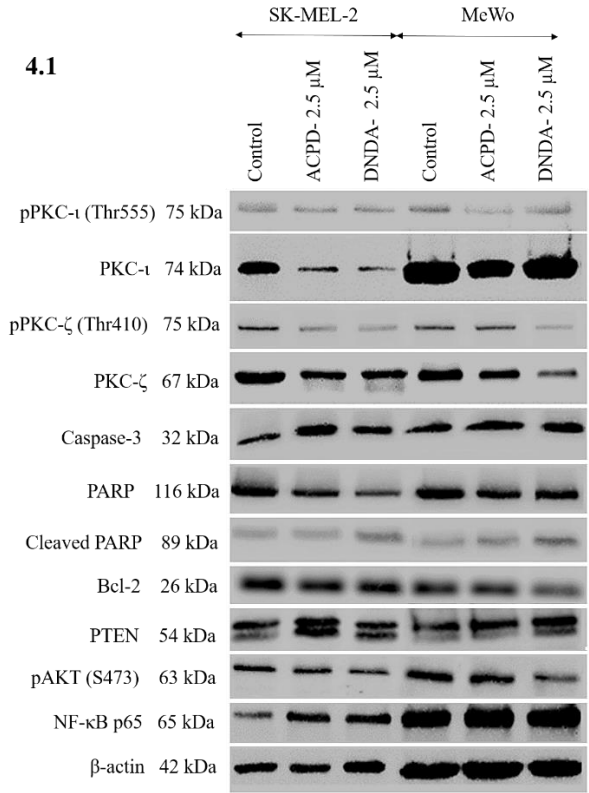
Figures 4.1-4.2. Western blots of the effects of ACPD and DNDA on aPKC expression and apoptosis on malignant melanoma cells. Fig. 4.1 represents the expression of phosphorylated PKC-ι, total PKC-ι, phosphorylated PKC-ζ, total PKC-ζ and apoptotic markers (Caspase-3, cleaved PARP, total PARP and Bcl-2) for the ACPD and DNDA (2.5 µM) treated malignant melanoma cell lines (SK-MEL-2 and MeWo) after the end of the 3rd day of treatments with respect to their controls. Fig. 4.2 indicates the densitometry values of 4.1 Western blots which are shown as the percentage change of the treated samples with respect to their controls and Mean ± SD are plotted. 40 µg of protein was loaded in to each well and β-actin was used as the loading control in each Western blot. Experiments (*N*=3) were performed.
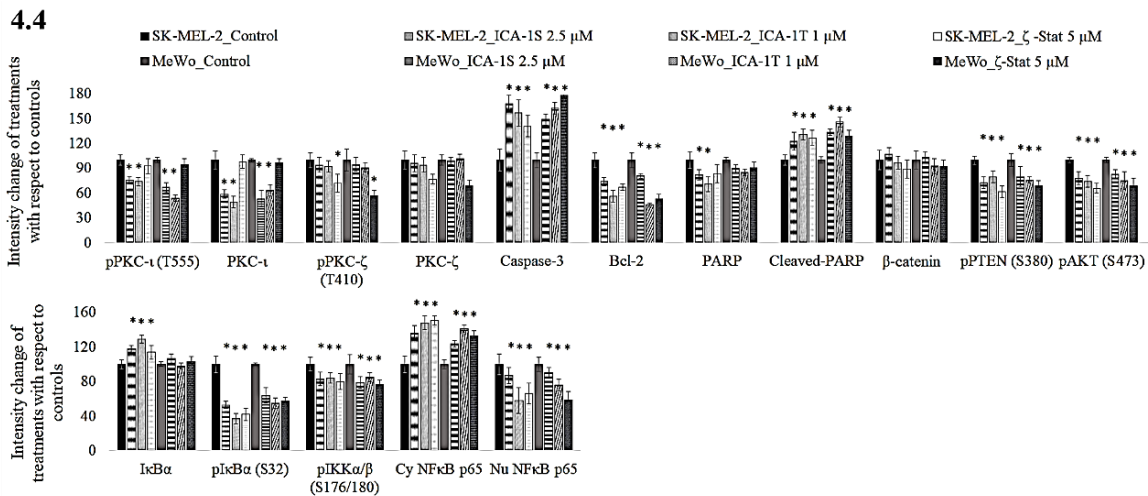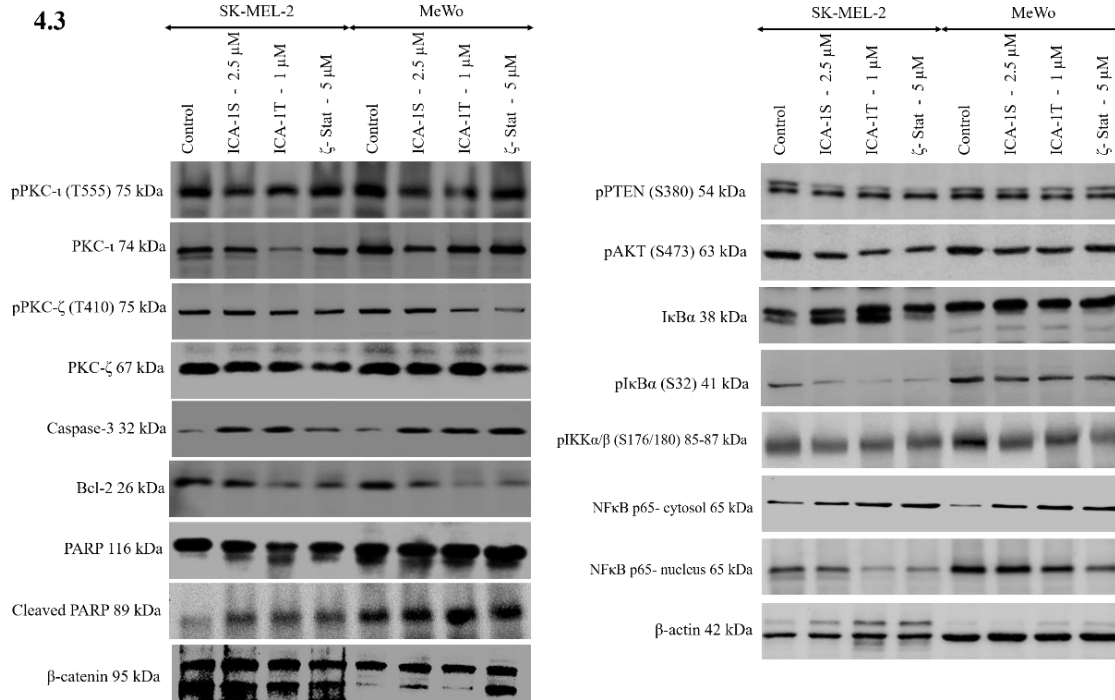
Figures 4.3-4.4: Effect of ICA-1S, ICA-1T and ζ-Stat on aPKC expression, apoptosis, and signaling pathways related to NF-κB and PI3K/AKT pathways in melanoma cells. Expression of the protein levels of phosphorylated PKC-ι, total PKC-ι, phosphorylated PKC-ζ, total PKC-ζ, Caspase-3, cleaved PARP, total PARP, Bcl-2, β-catenin, phosphorylated PTEN, RhoA, phosphorylated AKT and NF-κB p65, IκB, phosphorylated IκB and phosphorylated IKKα/β for the inhibitor treatments (2.5 µM of ICA-1S, 1 µM of ICA-1T and 5 µM of ζ-Stat) are shown in Fig. 4.3. 40-80 µg of protein was loaded in to each well and β-actin was used as the loading control in each Western blot. Fig. 4.4 represents the densitometry values for Western blots in Fig. 4.3. Experiments (*N*=3) were performed in each trial and representative bands are shown.

47
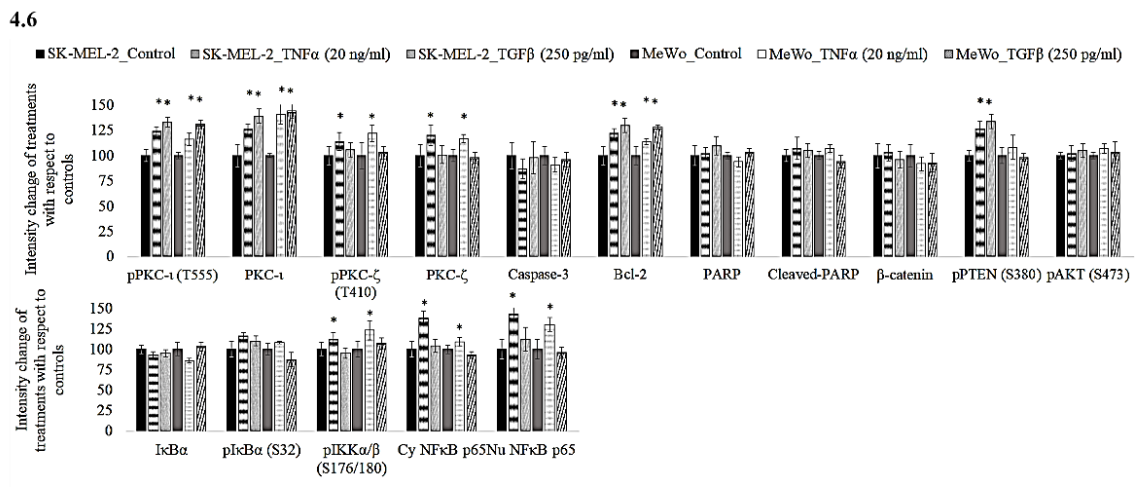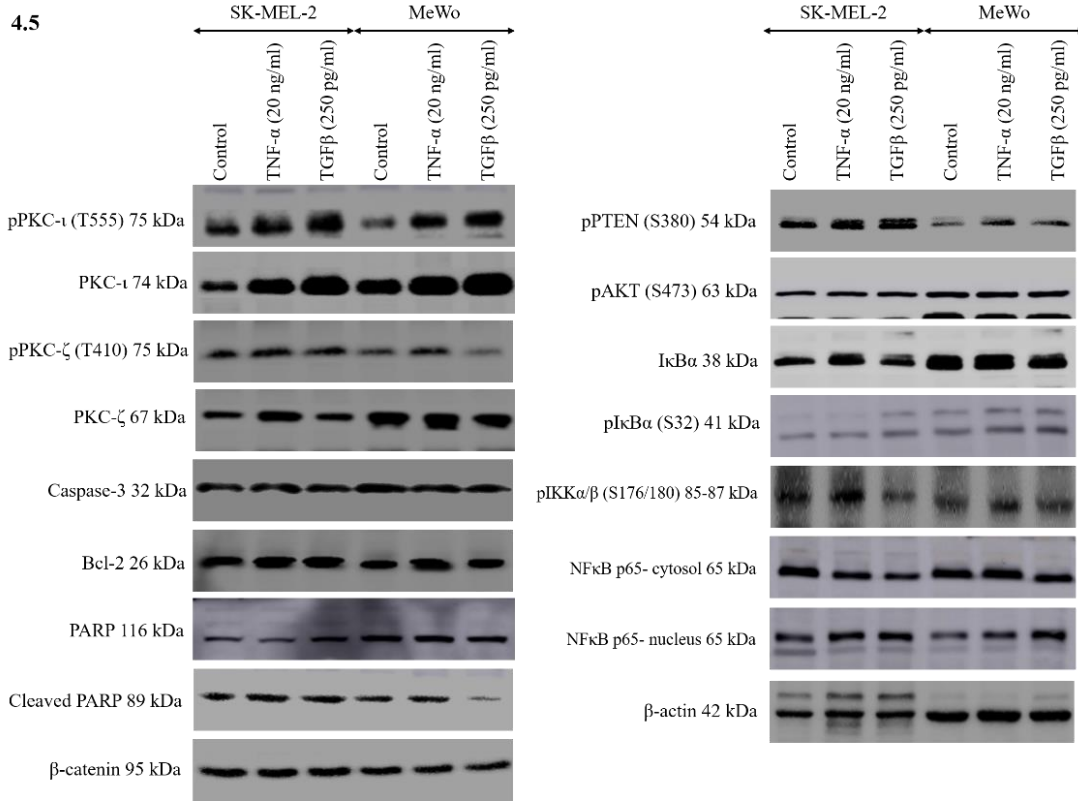
Figures 4.5-4.6: Effect of TNF-α and TGFβ on aPKC expression, apoptosis, and signaling pathways related to NF-κB and PI3K/AKT pathways in melanoma cells. Expression of the protein levels of phosphorylated PKC-ι, total PKC-ι, phosphorylated PKC-ζ, total PKC-ζ, Caspase-3, cleaved PARP, total PARP, Bcl-2, β-catenin, phosphorylated PTEN, RhoA, phosphorylated AKT and NF-κB p65, IκB, phosphorylated IκB and phosphorylated IKKα/β for the the TNF-α (20 ng/ml) and TGFβ (250 pg/ml) treatments are shown in Fig. 4.5 for malignant melanoma cell lines (SK-MEL-2 and MeWo). 40-80 µg of protein was loaded in to each well and β-actin was used as the loading control in each Western blot. Fig. 4.6 represents the densitometry values for Western blots in Fig. 4.5. Experiments (*N*=3) were performed in each trial and representative bands are shown.

4.3 Summary

Our Western blots data revealed that both ICA-1T and ICA-1S significantly reduced total and phosphorylated PKC-ι while having no effect on PKC-ζ. ζ-Stat showed a significant diminution of phosphorylated and total PKC-ζ levels without showing a significant effect of PKC-ι. On the other hand, both ACPD and DNDA showed specificity towards both aPKC isoforms. These data confirmed the kinase activity assay data and molecular docking predictions we reported in the previous chapter. As we demonstrated in Chapter 3, all inhibitors significantly reduce melanoma cell proliferation without showing a significant effect on normal melanocytes at IC_{50} concentrations. Therefore, here we tested the potential of the inhibitors to induce the apoptosis at the same concentrations.

As demonstrated in Figures 4.1 and 4.3, cleaved-PARP levels were significantly increased while Bcl-2 and PARP levels were significantly diminished upon inhibitor treatments. Increase in Caspase-3, increase in PARP cleavage, and decrease in Bcl-2 all indicate apoptosis stimulation (172–175). Increase in Caspase-3 levels is not always a direct indication of inducing apoptosis due to the tight binding of cleaved Caspase-3 with X-linked inhibitor of apoptosis protein (XIAP). XIAP undergoes auto-ubiquitination, but this process delays apoptosis until all XIAP is removed (176). Owing to this, we also tested direct PARP and cleaved PARP levels because PARP is a known downstream target for Caspase-3. PARP cleaves more upon inducing the apoptosis. We also tested Bcl-2 levels since it inhibits Caspase activity by preventing Cytochrome c release from the mitochondria and/or by binding to the apoptosis-activating factor (APAF-1) (177). All five inhibitor treatments depicted an increase in apoptotic activity in both SK-MEL-2 and MeWo cell lines. This data confirms that aPKCs have an anti-apoptotic effect.

One major anti-apoptotic pathway is NF-κB activation, which entails aPKC releasing NF-κB and NF-κB translocates to the nucleus to promote cell survival (178). Interestingly, aPKC inhibition increased the NF-κB production in both cells even though we observed an apoptotic stimulation. This was evident in the cytosolic NF-κB levels shown in Figures 4.3 and 4.4. But data shows a downregulation of AKT pathway which was evident from elevated levels of PTEN and lower levels of phospho AKT (S473), which agreed with apoptotic stimulation upon aPKC inhibition. In order to investigate further, we tested the effects of ICA-1T, ICA-1S and ζ-Stat on SK-MEL-2 and MeWo cell lines which provided specific inhibition of PKC-ι with ICA-1T and ICA-1S and the PKC-ζ inhibition with ζ-Stat. To interpret the fate of NF-κB pathway, we separated cytosol and nuclei and analyzed them separately. Figure 4.3 demonstrated that inhibition of PKC-ι and PKC-ζ expressively decreased the levels of phosphorylated PTEN and phosphorylated AKT (142). This specifies that PKC-ζ and PKC-ι may upregulate the PI3K/AKT pathway to induce cellular survival of melanoma cells. Our data demonstrated that aPKCs play a role in releasing NF-κB to translocate to the nucleus and promote cell survival in melanoma cells. PI3K stimulates IKKα/β through activation of AKT by phosphorylation at S473, which ultimately stimulates translocation of NF-κB complex into the nucleus, boosting cell survival (171). PTEN regulates the levels of PI3K. Phosphorylation at S380 leads to the inactivation of PTEN, thereby increasing the levels of PI3K followed by enhancement in phospho-AKT. Inhibition of PKC-ι and PKC-ζ significantly decreased the levels of phospho-PTEN and phospho-AKT but we still found increases in NF-κB p65 levels in the cytosol after inhibiting both aPKCs. This may seem illogical, but previous studies have shown that expression of NF-κB p65 has a corresponding increase in IκB, resulting in an auto-regulatory loop (171). Moreover, negative feedback is not inhibiting upstream signaling for NF-κB translocation because translocation has been inhibited downstream, resulting in more NF-

κB production. Knowing this, we tested the levels of NF-κB translocation by separating the nuclear extracts from the cell lysates and found that NF-κB levels in the nuclei decreased upon aPKC inhibition. This suggested that translocation of activated NF-κB in to nuclei is inhibited as a result of inhibition of aPKCs. Furthermore, we also found that aPKC inhibition increased the levels of IκB while decreasing the levels of phosphorylated IκB (S32) and phosphorylated IKKα/β (S176/180), confirming that both PKC-ι and PKC-ζ play a role in phosphorylation of IKKα/β and IκB: increased levels of IκB therefore remain bound to NF-κB complex and prevent the translocation to the nucleus to promote cell survival. As summarized in Figure 4.7, our data also demonstrate the effects of TNF-α stimulation on the expression of aPKCs. TNF-α is a cytokine, involved in the early phase of acute inflammation by activating NF-κB. TNF-α stimulation significantly increased NF-κB levels in both cytosol and nuclei. Increased NF-κB production promotes increases in total and phosphorylated aPKCs and increased the levels of Bcl-2, which enhanced melanoma cell survival. We observed amplified levels of IκB and NF-κB, which together enhanced the phosphorylation of IκB due to the augmented levels of aPKCs. On the other hand, PI3K/AKT signaling can be diminished by inhibiting aPKCs via downregulation of NF-κB. These results confirm that both PKC-ζ and PKC-ι are rooted in cellular survival via NF-κB and PI3K/AKT pathways.

4.7
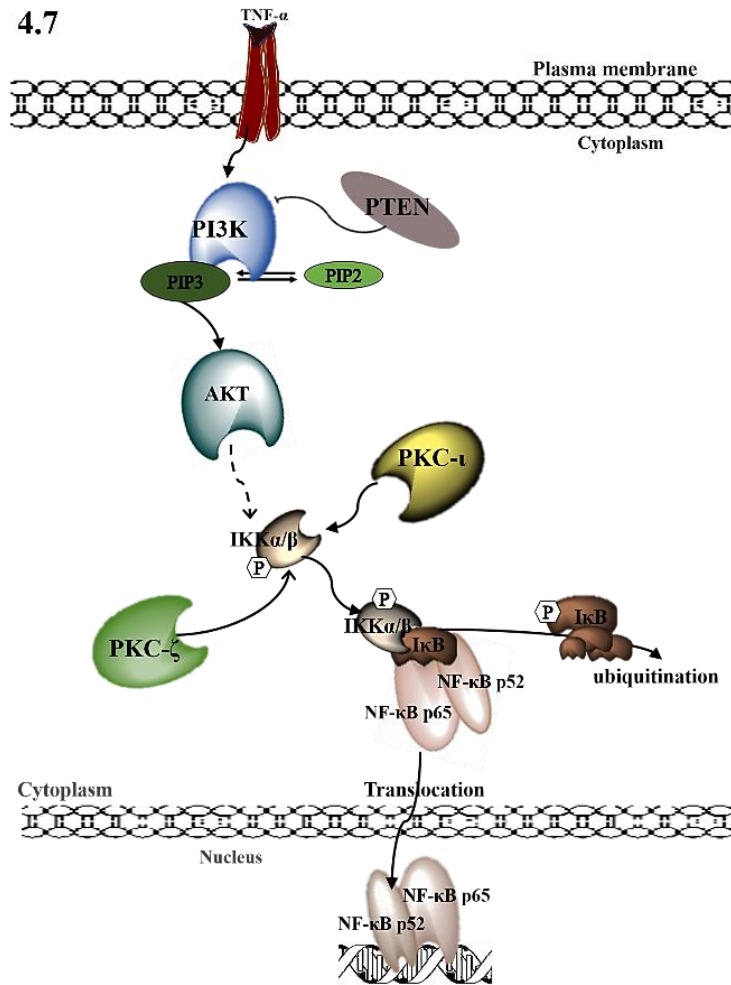
Figure 4.7: A schematic summary of the involvement of PKC-ι and PKC-ζ in melanoma progression via NF-κB and PI3K/AKT pathways. Upon extracellular stimulation with TNF-α, activation of AKT through PIP₃ takes place as a result of inactivation of PTEN. Activated AKT pathway can lead to cell survival, rapid proliferation and differentiation which are critical parts of melanoma progression. AKT could indirectly stimulate NF-κB pathway along with PKC-ι and PKC-ζ in which they play a stimulatory role on IKK-α/β in order to promote the releasing the NF-κB complex from IκB to translocate into nucleus.

CHAPTER 5

PKC-ι PROMOTES METASTASIS OF MELANOMA CELLS BY PROMOTING EPITHILIAL-MESENCHYMAL TRANSITION (EMT) AND ACTIVATING VIMENTIN

5.1 Introduction

Epithelial-mesenchymal transition as well as its reverse process mesenchymal-epithelial transition (MET), is essential for development and physiological response to an injury (such as wound healing) as well as in carcinogenesis (179,180). Under normal conditions, epithelial cells are linked together and the extracellular matrix (ECM) environment by different types of intercellular junctions such as desmosomes, adherens, and tight junctions, which enable tissue maintenance and stability (181). Epithelial cells can gain the ability to acquire a mesenchymal phenotype allowing for physiological circadian tissue changes but also for tissue loss or damage (182). Interestingly, this process is also associated with an transformation to intermediate stem cell phenotype, thus reflecting the highly conserved mechanisms during embryogenesis (179,183).

EMT represents the intersection of different aspects of human development which are sequential rather than parallel processes (181). During the early phase of human development, EMT is involved in morphogenesis and stem cell plasticity required for correct implantation, gastrulation and organogenesis (184,185). In the adult organism, subsequent processes relying on regulated EMT or MET are tissue maintenance allowing for reconstruction or maintenance of tissue, as well

53

as cell homeostasis after inflammatory or degenerative insults. In the case of chronic inflammatory and degenerative diseases, such as organ fibrosis, the EMT/MET system is over-regulated which may lead to organ insufficiency or failure (186–188).

EMT plays a key role in the initial steps of tumor cell dissemination and metastasis. Typically, EMT is found locally at the tumor front with a characteristically increased expression of vimentin paralleled by a loss of E-cadherin (189,190).

Throughout EMT, epithelial cells lose apical-basal polarity, remodel the extracellular matrix (ECM), rearrange the cytoskeleton, drive changes in signaling programs that control the cell shape maintenance and adapt gene expression to obtain mesenchymal phenotype, which is invasive and increases individual cell motility (191). EMT's key features comprise downregulation of E-cadherin to destabilize tight junctions between cells and upregulation of genes such as Vimentin that may assist mesenchymal phenotype.

Migration and invasion studies in cancer research are very important because the main cause of death in cancer patients is related to metastatic progression. For cancer cells to spread and distribute throughout the body, they must migrate and invade through ECM, undergo intravasation into blood stream and extravasation to form distant tumors. EMT is the driving force of this phenomenon (190).

Vimentin is a very important structural protein that belongs to the family of type III intermediate filament proteins. Intermediate filaments (IFs) make up a vast network of interconnecting proteins between the plasma membrane and the nuclear envelope and convey molecular and mechanical information between the cell surface and the nucleus. IF protein expression is cell type and tissue specific. Mesenchymal cells, fibroblasts, lymphocytes and most types of tumor cells express

54

Vimentin (192,193). Vimentin is essential for organizing microfilament systems, changing cell polarity, and thereby changing cellular motility. Moreover, increased Vimentin expression during EMT is a hallmark of metastasis which plays a very important role in gaining rear-to-front polarity for transforming epithelial cells. In addition to EMT, Vimentin expression is observed in cell mechanisms involved in cellular development, immune response and wound healing (142,143,194).

Vimentin is activated via phosphorylation and various kinases such as; RhoA kinase, protein kinase A, PKC, Ca^{2+}/calmodulin-dependent protein kinase II (CaM kinase II), cyclin-dependent kinase 1 (CDK1), RAC-alpha serine/threonine-protein kinase (AKT1) and RAF proto-oncogene serine/threonine-protein kinases (Raf-1-associated kinases) are known to play a role in regulation of Vimentin via phosphorylation. Studies show that amino acid sites S6, S7, S8, S33, S39, S56, S71, S72, and S83 amongst others, serve as specific phosphorylation sites on the head region of Vimentin (195–203).

Zinc finger protein SNAI1 (SNAIL1) and paired related homeobox 1 (PRRX1) are two very important transcription factors (TFs) which regulate EMT and we show that activated PKC-ι is being regulated via these TFs in relation to Vimentin in melanoma cells. The changes in gene expression that contribute to the repression of the epithelial phenotype and activation of the mesenchymal phenotype involve PRRX1 and SNAIL1. Their expression is activated early in EMT, and they have central roles in the progression of cancer. As these transcription factors have distinct expression profiles, their contributions to EMT depend on the cell or tissue type involved and the signaling pathways that initiate EMT. During EMT, these cells downregulate the expression of cell junction complex proteins such as E-cadherin (204). They also alter their gene expression program to promote mesenchymal behavior. SNAIL1 and PRRX1 are two known TFs

that upregulate Vimentin (205,206). They often control the expression of each other and functionally cooperate at targeted genes, and with additional transcription factors to further define the EMT transcription program that drives EMT progression.

5.2 Results

5.2.1 PKC-ι promotes migration and invasion of melanoma cells; a comparative study based on atypical PKC inhibitors

Wound healing assay was performed using ACPD and DNDA in the initial stage to investigate the effect of both PKC-ι and PKC-ζ on malignant melanoma cell migration *in-vitro*. Wound healing assay is commonly used to investigate *in-vitro* migration of cancer cells (207). Photographs for each cell line are compared as "day 0" (starting point) and "day 3" or "day 4" for both malignant cell lines (Fig. 5.1). Cells treated with ACPD 2.5 µM and DNDA 2.5 µM were compared with their respective controls. The areas of the scratch (wound) were calculated and compared to determine the statistical significance (Fig. 5.2). We found that both inhibitors significantly reduce the wound closure ($P \leq 0.01$) of both cell lines compared to their respective controls.

Basement membrane extract (BME) invasion assay was performed to investigate the effect of ACPD and DNDA on malignant melanoma cell invasion *in-vitro*. Although it is similar to Boyden chamber assay, it avoids scraping off the Matrigel and staining to assess the number of migrated cells through the filter. Hence, the method carries less human error compared to a conventional Boyden chamber assay (208). As demonstrated in Figures 5.3 and 5.4, invasion was significantly reduced ($P \leq 0.05$) by 24% and 21% in ACPD (2.5 µM) treated SK-MEL-2 and MeWo cells compared to its control. In DNDA (2.5 µM) treated samples, the invasion was significantly reduced

56

($P{\leq}0.05$) by 32% in both SK-MEL-2 and MeWo cell lines compared to its control. These data suggested that either inhibition of PKC-ζ and PKC-ι or both significantly retard the cellular migration and invasion of melanoma. Since ACPD and DNDA target both aPKCs it was not conclusive about specific impact of inhibition of PKC-ι and PKC-ζ on melanoma cell migration and invasion. Because of this, we later used ICA-1T, ICA-1S and ζ-Stat since they specifically inhibit aPKCs as explained before.

As shown in Figures 5.5 and 5.6, compared to 80% wound closure in SK-MEL-2 control, inhibitor treated samples showed fewer wound closures as 28% ($P{\leq}0.01$) for ICA-1T at 1 µM, 33% ($P{\leq}0.01$) for ICA-1S at 2.5 µM and 53% ($P{\leq}0.05$) ζ-Stat at 5 µM. Compared to 66% wound closure in MeWo control, inhibitor treated samples were 26% ($P{\leq}0.01$) for ICA-1T at 1 µM, 32% ($P{\leq}0.01$) for ICA-1S at 2.5 µM and 54% ($P{\leq}0.05$) ζ-Stat at 5 µM. Results suggested inhibition of PKC-ι is more effective in reducing cell migration *in-vitro* compared to PKC-ζ. Similarly, BME invasion assay was performed to investigate the effects of ICA-1S, ICA-1T and ζ-Stat on melanoma cell invasion *in-vitro*. Invaded cells adhered on the bottom surface of transwell inserts were stained with crystal violet and photographs were taken in randomly chosen fields as the visual representation of the invasion assay (Fig. 5.7). Crystal violet stained invaded cells were dissolved in 70% ethanol in the bottom chamber and absorbance was measured at 590 nm which is proportional to the number of invaded cells (Fig. 5.8). ICA-1T and ICA-1S significantly ($P{\leq}0.01$) reduced invasion by 55% and 43% in SK-MEL-2 cells and by 48% and 44% in MeWo cells, respectively. Interestingly, ζ-Stat did not show a significant effect on decreasing melanoma cell invasion. These data showed that PKC-ι inhibition showed a significant reduction of both melanoma cellular migration and invasion while PKC-ζ inhibition did not show any effect on

57

cellular invasion. These results confirmed that PKC-ι plays a crucial role in cellular migration and

invasion over PKC-ζ in melanoma.
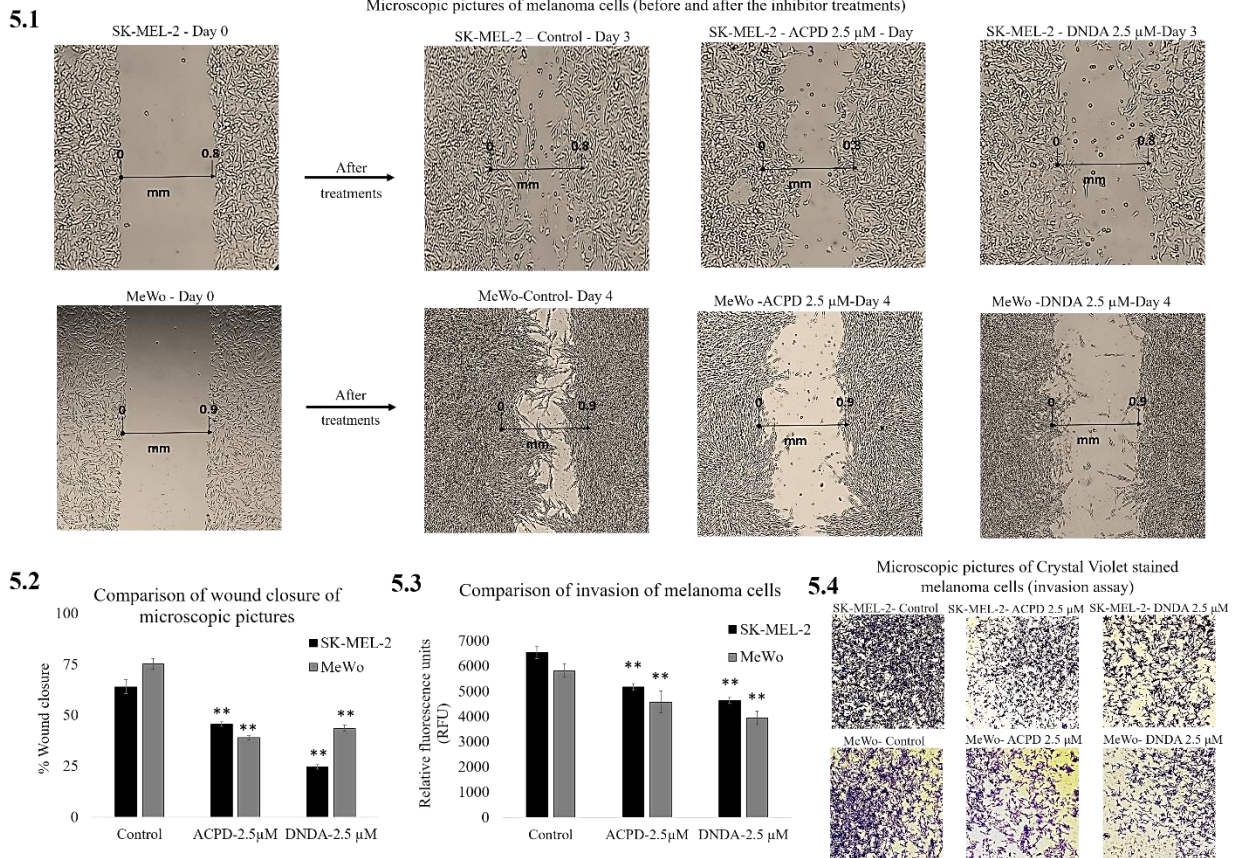
Figures 5.1-5.4: ACPD and DNDA decrease melanoma cell migration and invasion. Figure 5.1 and 5.2 represent the effect of aPKC inhibitors (2.5 µM of ACPD and DNDA) on melanoma cell migration in wound healing assay and Figure 5.3 represents the effect of inhibitors on melanoma cell invasion in Boyden chamber assay with basement extract. In wound healing assay, microscopic photographs of scratches on cells at the beginning (day 0) were compared with the photographs taken after 3 or 4 days. The effect of inhibitors are shown (Fig. 5.1) compared to their control for both ACPD and DNDA. Experiments (*N*=3) were performed for each cell line and randomly picked photographs are shown. Figure 5.2 represents a comparison of calculated percent wound closure for the photographs taken. For Boyden chamber assay (Fig. 5.3), relative fluorescence unit (RFU) values were reported after 2 h exposure of invaded cells with Calcein-AM, as a comparison of control and inhibitors (2.5 µM ACPD and DNDA) treated samples by subtracting the blanks (no cells). Figure 5.4 shows representative photographs of invaded cells after a three day incubation period. Mean ± SD are plotted. Statistical significance is indicated by asterisk as **P< 0.01.
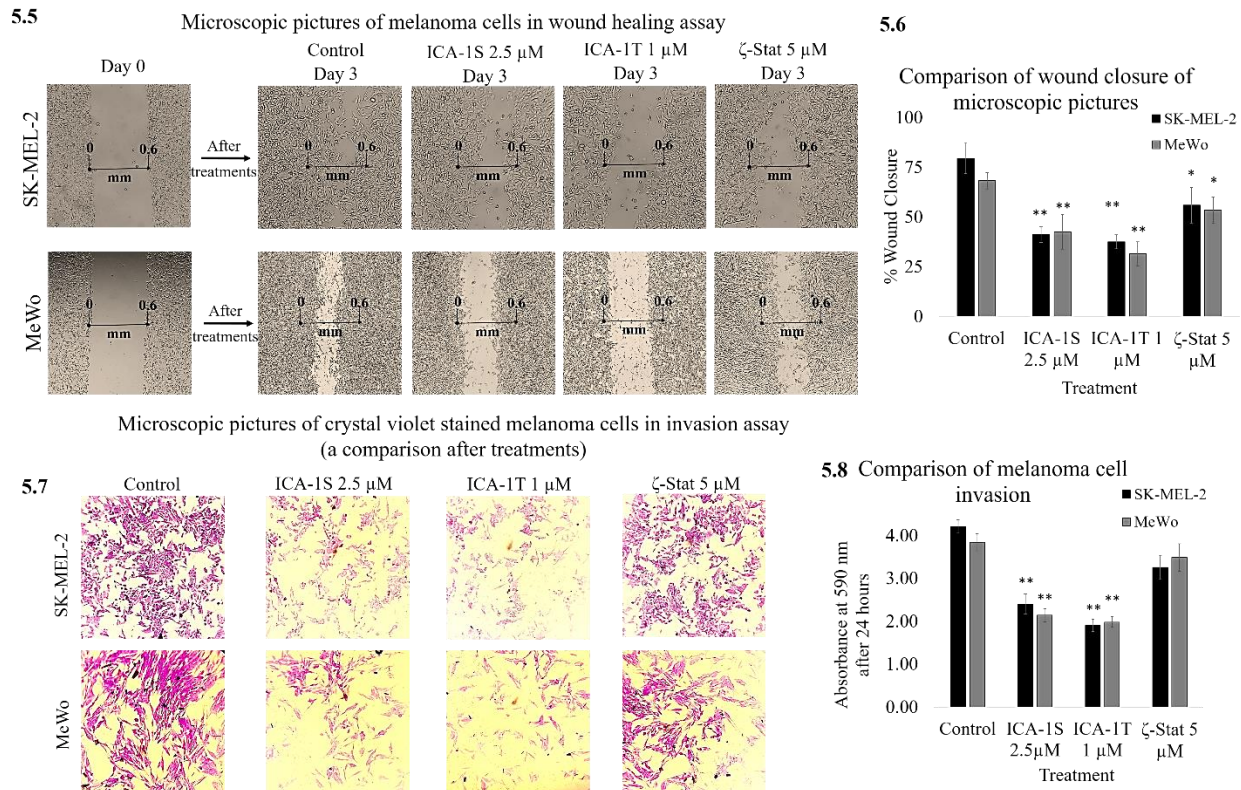
Figures 5.5-5.8: ICA-1S, ICA-1T and ζ-Stat decrease melanoma cell migration and invasion. Fig. 5.5 and 5.6 represent the effect of aPKC inhibitors (2.5 μM of ICA-1S, 1 μM of ICA-1T and 5 μM of ζ-Stat) on melanoma cell migration in wound healing assay and Figure 5.7 and 5.8 represent the effect of inhibitors on melanoma cell invasion in Boyden chamber assay with basement extract (BME). In the wound healing assay, microscopic photographs (40×) of scratches on cells at the beginning (day 0) were compared with the photographs taken after 3 days. The effect of inhibitors are shown (Fig. 5.5) compared to their controls. Experiments (*N*=3) were performed for each cell line and randomly picked photographs are shown. Figure 5.6 represents a comparison of calculated percent wound closure for the photographs taken using ImageJ (NIH, Rockville, MD, USA). For Boyden chamber assay (Fig. 5.7), invaded cells in the bottom surface of transwell insert were stained with 0.5% crystal violet and microscopic pictures were taken (100×). Subsequently, crystal violet was dissolved in 70% ethanol and absorbance was measured at 590 nm, which is directly proportional to the number of invaded cells. These absorbency values are included in Figure 5.8. Mean ± SD are plotted. Statistical significance is indicated by asterisk as **$P < 0.01$.

Our preliminary data showed that Vimentin was not detected in normal melanocytes compared to higher levels in melanoma cells, which was similar to the expression pattern of PKC-ι in these cell lines as we demonstrated in Figure 2.1 We have already shown that both ICA-1T and ICA-1S significantly reduced total and phosphorylated PKC-ι while having no effect on PKC-ζ. On the

59

other hand, ζ-Stat showed a significant diminution of phosphorylated and total PKC-ζ levels without affecting PKC-ι levels. Therefore, since these inhibitors were effectively inhibiting their targets, we also investigated the effects of aPKC inhibition on EMT signaling to understand how specific aPKC inhibition alters EMT stimulation in melanoma cells. We tested the levels of E-cadherin, phosphorylated Vimentin (S39), total Vimetin, Par6 and RhoA (Fig. 5.9 and 5.10). Interestingly, inhibition of PKC-ζ using ζ-Stat showed no significant effect on E-cadherin, Vimentin and phospho-Vimentin or Par6 and RhoA. Conversely, ICA-1T and ICA-1S inhibition on PKC-ι resulted in a significant increase of E-cadherin and RhoA while significantly decreasing Vimentin, phospho-Vimentin and Par6 (Fig. 5.9 and 5.10).

To fully establish these observations, we used *si*RNA for PKC-ι and PKC-ζ to knockdown the expression of the target proteins and subsequently investigated the levels of protein expression for the proteins E-cadherin, phosphorylated Vimentin (S39), total Vimetin, Par6 and RhoA (Fig. 5.11 and 5.12). These experiments showed a complementary situation for our inhibitor applications for the targeted proteins. Scrambled *si*RNA was also used in addition to the control and there was no significant difference observed between the control and scrambled *si*RNA treatments for the said proteins.

*si*RNA treatments of PKC-ι resulted in significant decrease in PKC-ι level by 87% and 64% in SK-MEL-2 and MeWo cell lines, respectively. PKC-ζ decreased by 11% and 0%, which is not significant, while Bcl-2 significantly decreased by 68% and 84%, Vimentin decreased by 73% and 67%, phospho Vimentin (S39) significantly decreased by 92% and 81%, E-cadherin increased by 59% and 46%, RhoA increased by 33% and 26%, and Par6 decreased by 42% and 55% in PKC-ι *si*RNA treated SK-MEL-2 and MeWo cells, respectively.

60

*si*RNA treatments of PKC-ζ resulted in significant decrease in PKC-ζ level by 83% and 76% in SK-MEL-2 and MeWo cell lines, respectively. As expected Vimentin, phospho Vimentin, E-cadherin, Par6 and RhoA levels of PKC-ζ *si*RNA treated samples did not show a significant difference to its control.

5.2.2 PKC-ι may induce EMT by upregulating TGFβ/Par6/RhoA and SMAD pathways

Earlier in Chapter 4, the effects of TNF-α and TGFβ stimulation on aPKC expression were demonstrated (Fig. 4.5 and 4.6). These experiments showed that both TNF-α and TGFβ upregulate PKC-ι while TGFβ did not increase the production of PKC-ζ.

As shown in Figures 5.13 and 5.14, we found that levels of Vimentin, Par6 and the degree of phosphorylation of Vimentin (S39) significantly increased for both cell lines in the presence of TGFβ while reducing the levels of E-cadherin and RhoA.

So far these results showed a strong relationship of PKC-ι with the melanoma cell migration and invasion over PKC-ζ. Whenever PKC-ι is inhibited or knocked down in its expression, melanoma cell motility decreased. In addition, it shows that PKC-ι inhibition leads to decreased mesenchymal markers; Vimentin and Par6 increase the expression of epithelial markers; E-cadherin and RhoA. These observations indicate a possible slowing down or reversing the EMT progression of melanoma cells upon PKC-ι diminution. Interestingly, Vimentin show a very strong relationship with PKC-ι as indicted in the Western blot analysis for inhibitor treatments (Fig. 5.9) and *si*RNA treatments (Fig. 5.11). Also data strongly suggest that PKC-ι inhibition effects the phosphorylation of Vimentin (S39), which is a crucial site for elevated Vimentin dynamics. Data shows that

Vimentin activity decreases as a result of PKC-ι diminution. On the other hand PKC-ζ did not show any involvement with the EMT process or Vimentin dynamics.
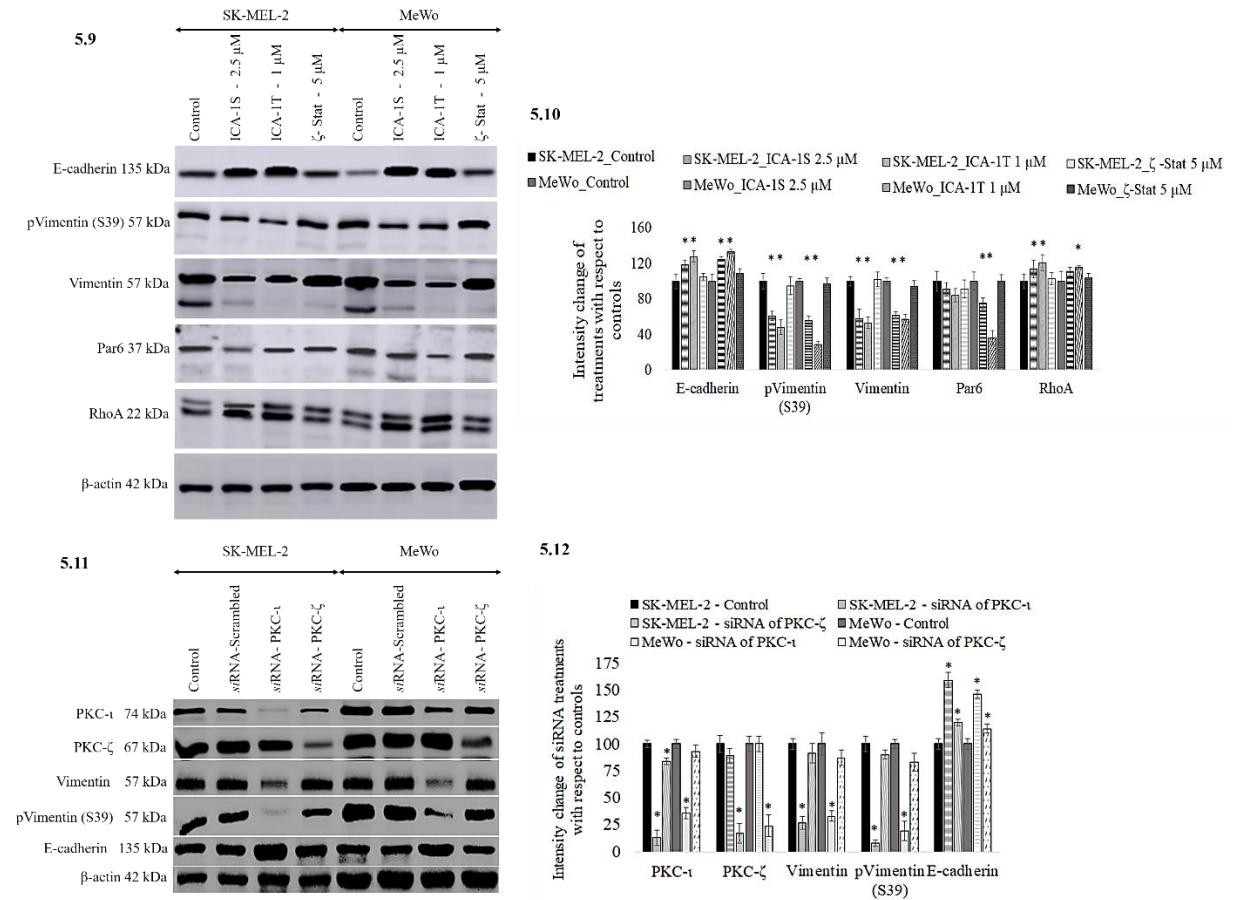
Figures 5.9-5.12: Effect of inhibitors (ICA-1S, ICA-1T and ζ-Stat) and *si*RNA knockdown of the expression of aPKCs on aPKC expression and EMT in melanoma cells. Expression of the protein levels of PKC-ι and PKC-ζ were depleted confirming the accuracy of *si*RNA. Protein levels of Vimentin, phosphorylated Vimentin, Par6, RhoA and E-cadherin are shown for the inhibitor treatments (2.5 µM of ICA-1S, 1 µM of ICA-1T and 5 µM of ζ-Stat) and for and for *si*RNA treatments are shown in Fig. 5.9 and 5.11, respecively. 40 µg of protein was loaded in to each well and β-actin was used as the loading control in each Western blot. Figures 5.10 and 5.12 represent the densitometry values for Western blots shown in 5.9 and 5.11, respectively. Experiments ($N = 3$) were performed in each trial and representative bands are shown.
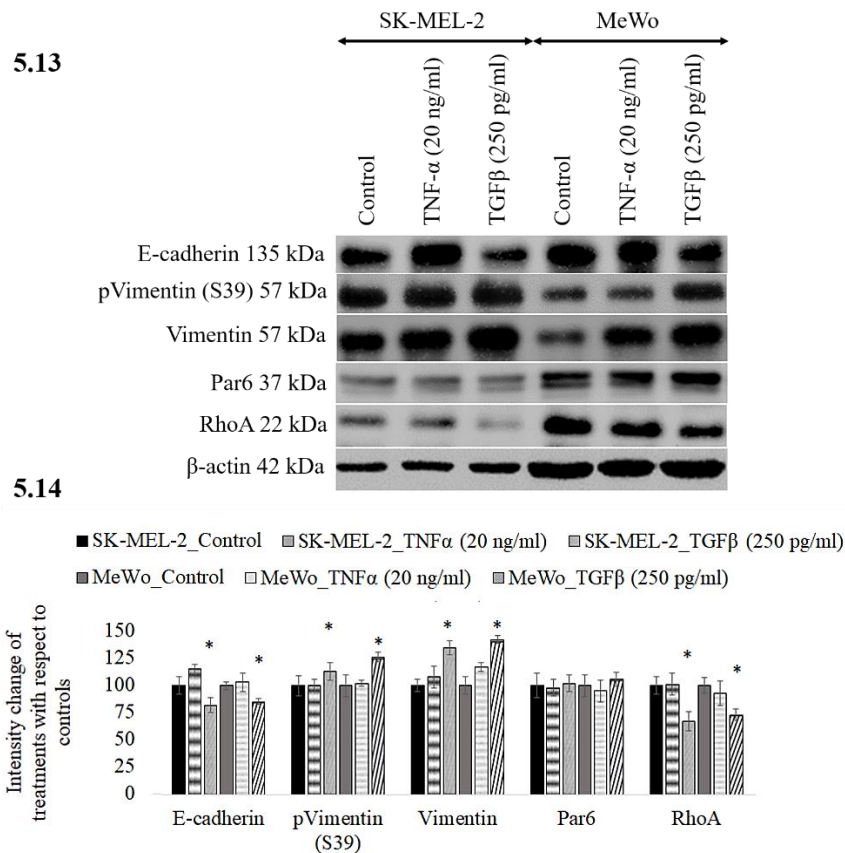
Figures 5.13-5.14: Effect of TNF-α and TGFβ on aPKC expression and EMT in melanoma cells. Protein levels of Vimentin, phosphorylated Vimentin, Par6, RhoA and E-cadherin are shown for the TNF-α (20 ng/ml) and TGFβ (250 pg/ml) treatments are shown in Fig. 5.13. 40 µg of protein was loaded in to each well and β-actin was used as the loading control in each Western blot. Figure 5.14 represents the densitometry values for Western blots shown in 5.13. Experiments ($N = 3$) were performed in each trial and representative bands are shown.

5.2.3 PKC-ι associates with Vimentin and play a critical role in upregulation of Vimentin dynamics in melanoma cells

To investigate the relationship of PKC-ι and Vimentin, an immunoprecipitation (IP) experiment was conducted. PKC-ι and PKC-ζ were separately immunoprecipitated (IP) and Western blot experiments were conducted independently for E-cadherin, CD44, Vimentin and NF-κB p65 (143). PKC-ζ IP samples did not show any association with these proteins. Only Vimentin immunoblots showed an association with PKC-ι IP samples (Fig. 5.15). This suggests that PKC-ι

associates with Vimentin. To confirm this association, Vimentin was immunoprecipitated, immunoblotted for above mentioned proteins, and only PKC-ι demonstrated an association with Vimentin. Both these IP and reverse IP of PKC-ι and Vimentin showed a strong direct association between them (Fig. 5.15 and 5.16). An association was essential between Vimentin and PKC-ι for PKC-ι to phosphorylate Vimentin.

Figures 5.17 and 5.18 show immunofluorescence staining studies, which also confirmed the association of PKC-ι and Vimentin depicting both proteins distributed throughout the cytoplasm. ICA-1T treated cells showed lesser amounts of those proteins (lighter in staining) compared to control samples. Inhibitor treatments for both cell lines also decreased the nuclei and overall cell sizes. In the controls of both cells, the invasive characteristics such as formation of lamellipodia, filopodia and invadopodia are observable clearly whereas ICA-1T treated cells showed less of such features.

Figures 5.19-5.28 demonstrate RT qPCR data, which revealed that PKC-ι mRNA levels decreased upon having been treated with ICA-1T and ICA-1S, by approximately 50% in SK-MEL-2 cells and 30% in MeWo cells. There was no significant difference observed between the inhibition of PKC- ι by ICA-1T and ICA-1S. Vimentin mRNA levels decreased by approximately 50% in SK-MEL-2 cells when treated with either PKC-ι inhibitor. Vimentin mRNA levels had no significant changes in MeWo cells treated with either ICA-1T or ICA-1S. ζ-Stat treatments had no significant effect on Vimentin mRNA levels in either cell line.

Immunofluorescence staining revealed that the shape of melanoma cells significantly changed upon inhibition of PKC-ι. Both Vimentin and PKC-ι levels were relatively low in ICA-1T treated cells in comparison to their respective controls. Additionally, invasive characteristics such as formation of lamellipodia, filopodia and invadopodia were distinctively visible in both controls,

64

though they were not apparent in treated cells. This also confirmed the growth retardation observed in melanoma cells upon aPKC inhibitor treatments that resulted in lesser growth in treated cells. As observed in qPCR experiments, treatments with PKC-ι specific ICA-1T and ICA-1S, specific for downregulation of PKC-ι suggested, that PKC-ι plays a role in its own regulation. Phosphorylation of Vimentin at S39 is required for its activation, and inhibition of PKC-ι diminishes this activation process. Very low levels of total Vimentin observed in Western blots for ICA-1T and ICA-1S treated cells indicate that without PKC-ι, unphosphorylated Vimentin undergoes rapid degradation. In addition to activating Vimentin, PKC-ι appears to play a role in regulating Vimentin expression in some carcinoma cells (209,210).

The effects of PKC-ι inhibition on the Vimentin intermediate filament (VIF) dynamics were examined in detail, while giving emphasis to the regulation of expression of Vimentin and PKC-ι. Here we knocked down the expression of two TFs; PRRX1 and SNAIL1 using *si*RNA. The changes in gene expression during EMT involve principal regulators such as SNAIL, Zinc finger E-box-binding homeobox1 (ZEB1), Twist-related protein1 (TWIST) and PRRX1. These TFs have highly specific expression profiles and are known to upregulate Vimentin expression during EMT (205,206,211–214). The direct effects of downregulation of PRRX1 and SNAIL1 on PKC-ι expression or PKC-ι activity has not been investigated before and herewith we analyze this phenomenon since the stimulation from TGFβ has shown an increased expression of PKC-ι along with Vimentin, as testified in the data. This observation suggested a close regulation of the expression of Vimentin and PKC-ι in melanoma cells. Overall, the results suggested that PKC-ι is a critical component in the regulation of Vimentin dynamics in which PKC-ι phosphorylates to activate Vimentin, thereby leading to the disassembly of VIF to support melanoma metastasis.

Results also indicated that PKC-ι activation and Vimentin expression regulation are interconnected and regulated by SNAIL1 and PRRX1.

As demonstrated in Figures 5.29 and 5.30, both inhibition from ICA-1T and *si*RNA depletion of PKC-ι, showed no significant effect on the PRRX1 and SNAIL1 levels. Reduction of both phosphorylated and total PKC-ι were significant similarly shown earlier in Figures 5.9 and 5.11 which indicated that both ICA-1T and *si*RNA applications were effective against their specific target PKC-ι. Depletion of PKC-ι resulted in a downregulation of total and phosphorylated Vimentin (S39) and upregulated E-cadherin (Fig. 5.29).

5.2.4 Effects of the knockdown of expression of SNAIL1 and PRRX1 on the expression of PKC-ι, Vimentin, E-cadherin and the activation of VIFs

Both Western blots (Fig. 5.31 and 5.32) and RT-qPCR results (Fig. 5.33-5.36) suggested that *si*RNA knockdown of PRRX1 and SNAIL1 significantly reduced the expression of PKC-ι and Vimentin and increased E-cadherin expression. As shown in Figure 5.31, *si*RNA of PRRX1 significantly reduced the PRRX1 expression by 90% and 93% ($P \leq 0.05$) in SK-MEL-2 and MeWo cells, respectively. SNAIL1 expression was reduced by 92% ($P \leq 0.05$) in both cell lines in SNAIL1 *si*RNA treatments. Subsequently, we analyzed the effects of these knockdown of expression of PKC-ι and Vimentin, along with the degree of phosphorylation. Phosphorylated PKC-ι (T555) was reduced by 48% ($P \leq 0.05$), while Vimentin level was reduced by 26% ($P \leq 0.05$), for PRRX1 knocked down in SK-MEL-2 while E-cadherin expression increased by 48% ($P \leq 0.05$). On the other hand, phosphorylated PKC-ι (T555) was reduced by 56% ($P \leq 0.05$) while Vimentin level was reduced by 45% ($P \leq 0.05$) for SNAIL1 knocked down in SK-MEL-2 while increasing E-cadherin

level by 37% ($P \leq 0.05$). This indicated that knockdown expression of SNAIL1 is more significant on down regulating the levels of phospho PKC-ι (T555) and Vimentin. Interestingly, total PKC-ι level did not change significantly. The same trend was observed in the MeWo cell line as well. Interestingly, phosphorylation of Vimentin at S39 demonstrated more than 80% ($P \leq 0.05$) reduction for these treatments. Previously reported data (Fig. 5.9 and 5.11) confirmed that PKC-ι knockdown expression using PKC-ι *si*RNA or inhibition using ICA-1T reduced the phosphorylation at S39. Current results also show that both PRRX1 and SNAIL1 transcriptionally upregulate the expression of Vimentin and activated PKC-ι levels which depends on the available amount of Vimentin. Knockdown of these TFs result a significant drop of the activated PKC-ι (T555) without changing the total PKC-ι significantly. As far as results show, Vimentin influenced PKC-ι regulation cycle to maintain sufficient levels of phosphorylated PKC-ι via PRRX1 and SNAIL1. Inhibited PKC-ι provides less phosphorylated PKC-ι levels which leads to a reduction of phosphorylated Vimentin. As a result of this negative impact upon PKC-ι inhibition on PRRX1 and SNAIL1, their transcriptional activities on Vimentin are reduced.

67
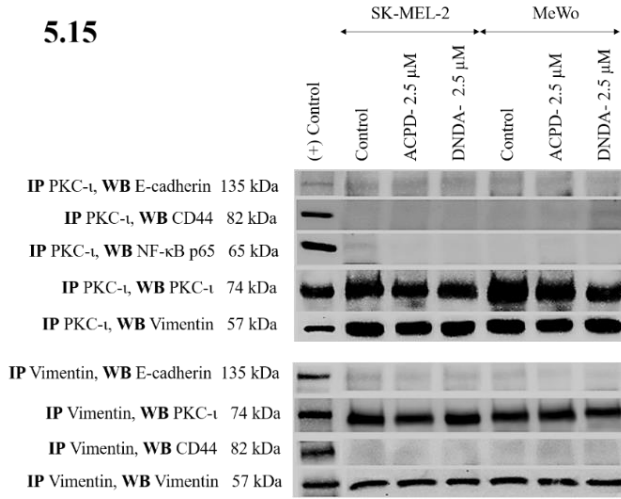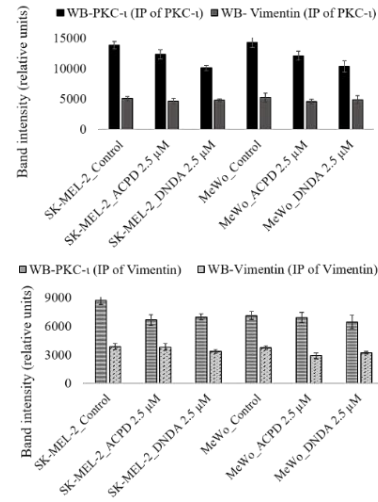
Figures 5.15-5.16. PKC-ι strongly associates with Vimentin. Whole cell lysates (100 µg) of malignant cells (SK-Mel-2 and MeWo) were IP separately for PKC-ι and Vimentin using specific antibodies. First column of the Western blot (Fig. 5.15) represents the (+) control, which contained 40 µg of MeWo whole cell extract, applied to ensure that bands appeared for the specific proteins in Western blots. Western blots (Fig5.15) of PKC-ι IP showed an association with Vimentin while no association was observed for E-cadherin, CD44 and NF-κB p65. Vimentin IP confirmed the association with PKC-ι in the Western blot while no association was observed with the above mentioned proteins. Experiments (*N*=3) were performed in each trial. Densitometry for each band was indicated in the bar graph in Fig. 5.16.
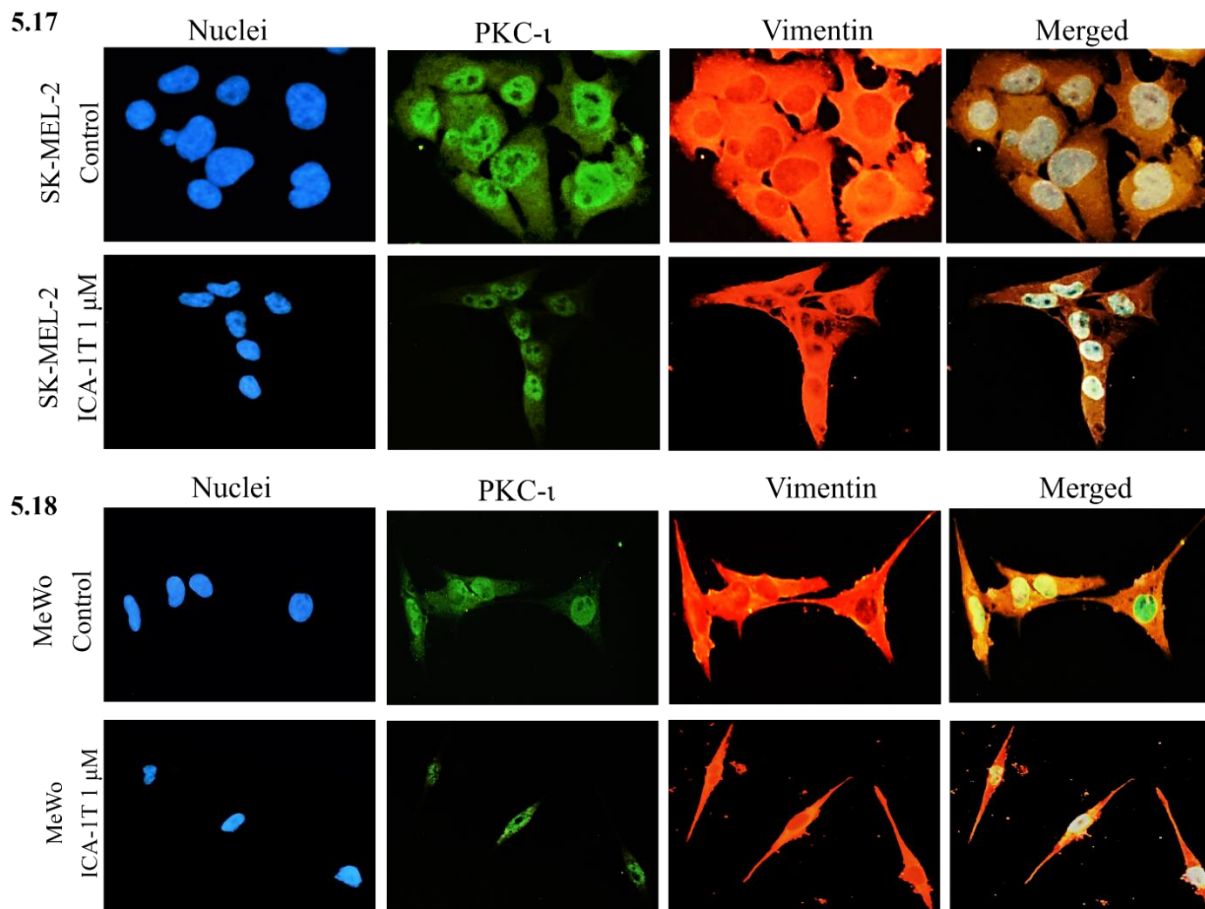
Figures 5.17-5.18: PKC-ι and Vimentin immunofluorescence in melanoma cells for ICA-1T treatments. Fig. 5.17 and 5.18 represents the immunofluorescence staining of nuclei (blue panel), PKC-ι (green panel) and Vimentin (red panel) for SK-MEL-2 and MeWo cells treated with ICA-1T (1 μM) against controls. A negative control for each secondary antibody was not tested. The images were captured at 200X magnification. Experiments ($N=3$) were performed in each trial and representative images are shown.
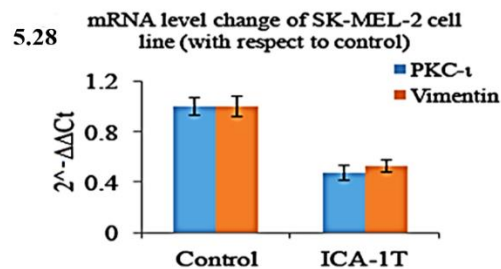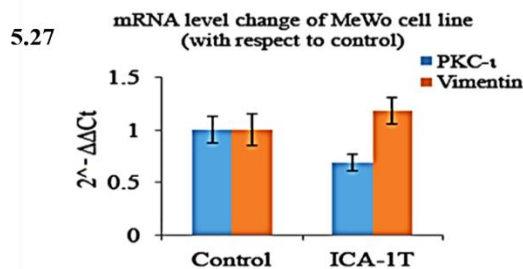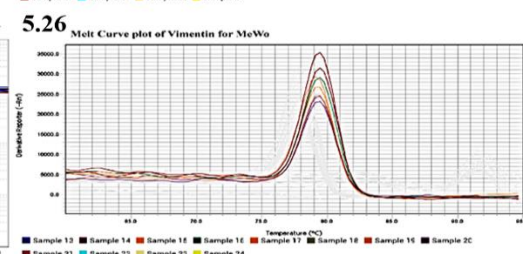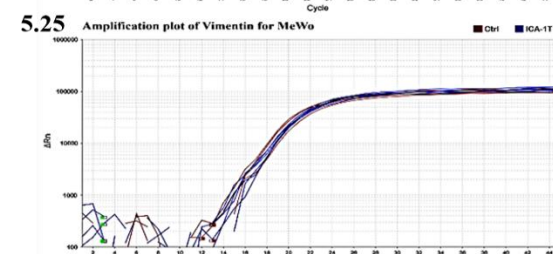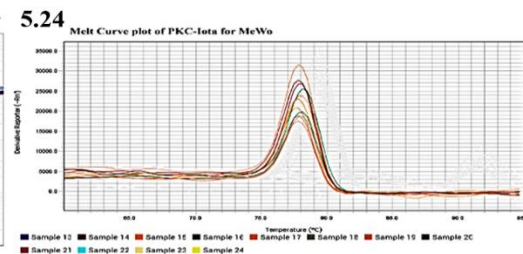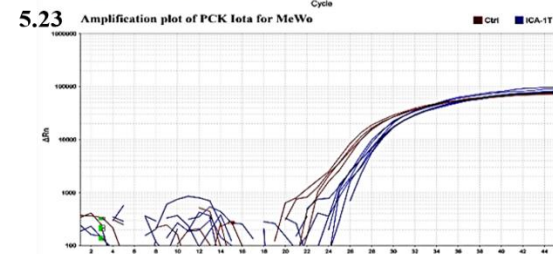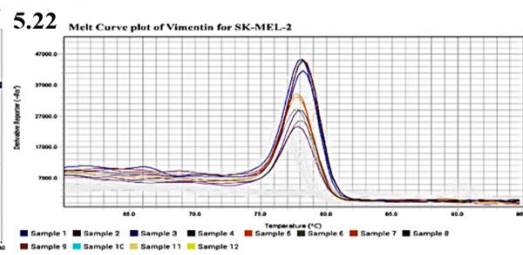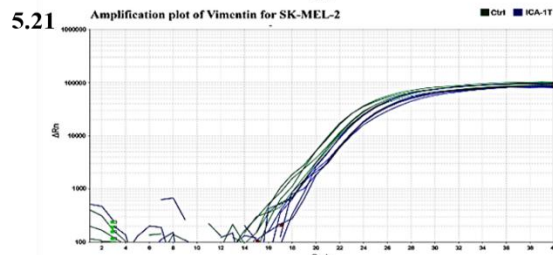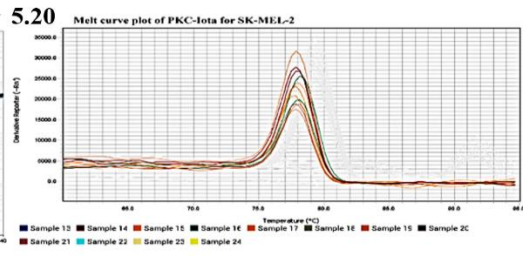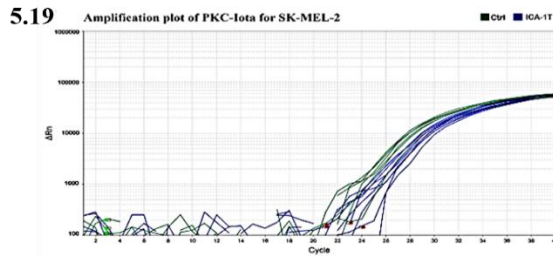
Figures 5.19-5.28: Quantitative real time PCR data of ICA-1T (1μM) treatments for PKC-ι and Vimentin for melanoma cell lines. Fig. 5.19 and 5.21 represent the amplification plots of PKC-ι and Vimentin for the SK-MEL-2 cell line. Fig. 5.23 and 5.25 represent the amplification plots of PKC-ι and Vimentin for the MeWo cell line. Fig. 5.20 and 5.22 represent the melt curve plots of PKC-ι and Vimentin for the SK-MEL-2 cell line. Fig. 5.24 and 5.26 represent the melt curve plots of PKC-ι and Vimentin for the SK-MEL-2 cell line. Fig. 5.27 and 5.28 demonstrate the mRNA level change of PKC-ι and Vimentin for ICA-1T treated MeWo and SK-MEL-2 cell lines, respectively. The ΔΔCT values were plotted with respect to the mRNA levels of control samples of each cell line. Statistical significance is indicated by asterisk as *$P < 0.05$. Experiments (N=3) were performed in each trial.
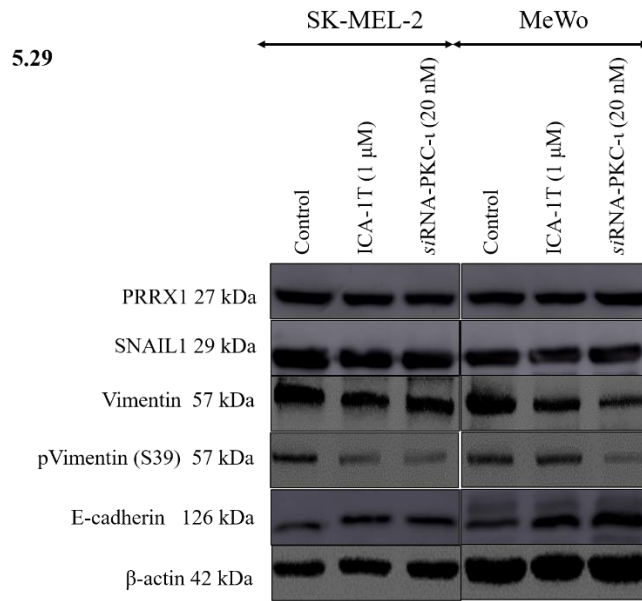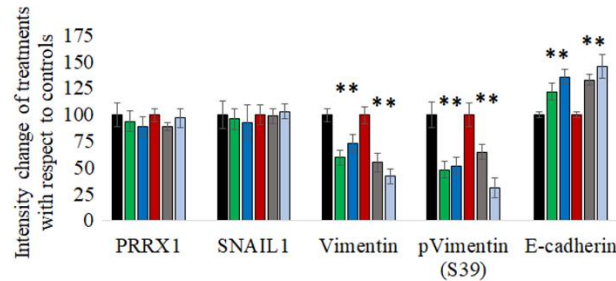
Figures 5.29-5.30: Effects of *si*RNA knockdown of expression and specific inhibition of PKC-ι on expression of Vimentin, E-cadherin, PRRX1 and SNAIL1 along with phosphorylation of Vimentin in melanoma cells (SK-MEL-2 and MeWo). Expression of the protein levels of Vimentin, phosphorylated Vimentin (S39) and E-cadherin for the *si*RNA treatment of PKC-ι (20 nM of *si*RNA) and PKC-ι specific inhibitor ICA-1T (1 μM) are shown in Fig. 5.29. 60 μg of protein was loaded in to each well and β-actin was used as the loading control in each Western blot. Fig. 5.30 represents the densitometry values for Western blots in Fig. 5.29. Experiments (*N*=3) were performed in each trial and representative bands are shown. Densitometry values are reported as mean ± SD. Statistical significance is indicated by asterisk as *$P \leq 0.05$.

5.31

SK-MEL-2   MeWo

Lanes: Control, siRNA-Scrambled (30 nM), siRNA-PRRX1 (30 nM), siRNA-SNAIL1 (30 nM) | Control, siRNA-Scrambled (30 nM), siRNA-PRRX1 (30 nM), siRNA-SNAIL1 (30 nM)

Blots:
- PRRX1 27 kDa
- SNAIL1 29 kDa
- pPKC-ι (T555) 74 kDa
- PKC-ι 74 kDa
- Vimentin 57 kDa
- pVimentin (S39) 57 kDa
- E-cadherin 126 kDa
- β-actin 42 kDa

5.32

Legend:
- SK-MEL-2_Control
- SK-MEL-2_siRNA_Scrambled 30 nM
- SK-MEL-2_siRNA_PRRX1 30 nM
- SK-MEL-2_siRNA_SNAIL1 30 nM
- MeWo_Control
- MeWo_siRNA_Scrambled 30 nM
- MeWo_siRNA_PRRX1 30 nM
- MeWo_siRNA_SNAIL1 30 nM

Y-axis: Intensity change of treatments with respect to controls

X-axis: PRRX1, SNAIL1, pPKC-ι (T555), PKC-ι, Vimentin, pVimentin (S39), E-cadherin

Figures 5.31-5.32: Effects of *si*RNA knockdown of expression of PRRX1 and SNAIL1 on expression of PKC-ι, Vimentin and E-cadherin along with phosphorylation of Vimentin and PKC-ι in melanoma cells (SK-MEL-2 and MeWo). Expression of the protein levels of phosphorylated PKC-ι, total PKC-ι, Vimentin, phosphorylated Vimentin (S39) and E-cadherin for the *si*RNA treatments of PRRX1 and SNAIL1 (30 nM of *si*RNA against scrambled *si*RNA) are shown in Fig. 5.31. 60 µg of protein was loaded in to each well and β-actin was used as the loading control in each Western blot. Fig. 5.32 represents the densitometry values for Western blots in Fig. 5.31. Experiments (*N*=4) were performed in each trial and representative bands are shown. Densitometry values are reported as mean ± SD. Statistical significance is indicated by asterisk as *P≤ 0.05.
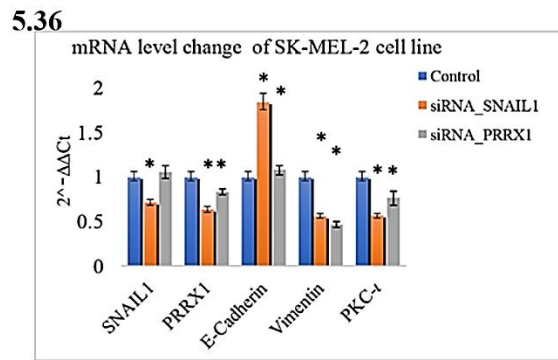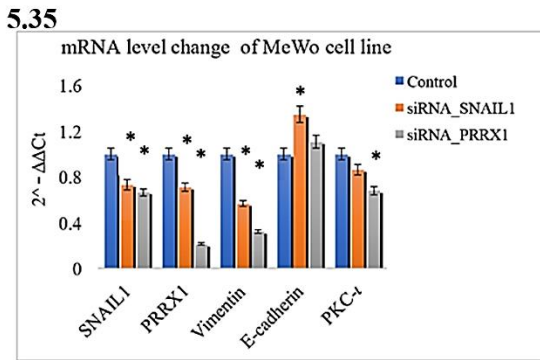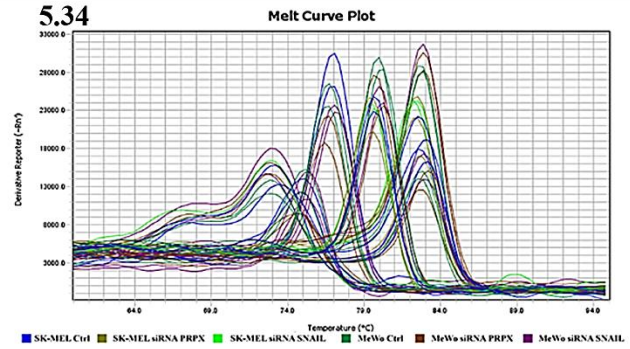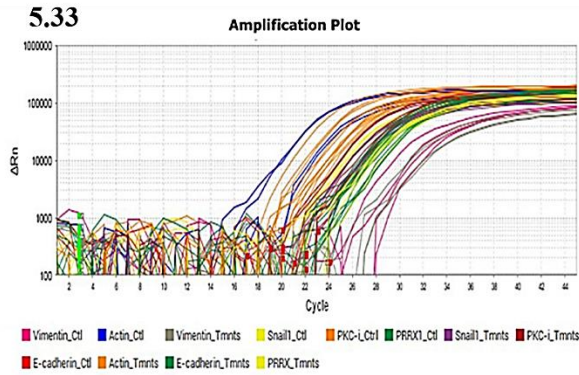
Figures 5.33-5.36: RT-qPCR data of *si*RNA knockdown of expression of PRRX1 and SNAIL1 on expression of PKC-ι, Vimentin and E-cadherin in melanoma cell lines (SK-MEL-2 and MeWo). Fig. 5.33 represents the amplification plots of SNAIL1, PRRX1, PKC-ι, E-cadherin and Vimentin for the MeWo cell line against β-actin. Fig. 5.34 represents the melt curve plots of SNAIL1, PRRX1, PKC-ι, E-cadherin, Vimentin and β-actin for the MeWo cell line, showing 6 different peaks recorded for each target which demonstrate high specificity and accuracy of the targeted primers. The ΔΔCT values were plotted with respect to the *m*RNA levels of control samples of each cell line (Fig. 5.35 for MeWo and Fig. 5.36 for SK-MEL-2). Experiments (*N*=3) were performed. Statistical significance is indicated by asterisk as *$P \leq 0.05$.

73
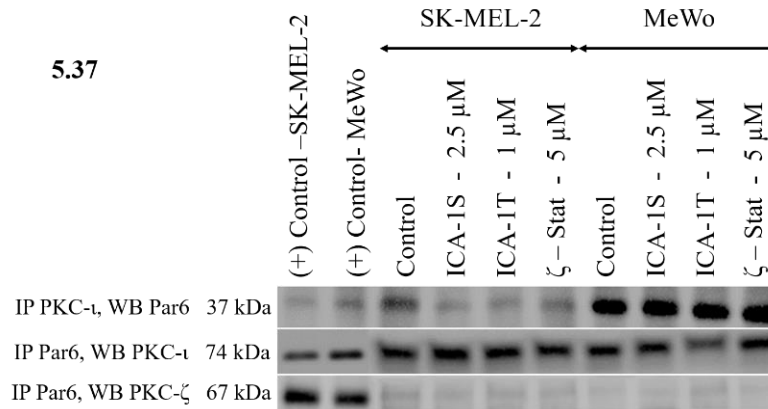
Figure 5.37: PKC-ι associates with Par6 in melanoma cells. Whole cell lysates (100 µg) of malignant cells (SK-Mel-2 and MeWo) were immunoprecipitated separately for PKC-ι and Par6 using specific antibodies. The first two lanes in Western blot represent the (+) control, which contained 40 µg of SK-MEL-2 and MeWo whole cell extracts, respectively, applied to ensure that bands appeared for the specific proteins in Western blots. Western blots of PKC-ι immunoprecipitation showed an association with Par6. Reverse-immunoprecipitation of Par6 confirmed the association with PKC-ι while no association was observed. Experiments ($N = 3$) were performed in each trial.

5.3 Summary

Our results demonstrated the effects of aPKC inhibition on melanoma cell migration and invasion. ACPD and DNDA treated samples demonstrated a reduction of melanoma motility but it was not conclusive which aPKC was responsible for upregulating metastasis, since both ACPD and DNDA inhibit PKC-ι and PKC-ζ. This was solved using specific PKC-ι inhibitors (ICA-1S and ICA-1T) and a PKC-ζ specific inhibitor ζ-Stat. Migration and invasion were markedly reduced for samples treated with ICA-1T and ICA-1S compared to ζ-Stat treated samples, suggesting that PKC-ι inhibition significantly diminishes melanoma cell migration and invasion suggesting that only PKC-ι is involved in EMT in melanoma. aPKC/Par6 signaling is known to stimulate EMT upon activation of TGF-β receptors in cancer cells. TGF-β activated aPKC/Par6 stimulates degradation of RhoA, which leads to the depolymerization of filamentous actin (F-actin) and loss of epithelial

74

structural integrity resulting in a reduction of cell-cell adhesion. RhoA is a GTPase, which promotes actin stress fiber formation thereby maintains cell integrity. Furthermore, TGFβ upregulates SNAIL1 and PRRX1 TFs that drive genetic reprogramming to facilitate EMT (215,216). Cells lose E-cadherin while gaining Vimentin during this process. This data showed that inhibition of PKC-ι using ICA-1T and ICA-1S significantly increased the levels of E-cadherin and RhoA while decreasing total and phosphorylated Vimentin (S39) and Par6 (142,143). None of these protein levels were significantly changed as a result of PKC-ζ inhibition. Data also showed that TGFβ treatments increased the expression of PKC-ι, Vimentin, phosphorylated Vimentin and Par6 while decreasing E-cadherin and RhoA. These results confirmed the involvement of PKC-ι in EMT stimulation. IP of PKC-ι confirmed a strong association with Par6 in both melanoma cells which was confirmed with reverse-IP of Par6 (Fig. 5.37). Previously published reports state that both aPKCs associate with Par6 and phosphorylate at S345 (217). Interestingly, only PKC-ι showed an association with Par6, which confirmed that PKC-ι is a major activator of EMT in melanoma. Moreover, IP of PKC-ι and Vimentin strongly confirmed an association between PKC-ι and Vimentin. *si*RNA knockdown of PKC-ι and PKC-ζ, immunofluorescent staining and RT-qPCR techniques were also used to study and confirm the association of Vimentin with PKC-ι. Immunofluorescence staining revealed that the shape of melanoma cells significantly changed upon inhibition of PKC-ι. Both Vimentin and PKC-ι levels were relatively low in ICA-1T treated cells in comparison to their respective controls. Furthermore, invasive characteristics such as formation of lamellipodia, filopodia and invadopodia were distinctively visible in both controls, though they were not apparent in PKC-ι inhibited cells. Reduction of nuclei volume and cell size, also confirmed the growth retardation we observed in melanoma cells upon aPKC inhibitor treatments that resulted in lesser growth in treated cells. As observed in qPCR experiments,

75

treatments with PKC-ι specific inhibiors ICA-1T and ICA-1S, depicted a corresponding downregulation of PKC-ι and suggested that PKC-ι plays a role in its own regulation. This is further discussed in the next chapter (Chapter 6).

Phosphorylation of Vimentin at S39 is required for its activation, and inhibition of PKC-ι diminishes this activation process. The reduced levels of total Vimentin observed in Western blots for ICA-1T and ICA-1S treated cells indicate that without PKC-ι, unphosphorylated Vimentin undergoes rapid degradation. In addition to activating Vimentin, PKC-ι appears to play a role in regulating Vimentin expression in some carcinoma cells (210).

As summarized in Figure 5.38, based on these results, we believe that TGFβ stimulated PKC-ι/Par6/RhoA and Smad2/3 pathways to induce EMT in melanoma through transcriptional activities of SNAIL1 and PRRX1. Vimentin and PKC-ι activation are upregulated simultaneously to facilitate EMT in melanoma. PKC-ι activated Vimentin thereby regulates the dynamic changes in melanoma metastasis. These results further confirm that PKC-ι inhibition using specific inhibitors such as ICA-1T and ICA-1S not only reduces melanoma cell survival but also negatively affects the melanoma metastatic progression by downregulating EMT. Taken together, this novel concept can be used to develop more specific effective therapeutics for melanoma patients based on PKC-ι being used as a novel biomarker to mitigate melanoma metastasis using specific inhibitors.
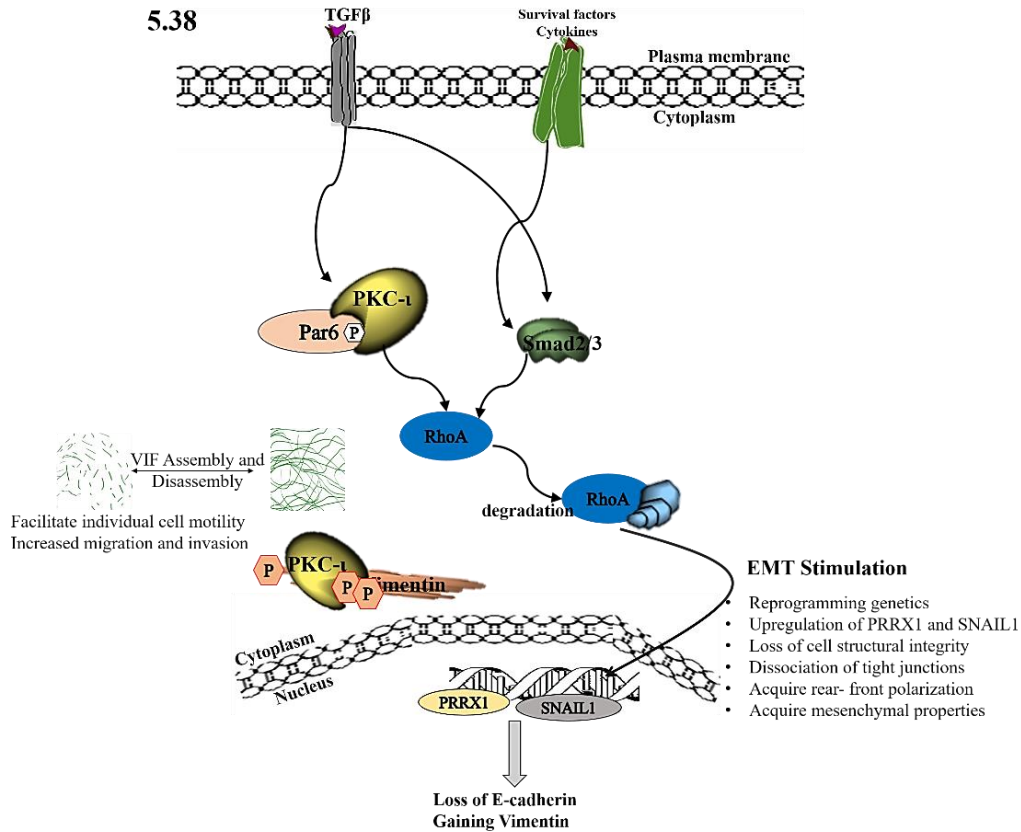
Figure 5.38: A schematic summary of the involvement of PKC-ι in melanoma progression via activation of EMT and Vimentin. Upon extracellular stimulation with TGFβ, PKC-ι associates and activates Par6, which stimulates the degradation of RhoA and upregulates EMT. SNAIL1 and PRRX1 are two very important transcription factors that drive the EMT process by upregulating Vimentin while downregulating E-cadherin. PKC-ι activates Vimentin by phosphorylation and initiates disassembly of VIF and facilitates cellular motility. During this process, cadherin junctions are disrupted as a result of loss of E-cadherin, and β-catenin is translocated to the nucleus to upregulate the production of facilitating proteins such as CD44, which further stimulate migration and EMT. Activated Vimentin changes cell polarity to maintain the mesenchymal phenotype of melanoma cells *in-vitro*.

CHAPTER 6

SELF-REGULATION OF PKC-ι IS A CRUCIAL MECHANISM MAKING PKC-ι AN IMPORTANT NOVEL TARGET IN MELANOMA ANTI-CANCER THERAPEUTICS

6.1 Introduction

So far collected data in the earlier chapters show that PKC-ι serves as an oncogene and therefore a potential therapeutic target for metastatic melanoma. On the other hand, the data has shown that PKC-ζ is involved in NF-κB activation and translocation, thereby regulating melanoma cell survival and growth. However, the data did not illustrate any significant involvement of PKC-ζ in cellular motility of metastatic melanoma cells. In addition, we showed that PKC-ι plays a crucial role in the activation of Vimentin increasing the motility of mesenchymal melanoma cells. This makes PKC-ι overexpression compared to PKC-ζ more lethal in melanoma progression which is associated with a poor prognosis.

The data confirmed that PKC-ι inhibition using specific inhibitors or the knockdown of its expression using *si*RNA significantly induces apoptosis, and reduces the migration and invasion of melanoma. Interestingly, this data demonstrated that PKC-ι inhibition not only affected the pathways regulated by PKC-ι, but also downregulated its protein expression on melanoma cells (Fig. 4.3). The data suggest that PKC-ι plays a role in a self-propagating cycle in melanoma cells, as observed in some other cycles related to cancer growth, such as TGFβ and CD147 (218). We

78

therefore designed further experiments to investigate the role of PKC-ι in its expression regulatory mechanisms in melanoma cells (144).

Transcription factors (TFs) play a key role in gene expression, controlling the rate of transcription of genetic information from DNA to messenger RNA by binding to a specific DNA sequence. Various cytokines often trigger such signaling. In this chapter, we sought to determine which transcription factors are the main regulators of PKC-ι expression in melanoma cells, giving emphasis to cytokine stimulation and expression.

We report the effects of the systematic silencing of PKC-ι, NF-κB, c-Jun and FOXO1 on PKC-ι levels in relation to NF-κB, PI3K/AKT/FOXO1, JNK/c-Jun and signal transducer and activator of transcription (STAT) signaling, along with cytokine production, to establish the mechanism of PRKCI (PKC-ι gene) regulation.

The PRKCI gene is located on chromosome 3 (3q26.2), a region identified as an amplicon with the tendency to undergo replication events (219). To determine TFs which regulate the PRKCI gene, a specific sequence was selected that includes the PRKCI promoter with a motif feature, promoter flank and an enhancer. This area provides the optimal platform for TFs to bind to regulate the transcription. Possible TF bindings were predicted using two different systems: PROMO and Genomatix Matinspector. Through these, we identified 5 TFs, including FOXO1 and c-Jun. We systematically silenced these TFs to analyze the downstream effect on PKC-ι expression (144).

The levels of both phosphorylated and total PKC-ι increased upon FOXO1 knockdown by *si*RNA and decreased upon the knockdown of c-Jun by *si*RNA. The results confirmed that c-Jun acts as a transcriptional activator and that FOXO1 acts as a transcriptional suppressor of PRKCI expression. Going forward, we establish the roles that these TFs play in an inflammation cycle that governs

79

PKC-ι expression and is dependent on PKC-ι for the cycle to continue. Furthermore, we established that major signaling pathways such as PI3K/AKT/FOXO1 and JNK/c-Jun play a vital role in regulation of PKC-ι expression. In addition, the cytokines interleukin (IL)-6 and IL-8 promote PKC-ι expression, thereby enhancing NF-κB activity, producing more cytokines as a part of a cycle such cancers use to develop and spread. IL-17E and intercellular adhesion molecule 1 (ICAM-1) induce FOXO1 to subdue PKC-ι expression. Overall, these results suggest that PKC-ι plays a central role in melanoma progression with a complex and tightly regulated expression profile. The specific inhibition of PKC-ι can disrupt its own regulatory cycle, leading to the disruption of its oncogenic role in melanoma (144).

6.1.1 c-Jun and FOXO1

c-Jun is a TF that combines with activator protein 1 (AP-1) and c-Fos to form an early response TF complex (220). c-Jun is activated by phosphorylation at S63 and S73 by c-Jun N-terminal kinases (JNKs), and c-Jun expression is regulated by various extracellular stimuli, such as cytokines (221). Extracellular signal-regulated kinase (ERK) increases c-Jun transcription (222). c-Jun is the first discovered oncogenic TF that is associated with metastatic breast cancer, non-small cell lung cancer and several other types of cancer (223–225). Phosphorylation at S63 and S73 activates c-Jun, thereby increasing transcription of c-Jun targeted genes. c-Jun promotes the oncogenic transformation of 'ras' and 'fos' in several types of cancer (226,227). Moreover, FOXO1 regulates gluconeogenesis, insulin signaling and adipogenesis. Phosphorylation plays a key role in the function of FOXO1 (228,229). AKT phosphorylates FOXO1 at T24, which causes FOXO1 to drive nuclear exclusion, leading to ubiquitination (230,231). Therefore, the phosphorylation of FOXO1 is an indication of its downregulation. FOXO1 is a well-known, bona

fide tumor suppressor (232–234). It plays a regulatory role in both the intrinsic and extrinsic pathways of apoptosis in many types of cancer, exhibiting an association between FOXO dysregulation and cancer progression (235,236). Furthermore, the overexpression of FOXO1 decreases cancer cell proliferation and inhibits migration and tumorigenesis. *In-vitro* and *in-vivo* experiments have proven this tumor suppressing activity (237). Importantly, FOXO1 can also be downregulated by ERK1/2 and PKC-ι, in addition to AKT (234). In the current study, we demonstrate that, due to PKC-ι inhibition, the availability of active PKC-ι decreases so that it becomes ineffective at deactivating FOXO1 through phosphorylation. Importantly, this is one of the direct involvements of PKC-ι in its own expression regulation and PKC-ι inhibition that leads to continuous upregulation of FOXO1.

6.2 Results

The specific sequence of the PRKCI gene (chromosome 3; 170220768-170225128), which was selected to contain the promoter, promoter flank, enhancer and a motif feature, was 4,360 bp in length. The promoter allows TFs to bind and initiate transcription, and the enhancer is a regulatory region in the flank that facilitates TF binding. We narrowed down possible hits by allowing only TFs, which can bind within a dissimilarity margin ≤10%, thereby achieving high specificity. We obtained approximately 70 TF hits to the given target after comparing the outcomes of PROMO analysis and Genomatix Matinspector. c-Jun, interferon regulatory factor 9 (ISGF3), paired box gene 3 (PAX3), Early growth response protein 1 (EGR1) and FOXO1 were selected as the top 5 TFs with the highest binding probability to the selected sequence of the PRKCI gene (144).

FOXO1 and c-Jun stand out as the main transcriptional regulators of PKC-ι expression in melanoma cells. As shown in Figure 6.1, the results of Western blot analysis revealed that transfection with each *si*RNA for EGR1, FOXO1 and c-Jun significantly reduced expression levels of these proteins. Figure 6.2 illustrates the densitometry analysis for the Western blots on Figure 6.1. The *si*RNA for EGR1 decreased the expression of EGR1 by 72% ($P \leq 0.05$) and 76% ($P \leq 0.05$) in the SK-MEL-2 and MeWo cells, respectively. The *si*RNA of FOXO1 decreased the expression of FOXO1 by 87% ($P \leq 0.05$) and 83% ($P \leq 0.05$), while the levels of phospho FOXO1 (T24) decreased by 75% ($P \leq 0.05$) and 73% ($P \leq 0.05$) in the SK-MEL-2 and MeWo cells, respectively. The *si*RNA of c-Jun decreased the expression of c-Jun by 82% ($P \leq 0.05$) and 73% ($P \leq 0.05$), while the levels of phospho c-Jun (S73) decreased by 76% ($P \leq 0.05$) and 67% ($P \leq 0.05$) in the SK-MEL-2 and MeWo cells, respectively. These results suggested that transfection with each of the *si*RNAs knocked down the expression of its respective target. Only the knockdown of FOXO1 and c-Jun was found to have an effect on the levels of total and phosphorylated PKC-ι (T555) in both cell lines. The knockdown of FOXO1 by *si*RNA increased the expression of total PKC-ι by 34% ($P \leq 0.05$) and 24% ($P \leq 0.05$), while it increased the level of phospho PKC-ι (T555) by 28% ($P \leq 0.05$) and 32% ($P \leq 0.05$) in the SK-MEL-2 and MeWo cells, respectively. The knockdown of c-Jun by *si*RNA decreased the expression of total PKC-ι by 17% ($P \leq 0.05$) and 16% ($P \leq 0.05$), and decreased the level of phospho PKC-ι (T555) by 21% ($P \leq 0.05$) and 17% ($P \leq 0.05$) in the SK-MEL-2 and MeWo cells, respectively. The knockdown of the expression of the TFs, ISGF3, EGR1 and PAX3, by *si*RNA was not found to have a significant effect on the expression of total and phosphorylated PKC-ι (T555) in both cell lines. Therefore, a decision was made to omit ISGF3, EGR1 and PAX3, and only FOXO1 and c-Jun were selected for use in the subsequent experiments. As shown in Figure 6.1, only the EGR1 negative results were included (144).
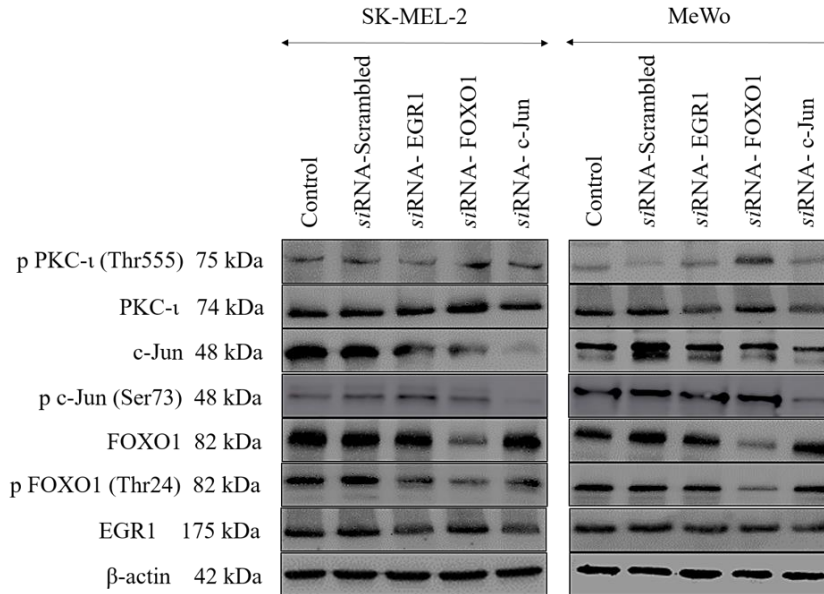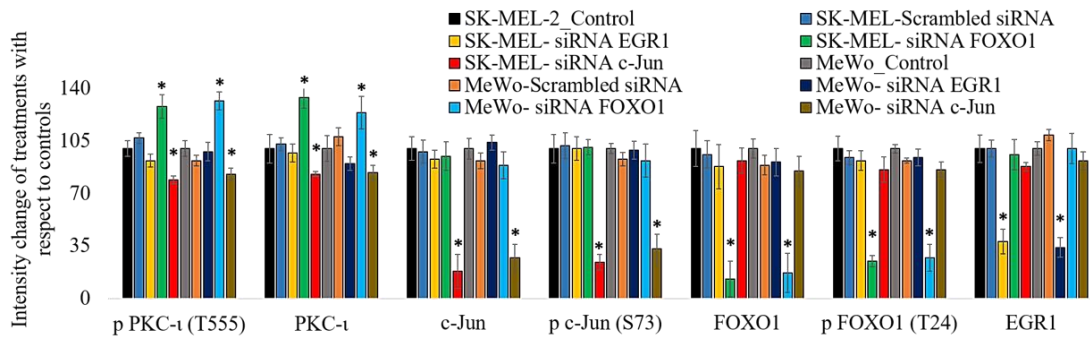
Figures 6.1 and 6.2: Effects of RNA interference (*si*RNA) of the transcription factors of EGR1, FOXO1 and c-Jun on the expression of PKC-ι and targeted transcription factors in melanoma cells (SK-MEL-2 and MeWo). Fig. 6.1 shows the expression of the protein levels of phosphorylated PKC-ι (T555), total PKC-ι, c-Jun, phosphorylated c-Jun (S73), FOXO1, phosphorylated FOXO1 (T24) and EGR1 for the *si*RNA knockdown of the expression of EGR1, FOXO1 and c-Jun (20 nM of each *si*RNA for 48 h) for SK-MEL-2 and MeWo cell lines. Total protein (80 µg) was loaded into each well and β-actin was used as the internal control in each western blot. Fig. 6.2 shows the densitometry values for the western blots in 6.1. Experiments (*N*=4) were performed in each trial and representative bands are shown. Densitometry values are reported as the means ± SD. Statistical significance is indicated by an asterisk (*$P \leq 0.05$).

83

6.3 Amplification Plot

6.4 Melt Curve Plot
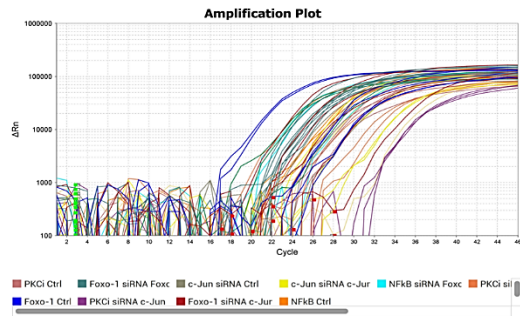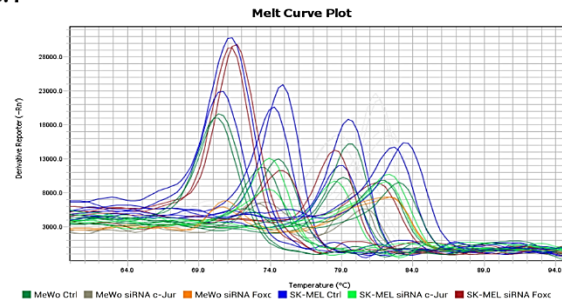
6.5
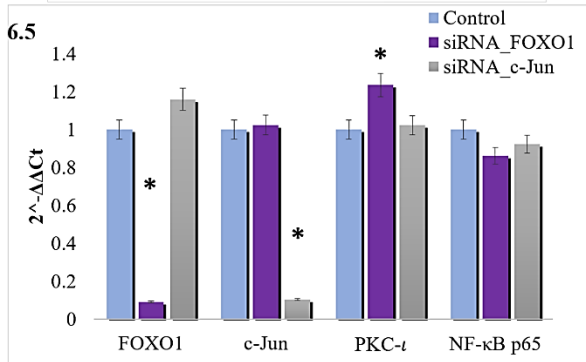
6.6
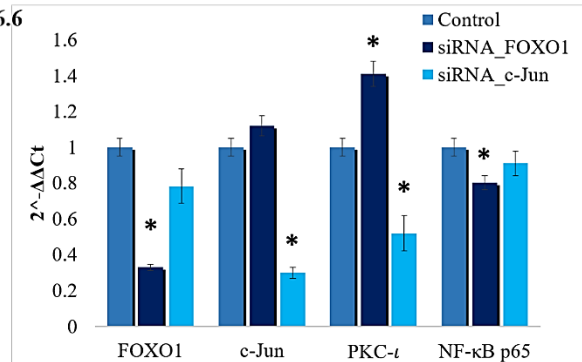
Figures 6.3-6.6: RT-qPCR analysis of *si*RNA knockdown of FOXO1 and c-Jun for SK-MEL-2 and MeWo cells. mRNA levels of FOXO1, c-Jun, PKC-ι, NF-κB p65 were plotted against β-actin as the internal control. Fig. 6.3 shows the amplification plots for the targets and melt curves (Fig. 6.4) of the RT-qPCR analysis for tested primers for SK-MEL-2 and MeWo cells, respectively. Quantitative data for the amplification plots shown in (Fig. 6.5 and 6.6) for the SK-MEL-2 and MeWo cells, respectively. Experiments (N=3) were performed in each cell lines and the means ± SD are plotted. Statistical significance is indicated by an asterisk ($^*P \leq 0.05$).

84

As shown in qPCR (Fig. 6.3, 6.5 and 6.6), the mRNA level of FOXO1 significantly decreased by 90.8% and 67.3% in the SK-MEL-2 and MeWo cells, respectively, following transfection with FOXO1 *si*RNA. The mRNA level of c-Jun significantly decreased by 89.7% and 30.15% in the SK-MEL-2 and MeWo cells, respectively, following transfection with c-Jun *si*RNA. These data confirmed the efficiencies and specificities of the applied *si*RNAs. The RT-qPCR data revealed that the PKC-ι mRNA levels decreased (by 47.2%) following transfection with *si*RNA for c-Jun in the MeWo cells, even though the PKC-ι levels in the SK-MEL-2 cells were not significantly altered. On the other hand, the PKC-ι mRNA levels were significantly increased by 23.5% and 42% in the SK-MEL-2 and MeWo cells transfected with FOXO1 *si*RNA, respectively. Therefore, these RT-qPCR results agree with the protein expression, which is shown in Figure 6.1. These results indicate that the downregulation of FOXO1 expression enhances PKC-ι expression, while the silencing of-Jun expression reduces PKC-ι expression. This indicates that FOXO1 downregulates the expression of PKC-ι and c-Jun upregulates PKC-ι expression in melanoma cells *in-vitro*.

FOXO1 holds the key to PKC-ι expression in melanoma cells. As shown in Figures 6.7 and 6.8, the results of Western blot analysis revealed that the knockdown of the expression of NF-κB by *si*RNA significantly decreased the levels of phosphorylated PKC-ι by 23% ($P \leq 0.05$) and 18% ($P \leq 0.05$) in the SK-MEL-2 and MeWo cells, respectively. The levels of total PKC-ι significantly decreased by 14% ($P \leq 0.05$) and 12% ($P \leq 0.05$) in the SK-MEL-2 and MeWo cells, respectively. Of note, FOXO1 expression increased by 17% ($P \leq 0.05$) and 18% ($P \leq 0.05$) in the SK-MEL-2 and MeWo cells, whereas the levels of phosphorylated FOXO1 decreased in the cells transfected with NF-κB *si*RNA. As we have reported previously in Chapter 4, the inhibition of PKC-ι significantly downregulated the PI3K/AKT pathway, thereby suppressing the activation of AKT.

Phosphorylated AKT (S473) phosphorylates FOXO1 to cause nuclear exclusion and thereby the degradation of FOXO1. This explains the elevated levels of active FOXO1 that are due to the downregulation of phospho AKT upon the downregulation of NF-κB caused by PKC-ι knockdown by *si*RNA. As shown in Figures 6.7 and 6.8, silencing NF-κB led to decrease the levels of phosphorylated AKT (S473) by 13% ($P \leq 0.05$) and 11% ($P \leq 0.05$) in the SK-MEL-2 and MeWo cells, respectively. Notably, the levels of phosphorylated c-Jun (S73) and total c-Jun were not significantly altered upon NF-κB knockdown. Similar results were obtained with NF-κB inhibition using a well-known NF-κB inhibitor, JSH-23 (100 nM).

Results of enzyme-linked immunosorbent assay (ELISA) confirm an interplay between the PI3K/AKT, JNK, NF-κB and STAT signaling pathways upon PKC-ι inhibition to coordinate the regulation of its expression (Fig. 6.9 and 6.10). ICA-1T (1 μM) was used to specifically inhibit PKC-ι, which allowed to obtain a broad picture of how multiple pathways may influence melanoma cells *in-vitro* as a result of PKC-ι inhibition related to PKC-ι regulation. Immuno paired antibody detection (IPAD) assay is an array-based ELISA allowing the simultaneous detection of multiple proteins. As shown in Figures 6.9 and 6.10, Caspase-3, CD44 antigen (CD44), CCAAT/enhancer-binding protein homologous Protein (CHOP), E-cadherin, IκBα, Myc, NOTCH, phospho eukaryotic translation initiation factor 4E-binding protein 1 (p-4E-BP1) (T37/46), p-AKT (S473), p-β-catenin (S33/37), p-HER3 (Y1289), phospho insulin receptor substrate 1 (p-IRS-1) (S1101), phospho jun N-terminal kinase (p-JNK) (T183), p-MEK1 (S217/221), p-mTOR (S2448), p-NF-κB p65 (S536), p-SMAD1 (S463), p-SMAD2 (S465/467), phospho signal transducer and activator of transcription (p-STAT3) (Y705), p-STAT5 (Y694), phospho yes-associated protein 1 (p-YAP1) (S127), phospho zeta-chain-associated protein kinase 70 (p-ZAP70) (Y493), cyclin-dependent kinase inhibitor 1 (p21) and PARP levels were reported

86

upon ICA-1T treatments against the controls for both cell lines. The caspase-3, E-cadherin, p-NF-κB p65 (S536), p-ZAP70 (Y493) and p21 levels significantly increased upon PKC-ι inhibition, while the CD44, p-4E-BP1 (T37/46), p-AKT (S473), p-IRS-1 (S1101), p-STAT3 (Y705), p-STAT5 (Y694), p-YAP1 (S127) and PARP levels significantly decreased (Fig. 6.9 and 6.10).
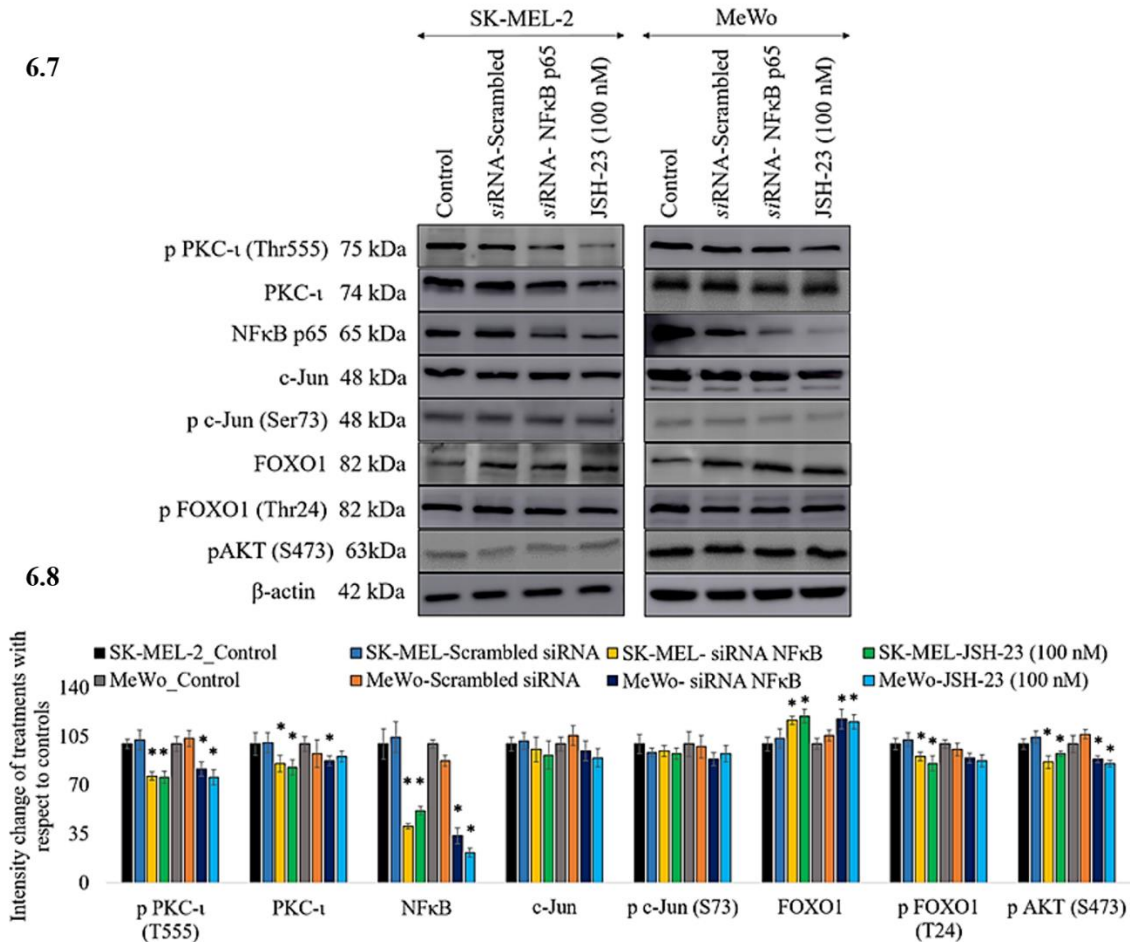
Figures 6.7 and 6.8: Effects of RNA interference (*si*RNA of the transcription factor NF-κB) and NF-κB inhibitor JSH-23 on the expression of PKC-ι and targeted transcription factors in melanoma cells (SK-MEL-2 and MeWo). Fig. 6.7 shows protein levels of phosphorylated PKC-ι (T555), total PKC-ι, NF-κB p65, c-Jun, phosphorylated c-Jun (S73), FOXO1, phosphorylated FOXO1 (T24) and phosphorylated AKT (S473) for the *si*RNA knockdown of the expression of NF-κB (20 nM of each *si*RNA for 48 h) and JSH-23 treatments (100 nM) for SK-MEL-2 and MeWo cell lines. Total protein (80 µg) was loaded into each well and β-actin was used as the internal control in each western blot. Fig. 6.8 shows the representative densitometry values for the western blots in Figure 6.7. Experiments (*N*=4) were performed in each trial and representative bands are shown. Densitometry values are reported as the means ± SD. Statistical significance is indicated by an asterisk ($^{*}P \leq 0.05$).
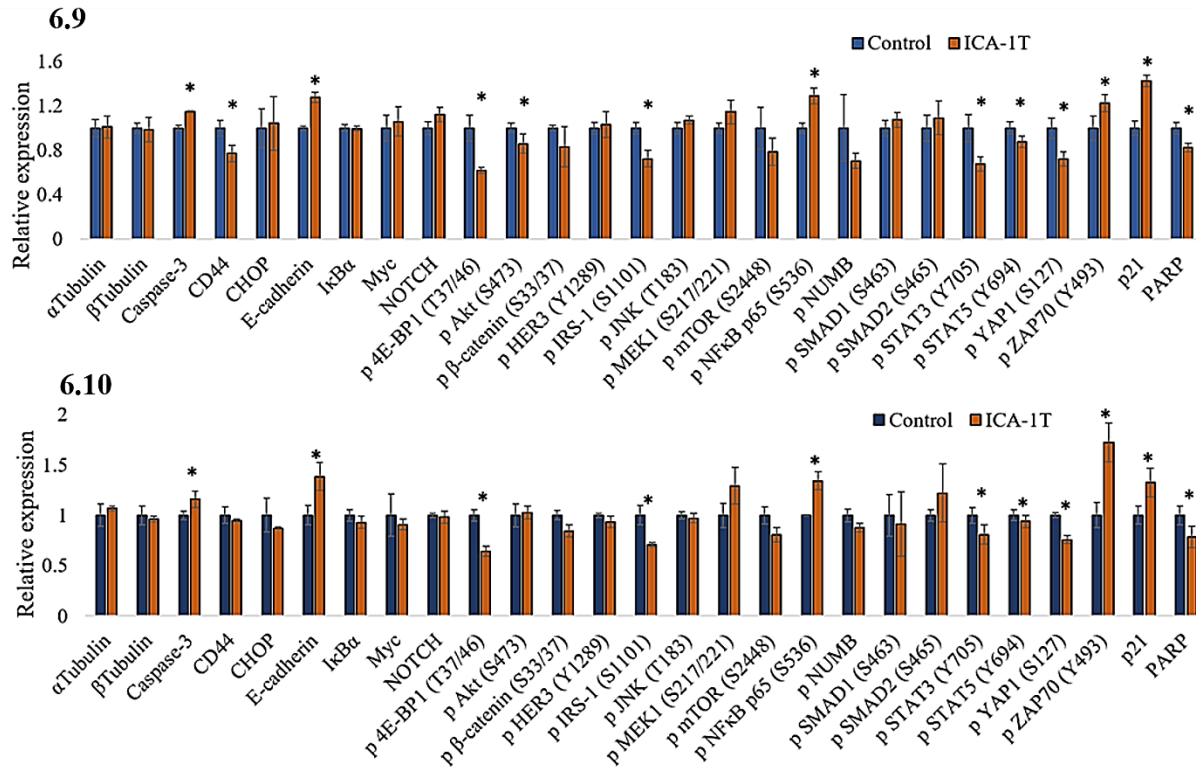
Figures 6.9 and 6.10: Immuno paired antibody detection assay (IPAD) for melanoma cells (SK-MEL-2 and MeWo). Fig. 6.9 and 6.10 shows the expression of IPAD assay targets for SK-MEL-2 and MeWo cell lines, respectively. Approximately 1×10^5 cells were cultured in T75 flasks and 24 h post-plating, fresh medium was supplied and the cells were treated with either volume of sterile water (control) or IC_{50} concentration of ICA-1T (1 μM). Additional doses were supplied every 24 h during a 3-day incubation period. The cells were then lysed and prepared lysates with the final total protein concentration to be >2 µg/ml and then sent them to ActivSignal, LLC facility to conduct the IPAD assay. IPAD platform is a proprietary multiplexed ELISA technology for analyzing the activity of multiple signaling pathways in one reaction. Activities of multiple signaling pathways were monitored simultaneously in a single well through assessing the expression or protein phosphorylation of 25 target human proteins, such as Caspase-3, CD44, CHOP, E-cadherin, IκBα, Myc, NOTCH, p-4E-BP1, p-AKT (S473), p-β-catenin, p-HER3, p-IRS-1, p-JNK, p-MEK1, p-mTOR, p-NF-κB, p-NUMB, p-SMAD1, p-SMAD2, p-STAT3, p-STAT5, p-YAP1, p-ZAP70, p21 and PARP. α-tubulin and β-tubulin were used as internal controls in each trial. Experiments (N=3) were performed in each cell lines and the means ± SD are plotted. Statistical significance is indicated by an asterisk ($^*P \leq 0.05$).
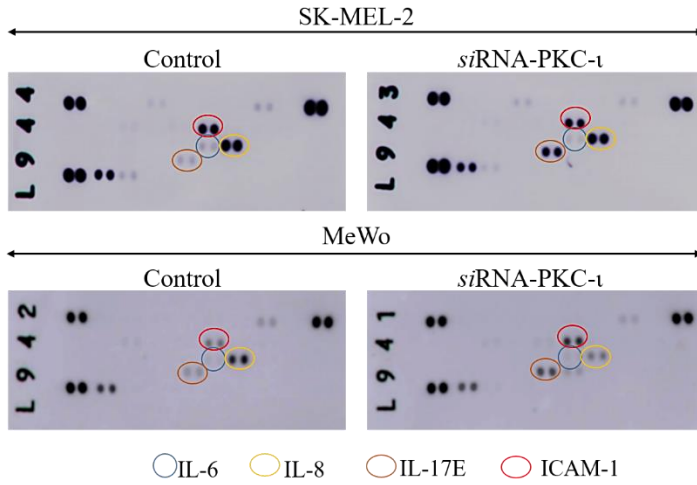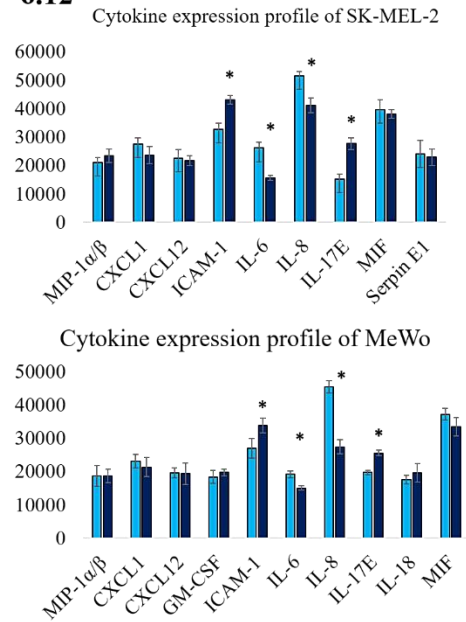
Figures 6.11 and 6.12: Cytokine expression analysis of melanoma cells upon PKC-ι knockdown of expression. Fig. 6.11 shows the Western blot array of the PKC-ι silenced SK-MEL-2 and MeWo cells against the controls. Fig. 6.12 shows the quantified results of the western blots shown in 6.11 for the SK-MEL-2 and MeWo cells, respectively. IL-6, IL-8, IL-17E, ICAM-1, CXCL-1, CXCL-12, GM-SCF, MIF and Serpin were found in detectable levels in western blot analysis for the two melanoma cell lysates. Experiments ($N=3$) were performed in each cell lines and the means ± SD are plotted. Statistical significance is indicated by an asterisk ($^*P \leq 0.05$).
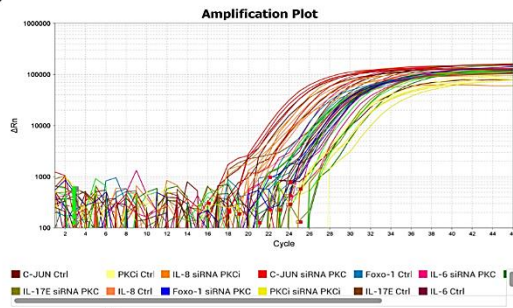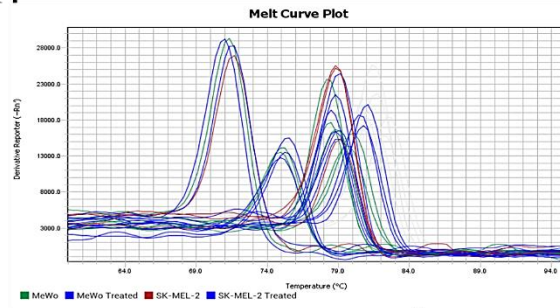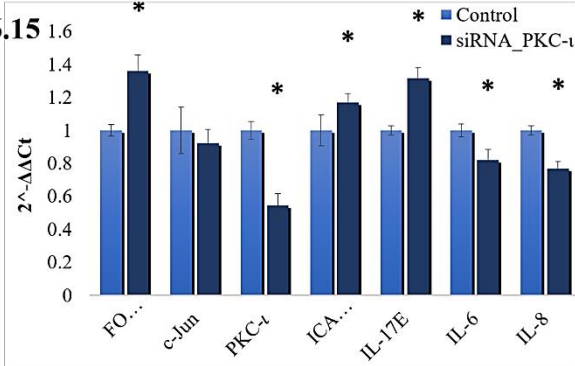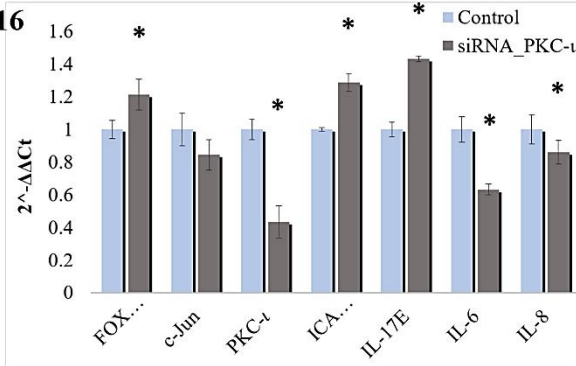
Figures 6.13-6.16: RT-qPCR analysis of cytokines (IL-6, IL-8, IL-17E and ICAM-1), FOXO1, c-Jun for PKC-ι *si*RNA knockdown in SK-MEL-2 and MeWo cells. Fig. 6.13 amplification plots of the said markers for SK-MEL-2 and MeWo cells, respectively. Fig. 6.14 indicates the melt curves of the RT-qPCR analysis for tested primers for SK-MEL-2 and MeWo cells, respectively. Fig. 6.15 and 6.16 show the quantitative data for the amplification plots shown in Fig. 6.13. Experiments (*N*=3) were performed in each cell lines and the means ± SD are plotted. Statistical significance is indicated by an asterisk (*$P \leq 0.05$).

IL-6, IL-8, IL-17E and ICAM-1 may participate in PKC-ι regulation in an autocrine manner through transcriptional activation/deactivation. As shown in Figures 6.11 and 6.12, the Western blot cytokine expression profile for the two melanoma cell lysates exhibited a significant decrease in the levels of IL-6 and IL-8, while the levels of IL-17E and ICAM-1 increased in the cells transfected with PKC-ι *si*RNA (*si*RNA for PKC-ι, 20 nM) compared to the control (scrambled *si*RNA, 20 nM). C-X-C motif chemokine (CXCL)-1, CXCL-12, granulocyte-macrophage colony-stimulating factor (GM-SCF), macrophage migration inhibitory factor (MIF) and Serpin were also found in detectable levels, although these were not significantly altered due to PKC-ι knockdown. The results of the RT-qPCR analysis of the same lysates are shown in Figure 6.13. Since only IL-6, IL-8, IL-17E and ICAM-1 exhibited a significant change in expression upon PKC-ι silencing by *si*RNA, they were only tested for those mRNA levels in the RT-qPCR experiments. As demonstrated in Figures 6.15 for SK-MEL2 and 6.16 for MeWo cell line, RT-qPCR data revealed how the mRNA levels of PKC-ι significantly decreased by 35.6% and 56.7% in the SK-MEL-2 and MeWo cells, respectively following transfection with PKC-ι siRNA. We observed a significant decrease in the mRNA levels of both IL-6 and IL-8, with a simultaneous significant increase in the levels of IL-17E and ICAM-1 upon the knockdown of expression of PKC-ι in both cell lines. In addition, we found that the FOXO1 mRNA levels increased significantly by 36.1% and 21.5% in the SK-MEL-2 and MeWo cells, respectively; the c-Jun mRNA levels decreased by 8% and 15.5% in the SK-MEL-2 and MeWo cells, respectively. These data confirm the association between PKC-ι, FOXO1 and c-Jun presented in Figures 6.1 and 6.3.

Figure 6.17 shows a schematic summary of the regulation of the expression of PKC-ι in melanoma based on the current and previous data. This model depicts the interactions between NF-κB, PI3K/AKT/FOXO1, JNK/c-Jun and STAT3/5 signaling pathways during PKC-ι regulation. It is

shown that PKC-ι plays a very important role in the regulation of its expression through the transcriptional activation/deactivation of c-Jun and FOXO1. PKC-ι is overexpressed as a result of c-Jun transcriptional activity with the help of pro-survival, oncogenic PI3K/AKT, NF-κB, STAT3/5 signaling cascades in melanoma cells. Specific inhibitors of PKC-ι initiates a disruption to rapid PKC-ι expression cycle where the reduced activity of PKC-ι downregulates the NF-κB pathway and its transcriptional activity thereby decreases the expression of IL-6 and IL-8. The activity of AKT decreases as a result of lacking the stimulation from cytokines, such as IL-6, IL-8 and TNF-α, which leads to the upregulation of FOXO1, which turns out to be the most important TF regulating PKC-ι expression after the disruption initiated as a result of PKC-ι inhibition. FOXO1 negatively regulates the expression of PKC-ι and also diminishes the JNK activity to retard its activation of c-Jun which serves as the transcription component which upregulates PKC-ι expression. This process continues and leads to the further downregulation of NF-κB and c-Jun. Therefore, the upregulation of FOXO1 leads to the continuation of the diminution of PKC-ι expression. As a result, the total PKC-ι level decreases in melanoma cells. These findings strongly support our previous data where a reduction in total PKC-ι levels was observed upon the specific inhibition using PKC-ι inhibitors, such as ICA-1T and ICA-1S.
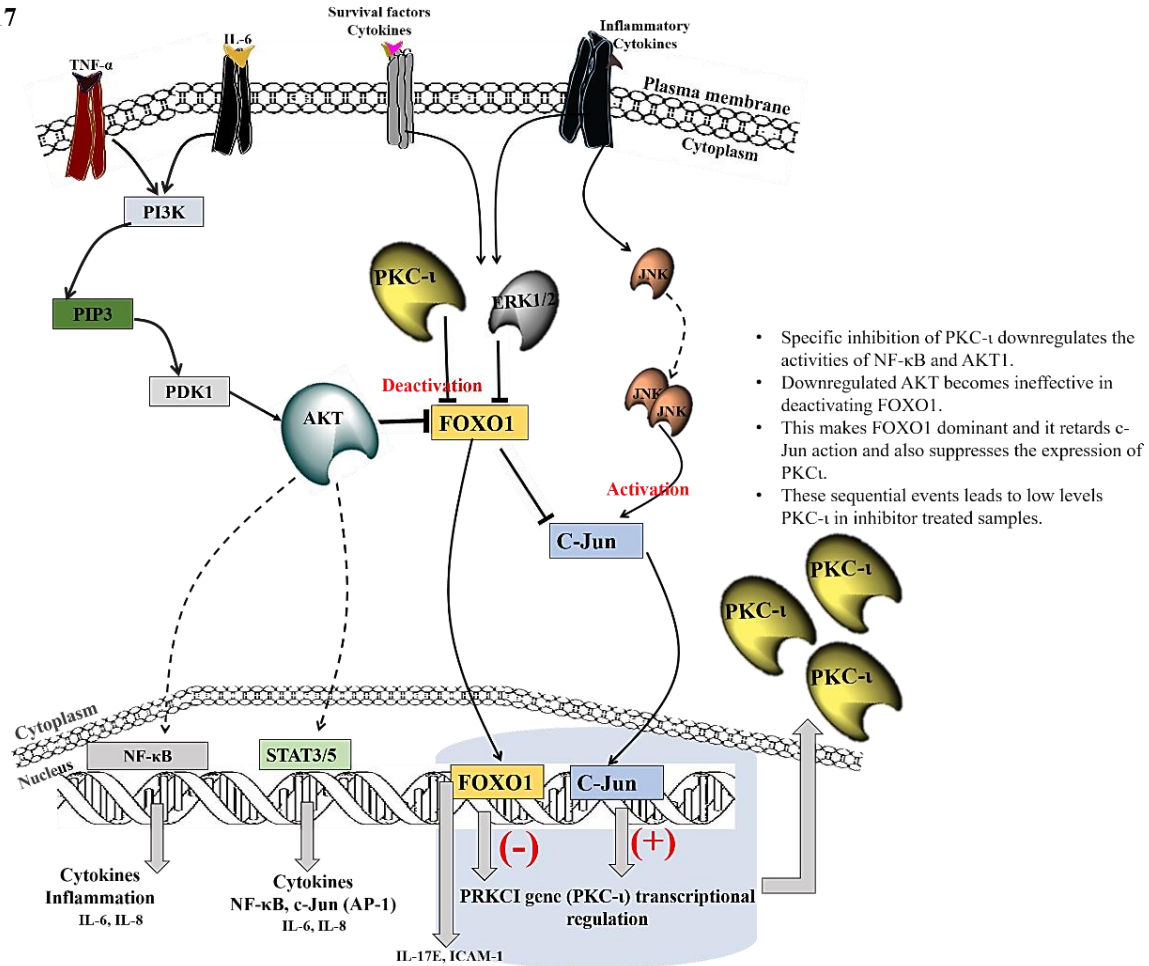
Figure 6.17: A schematic summary of the regulation of the expression of PKC-ι in melanoma. This model depicts the interactions between NF-κB, PI3K/AKT/FOXO1, JNK/c-Jun and STAT3/5 signaling pathways during the PKC-ι regulation. PKC-ι plays an important role in the regulation of its own expression in an intricate signaling web through c-Jun and FOXO1. PKC-ι is overexpressed in melanoma cells due to elevated transcriptional activity of c-Jun with the aid of PI3K/AKT, NF-κB, STAT3/5 signaling. The specific inhibition of PKC-ι initiates a disruption to rapid PKC-ι expression cycle in melanoma where the reduced activity of PKC-ι downregulates the NF-κB pathway and its transcriptional activity, which in turn diminishes the expression of IL-6/8. As a result of this AKT activity reduction, FOXO1 gets upregulated. FOXO1 turns out to be the most important TF regulating PKC-ι expression after the disruption initiated as a result of PKC-ι inhibition. Dominant FOXO1 negatively regulates the expression of PKC-ι and also diminishes the JNK activity to retard its activation of c-Jun. We found c-Jun as the transcription component that upregulates PKC-ι expression. The downregulation of IL-6 and IL-8 expression leads to the lessened STAT3/5 signaling, which causes c-Jun transcriptional reduction. This whole process continues and leads to the further downregulation of NF-κB, AKT and JNK/c-Jun while upregulating FOXO1, which leads to the continuation of the attenuation of PKC-ι expression. As a result, the total PKC-ι level decreases in melanoma cells.

6.3 Summary

On the other hand, our previous data showed that PKC-ι inhibition significantly downregulated the PI3K/AKT pathway, thereby suppressing the activation of AKT. In this Chapter, we discussed the mechanism for the downregulation of NF-κB, which reduces the activity of AKT upon PKC-ι inhibition. PKC-ι inhibition affects FOXO1, as shown by the significantly higher levels of total FOXO1, while a reduction in its phosphorylated levels was observed, suggesting that NF-κB downregulation upregulates FOXO1 activity. The elevated levels of FOXO1 negatively influenced PKC-ι expression and phosphorylation as shown in Figures 6.7 and 6.8 as a result of NF-κB depletion. This further confirms our previous observations with PKC-ι inhibition with ICA-1T and ICA-1S (Fig. 4.1), where total PKC-ι, phosphorylated PKC-ι, NF-κB activation and activated AKT (S473) were significantly reduced. These results could be due to the tight regulation of PKC-ι expression by FOXO1, which retards PRKCI from transcription. Such results confirmed that FOXO1 is a major regulator which suppresses the expression of PKC-ι regulation. Of note, the c-Jun and phosphorylated c-Jun (S63) levels were not significantly altered as a result of NF-κB *si*RNA knockdown. This advocates that NF-κB downregulation does not affect PKC-ι expression through c-Jun. Instead, c-Jun protects cancer cells from apoptosis by cooperating with NF-κB to prevent apoptosis upon TNF-α stimulation (220). Our data in Chapter 4 showed how TNF-α upregulates NF-κB, phospho AKT and PKC-ι expression in these two melanoma cell lines (Fig 4.5 and 4.6). However, the data from the current experiment suggest that the TNF-α downstream target is mainly FOXO1, where it 'switches off' through the phosphorylation of elevated AKT. The inhibition of PKC-ι diminishes this AKT activation, thereby upregulating FOXO1 activity.

On the other hand, our systematic silencing of c-Jun, FOXO1 and EGR1 revealed that (Fig. 6.1 and 6.2 for Westerns blots and 6.3, 6.4 and 6.5 for qPCR) c- Jun also seemed to regulate PKC-ι

expression, apart from FOXO1. To explain the crosstalk between these cell signaling pathways in relation to PKC-ι regulation, we conducted two other *in-vitro* experiments, ELISA using IPAD assay and a cytokine array. These findings demonstrated links between PKC-ι expression with the cytokines, IL-6, IL-8, IL-17E and ICAM-1, along with some other key cellular signaling points.

As shown in Figures 6.9 and 6.10, the IPAD ELISA data revealed a significant increase in the levels of Caspase-3, E-cadherin, p-NF-κB p65 (S536), p-ZAP70 (Y493) and p21 levels upon PKC-ι inhibition, while the levels of CD44, p-4E-BP1 (T37/46), p-AKT (S473), p-IRS-1 (S1101), p-STAT3 (Y705), p-STAT5 (Y694), p-YAP1 (S127) and PARP levels significantly decreased. We have already shown in previous Chapters (Chapter 4), using various apoptotic markers, that PKC-ι inhibition induced the apoptosis of melanoma cells (Fig. 4.1 and 4.3). This is again evident from increases in the levels of Caspase-3 and the cleavage of PARP in the IPAD assay. Additionally, PKC-ι inhibition delayed EMT in melanoma and we observed elevated levels of E-cadherin with downregulation of Vimentin and CD44 expression. Therefore, this IPAD assay provided additional data for the results we have shown in Chapter 4. Phosphorylation at S536 on the NF-κB p65 transactivation domain is an indication of dimerization of NF-κB subunits. Since PKC-ι inhibition downregulates NF-κB translocation to the nucleus, phospho NF-κB levels increase in order to diminish the effect of PKC-ι inhibition. However, elevated FOXO1 does not allow NF-κB to take over the control since it is missing the crucial assistance needed from PKC-ι due to its inhibition from ICA-1T and ICA-1S inhibitors. Aberrant STAT3/5 activity has been shown to be connected to multiple types of cancer (238–243). The cytokines, IL-6 and IL-5, are known to upregulate STAT signaling, which induces cell survival in many types of cancers (238,239,244). Upregulated STAT3 increases the transcription of c-Jun (238,245). Our IPAD results indicated that STAT3 and STAT5 activities were downregulated due to PKC-ι inhibition, suggesting that c-Jun expression

95

can be retarded. Few studies, including the one by Hornsveld *et al*. provided connections between the JNK pathway and FOXO1, elaborating its tumor suppressing features for weakening JNK activity (234,246,247). However, JNK activates c-Jun. The data from our Western blot and RT-qPCR analysis demonstrated that c-Jun depletion diminished PKC-ι expression, which suggested that c-Jun acts as an activator of PKC-ι expression. It is therefore evident that both FOXO1 and c-Jun are involved in regulating PKC-ι expression. The results suggest that FOXO1 plays a major role over c-Jun only upon PKC-ι inhibition, possibly through multiple mechanisms, such as the reduction of JNK signaling, retarding PKC-ι expression and cell cycle arrest. Upregulated FOXO1 is well known to induce cell cycle arrest by promoting the transcription of cell cycle kinase inhibitors or cyclin-dependent kinase inhibitor (CKI). p21 and p27 are two of the most well-known downstream CKIs induced by FOXOs (234,246). Notably, FOXO1 is also believed to induce anoikis, which is apoptosis that occurs when cells detach from the extracellular matrix. Our IPAD-ELISA results revealed significantly elevated levels of p21 by approximately 25% in both cell lines, suggesting that the inhibition of PKC-ι induces cell cycle arrest through FOXO1. This is another indirect downstream effect of PKC-ι involvement in its expression where inhibition of PKC-ι enhances FOXO1 anti-tumor activity.

As shown in Figure 6.17, our results summarize that PRKCI expression is negatively regulated by FOXO1 and positively regulated by c-Jun. When PKC-ι is inhibited, the following series of downstream effects take place. The downregulation of NF-κB activity decreases the levels of phospho AKT (S473). As a result of a low activity of AKT along with diminished levels of PKC-ι, the phosphorylation of FOXO1 is reduced and therefore active FOXO1 (unphosphorylated FOXO1) levels are being elevated. Elevated FOXO1 suppresses PRKCI gene expression similar to 'switch off' effect. The downregulation of PKC-ι also diminishes STAT3/5 activity, as shown

96

by the IPAD assay data. STAT3 and STAT5 are known to upregulate the transcription of c-Jun and NF-κB (245,248). Therefore, it is evident that PKC-ι inhibition induces the downregulation of STAT3/5, which decreases the transcription and activation c-Jun. These data suggest that PKC-ι levels were decreased when c-Jun expression is silenced by *si*RNA (Fig. 6.1 and 6.2), and as shown by RT-qPCR in Figures 6.3, 6.5 and 6.6, the knockdown of PKC-ι decreased c-Jun mRNA expression, but not significantly.

As shown in Figures 6.11 and 6.12, further *in-vitro* experiments demonstrated changes in cytokine expression (IL-6, IL-8, IL-17E and ICAM-1) in melanoma cells upon PKC-ι knockdown. As shown by the results of both Western blot and RT-qPCR analyses, the protein levels of IL-6 and IL-8 (as well as their mRNA levels) decreased, while the levels of IL-17E and ICAM-1 increased significantly in both cell lines upon PKC-ι knockdown by *si*RNA. This suggests that the PKC-ι self-regulated expression cycle is involved in autocrine signaling. The cellular environment of a tumor, and in particular melanoma, is frequently exposed to various inflammatory factors and immune cells. The effect of these factors function to either promote chronic inflammation or engage in antitumor activity (249). Cytokines are examples of these inflammatory factors; they play an essential role in regulating tumor microenvironments (250). Cytokines utilize several signaling pathways to carry out their functions. They act to promote or dysregulate tumor progression and metastasis. Cytokines, such as CXCL-1, CXCL-12, IL-18, CXCL-10, IL-6 and IL-8 promote cancer progression by facilitating metastasis. CXCL1, also known as melanoma growth-stimulatory activity/growth-regulated protein α, is secreted by melanoma cells and is associated with roles in wound healing, angiogenesis and inflammation. In particular, it has been linked to tumor formation. High levels of CXCL10/CXCR3 expressed in melanoma have been linked to metastasis regulation (251). CXCL10 plays an important role in promoting tumor growth

97

and metastasis (252). CXCL12, also known as stromal-derived factor-1, utilizes the receptors CXCR4 and CXCR7. CXCL12 and its receptors have been linked to roles in regulating tumor metastasis. CXCL-1, CXCL-10, CXCL-12 and IL-18 levels were not significantly altered due to PKC-ι depletion.

IL-6 is a very important cytokine and contributes to the degradation of IκB-α, leading to the upregulation of NF-κB translocation. Our data indicated that PKC-ι stimulates NF-κB translocation through IκB-α degradation. The translocation of NF-κB to the nucleus induces cell survival through the transcription of various survival factors as well as other cytokines (104,238,244). IL-8 is an example of such a cytokine. IL-8 plays a role in regulating polymorphonuclear neutrophil mobilization. In melanoma, IL-8 has been attributed to extravasation, a key step in metastasis. Studies have shown that the expression of IL-8 in melanoma is regulated via NF-κB. When NF-κB is translocated to the nucleus, IL-8 expression increases, leading to the promotion of a more favorable microenvironment for metastasis (253,254). The results of this study indicated that both IL-6 and IL-8 expression levels decrease upon transfection with PKC-ι *si*RNA. As is summarized by the diagram in Figure 6.17, IL-6 expression is regulated by NF-κB, and IL-8 expression is regulated by both NF-κB and STATs. Our data justified how the PKC-ι inhibition/knockdown downregulates the NF-κB and STAT signaling pathways. The results suggested that IL-6 and IL-8 play an important role in upregulating PKC-ι expression, activating c-Jun, while deactivating FOXO1.

Some cytokines promote anti-tumor activity by utilizing an immune response. ICAM-1 plays a key role in the immune response, including antigen recognition and lymphocyte activation (255,256). ICAM-1 has been linked to the inhibition of tumor progression through the inhibition of the PI3K/AKT pathway. The inhibition of this pathway via ICAM-1 exposes tumor cells to

death via cytotoxic T-lymphocytes (256). Clinical research has also proven that, within the first 5 years of ovarian cancer diagnosis, ICAM-1 expression inhibition is associated with an increased risk of metastasis (255,256). Another anti-tumor cytokine is IL-17E. IL-17E belongs to a family of cytokines known as IL-17. In various forms of cancer, including melanoma and pancreatic cancers, treatment with recombinant IL-17E has been shown to decrease tumor growth (257,258). The upregulation of IL-17E is linked to the increased expression of TH17 cells. T cells, such as TH17 have been implicated in the inhibition of tumor-infiltrating effector T cells. The exact mechanism of IL-17E function in the anti-tumor effect has not been thoroughly explored (259). Notably, the results of our western blot and RT-qPCR analyses indicated that ICAM-1 and IL-17E protein and mRNA expression increased upon the silencing of PKC-ι by *si*RNA. This confirms that anti-tumor/pro-apoptotic signaling is upregulated upon the knockdown of oncogenic PKC-ι via an autocrine manner through IL-17E and ICAM-1. Moreover, the results suggest that IL-17E and ICAM-1 play an important downregulatory role in the regulation of PKC-ι expression along with FOXO1, opposite to c-Jun, IL-6 and IL-8.

In conclusion, our overall results demonstrate PKC-ι itself to play an important role in its expression in a complex signaling network through the transcriptional activation/ deactivation of c-Jun and FOXO1. The reduced activity of PKC-ι due to its specific inhibition, downregulates the NF-κB pathway and its transcriptional activity, which turns out to 'strike' the expression of IL-6 and IL-8. As a result, the activity of AKT decreases, which leads to the upregulation of FOXO1. FOXO1 is the most important TF regulating PKC-ι expression upon receiving stimulation from IL-17E and ICAM-1. FOXO1 negatively regulates the expression of PKC-ι, diminishing JNK activity to retard the activation of c-Jun. IL-6 and IL-8 expression are downregulated via PKC-ι-mediated NF-κB transcriptional activity reduction. This leads to STAT3/5 signaling

99

downregulation, reducing c-Jun expression. This whole process continues and leads to the further downregulation of NF-κB, c-Jun and upregulation of FOXO1, which leads to the continuation of the depletion of PKC-ι expression. As a result of this sequence of events, the total PKC-ι level decreases in melanoma cells, which began as a result of PKC-ι inhibition. These results indicate that PKC-ι is being regulated in a rather complex manner, which involves itself as a key component. PKC-ι inhibition leads to a decrease in its own production, and during this process, PKC-ι inhibition also triggers multiple anti-tumor/pro-apoptotic signaling. This makes PKC-ι one of the central key point of interest to specifically target and diminish as a means of treating melanoma *in-vitro*. Therefore, our overall results confirm that PKC-ι inhibition using specific and effective inhibitors, such as ICA-1T and ICA-1S, is significantly effective in the treatment of melanoma *in-vitro*. These inhibitors must test against more melanoma cell lines in-vitro and in-vivo studies must be done in order to solidify the results presented in this dissertation. The current results strongly suggest that PKC-ι is a prime novel biomarker that can be targeted to design and develop personalized and targeted therapeutics for melanoma.

100

CHAPTER 7

DISCUSSION AND FUTURE DIRECTIONS

7.1 Discussion

Identifying aPKC specific inhibitors is a great challenge due to a largely conserved carboxyl-terminal catalytic domain among the PKC superfamily as explained in Chapter 1. This similarity in the kinase domains is the pivotal factor placing them under one parent family. However, the amino-terminal regulatory domain differs between the subclasses, playing a vital role in secondary messenger binding, binding to the membrane and protein-protein interactions affecting PKC activation.

Atypical PKCs were first considered as a novel therapeutic target by Stallings-Mann *et al.* in 2006 (146). They screened ATM as a potent inhibitor of the interaction between the PB1 domain of PKC-ι and Par6. ATM, is currently in phase I clinical trial evaluation for lung cancer treatments and the outcome of the trials are unknown to date. Gunaratne *et al.* reported that both aPKCs interact with Par6 and thereby phosphorylate Par6 at S245 (215). This suggested that ATM may also interact with the complex of Par6 and PKC-ζ. However, Stallings-Mann *et al.* reported that ATM demonstrated a specificity on PKC-ι versus PKC-ζ by targeting the interaction between Par6 and PKC-ι (146). The ATM mechanism of action is not fully understood, and *in-vitro* results demonstrated off target effects (94,98).

101

Blázquez *et al.* tested calphostin C and chelerythrine against West Nile virus (WNV), in a cell culture system which significantly inhibit WNV multiplication without affecting cell viability. They reported that PKCs have also been implicated in different steps during viral replication (260). Calphostin C and chelerythrine are two wide range PKC inhibitors that target all three PKC classes. Results indicated that atypical PKCs are involved in WNV multiplication process which can be effectively retard using said inhibitors (260). Kim *et al.* reported the application of Echinochrome A as a cardiomyocyte differentiation agent in mouse embryonic stem cells. They investigated the potential use of Echinochrome A as an aPKC specific inhibitor and found that IC_{50} for PKC-ι is 107 μM under *in-vitro* kinase assay conditions. IC_{50} values for ICA-1T and ICA-1S were approximately 1 μM and 2.5μM, respectively. Molecular docking simulation results suggested a direct binding of Echinochrome A with PKC-ι (261). Another study by Kwiatkowski *et al.* identified an azaindole-based scaffold for the development of more potent and specific PKC-ι inhibitiors (262). They described a fragment based approach and introduced a new class of potential aPKC inhibitors based on azaindole (262). As indicated in earlier chapters PKC-ι and PKC-ζ are 84% homologous, make it difficult to identify specific inhibitors. In the current study, we targeted the amino acid residues 469-475 (glutamine, isoleucine, arginine, isoleucine, proline, arginine and serine). Data confirms the presence of a potentially druggable allosteric site in the structure of PKC-ι using the solved crystal structure of PKC-ι. The pocket is located in the C-lobe of the kinase domain of PKC-ι, which is framed by solvent exposed residues of helices αF-αI and the activation segment. Tested inhibitors were predicted to interact with this site with moderate-high affinity based on molecular docking. Experimental evidences based on kinase activity assay for ICA-1S and ICA-1T confirmed the affinity predicted for the identified allosteric site. Combinations of drugs targeting the ATP binding site and allosteric sites would be expected to

102

more effectively inhibit cancer cell growth since it will change the protein dynamics of PKC-ι both in kinase and regulatory domains. The other important characteristic of this approach is that it eliminates potential candidates that are capable of binding the ATP binding pocket (which is conserved between PKC isoforms). The identified allosteric hollow is a potential pocket within diverse structural elements in PKC-ι and also demonstrated ATP binding did not affect the drug binding, the predicted specificities were tested *in-vitro*. Kinase activity studies with MBP as an aPKC substrate confirmed the molecular docking predictions for their specificity and affinities. ζ-Stat demonstrated a mild activity against PKC-ι at the highest tested concentration (20 μM) and at the IC_{50} concentration used, it did not show a significant activity on PKC-ι. Therefore, data confirmed that ACPD and DNDA target both aPKCs while ICA-1T and ICA-1S target PKC-ι and ζ-Stat targets PKC-ζ.

Cytotoxicity determinations of the inhibitors to establish their therapeutic potential was very important. None of the inhibitors demonstrated a significant toxicity to normal melanocytes at the IC_{50} concentrations used for two melanoma cell lines. Importantly, all inhibitors displayed increased cytostatic properties rather than being toxic. These results indicate that inhibitors effectively arrest melanoma cell growth, differentiation and proliferation before they induce apoptosis. This confirms that malignant melanoma cells are highly dependent on aPKCs to remain viable, which was evident as seen by both melanoma cell lines overexpressing aPKCs compared to the undetectable PKC-ι and low levels of PKC-ζ in normal melanocytes.

Overexpression of aPKCs induces anti-apoptotic effects in many cancers (80,142,143,146). Apoptosis analysis for inhibitor treatments on melanoma cells demonstrated apoptotic stimulation upon aPKC inhibition.

103

An increase in PARP cleavage and Caspase-3, and a diminution in Bcl-2 all indicate apoptosis stimulation upon inhibition of both PKC-ι and PKC-ζ. Data showed that both aPKC inhibition retards the activity of PI3K/AKT mediated NF-κB activation, in which both aPKCs play a role in releasing NF-κB to translocate to the nucleus and promote cell survival. The data showed that aPKC inhibition increased the levels of IκB while decreasing the levels of phospho-IκB (S32) and phospho-IKKα/β (S176/180), confirming that both PKC-ι and PKC-ζ play a role in phosphorylation of IKKα/β and IκB: increased levels of IκB therefore remain bound to NF-κB complex and prevent the translocation to the nucleus to promote cell survival. TNF-α stimulation significantly increased NF-κB levels in both cytosol and nuclei but aPKC inhibition mitigated this effect significantly. The overall data confirms that both PKC-ζ and PKC-ι are embedded in cellular survival via NF-κB and PI3K/AKT pathways.

Our *in-vitro* migration and invasion assays for the two tested human melanoma cell lines demonstrated that both invasion and migration were markedly reduced by PKC-ι inhibition using PKC-ι specific inhibitors such as ICA-1T and ICA-1S. Moreover, the data confirmed that PKC-ι activates Par6 and induced the degradation of RhoA to stimulate the EMT in melanoma cells (Fig. 5.9). Also, IP, immunofluorescence and Western blot techniques demonstrated that PKC-ι strongly associates with Vimentin and actively participates in the phosphorylation at the S39 position, which is an important site of Vimentin, essential for Vimentin intermediate filament disassembly to facilitate increased migration of melanoma cells. Data showed that by inhibiting PKC-ι, the S39 phosphorylation decreases significantly in addition to total Vimentin expression. In addition, upon PKC-ι diminution we observed cells that are constricted, have a rounded in shape and tend to form cell colonies, which are all characteristics of epithelial phenotype behavior. However in Vimentin-rich mesenchymal conditions, Vimentin wraps around and control the distribution of microtubules

towards one direction to facilitate rear-front polarity. This is achieved as VIF assembles along microtubules to form a copy of the previously polarized microtubule network which has a slower rate of turn over. This is important as the orientation of microtubules is responsible for conferring the front-rear polarity that is characteristic of mesenchymal cells. Gan *et al.* showed that disruption of VIF network on microtubules leads to dramatic changes in the microtubule network and changes the polarity of cells (263). Ivaska *et al.* discussed the involvement of PKC-ε on phosphorylation of Vimentin and control of integrin recycling to facilitate cell motility. Integrins are heterodimeric cell surface receptors, which mediate cell adhesion and migration via cell to cell and cell to matrix interactions. Ivaska *et al.* discuss three major steps in motility; (I) formation of protrusion and new adhesion sites at leading edge (II) contraction of cell body (III) detachment from trailing end. Phosphorylation of Vimentin is central in regulation of these dynamics and Vimentin expression correlates with increased migration following EMT (195). Our data confirms that once PKC-ι is inhibited both PKC-ι and Vimentin expressions are decreased and E-cadherin expression is amplified suggesting a slowdown or a possible reversal of the EMT process. Once this happens, experimental results suggested that the cell shape changes to a more rounded shape and cell form colonies rather than showing individual mesenchymal behavior as seen in control samples.

As discussed in earlier Chapters, data showed that PKC-ι inhibition significantly downregulated the PI3K/AKT1 pathway, thereby suppressing the activation of AKT. Downregulation of NF-κB due to PKC-ι inhibition, results in downregulation of AKT. Data indicates that it increases total FOXO1 level, while reducing its phosphorylated FOXO1 levels. This suggested that NF-κB downregulation causes upregulation of FOXO1 activity as a result of PKC-ι inhibition. Therefore FOXO1 upregulation negatively influences PKC-ι expression and phosphorylation at T555. This further confirms our previous observations with PKC-ι inhibition with ICA-1T and ICA-1S, where

105

total PKC-ι, phosphorylated PKC-ι, NF-κB activation and activated AKT (S473) were significantly reduced. These results could be due to the tight regulation of PKC-ι expression by FOXO1, which retards PRKCI transcription. Therefore FOXO1 is a major regulator which suppresses the expression of PRKCI. Interestingly, c-Jun and phosphorylated c-Jun (S63) levels were not significantly altered as a result of NF-κB depletion and which suggests that NF-κB diminution does not affect PKC-ι expression over c-Jun. Instead, c-Jun is known to protect cancer cells from apoptosis by cooperating with NF-κB signaling to facilitate survival upon TNF-α stimulation (220). Our data indicated how TNF-α upregulates NF-κB and AKT pathways along with PKC-ι expression in these two melanoma cell lines. Our data also suggests that the TNF-α downstream target is mainly FOXO1, where it transcriptionally deactivates through the phosphorylation of elevated AKT. The inhibition of PKC-ι diminishes this AKT activation, thereby upregulating FOXO1 activity.

Our data also revealed that c-Jun also plays a role in PKC-ι expression, in addition to FOXO1. The ELISA results identifies links between PKC-ι expression with the cytokines, IL-6, IL-8, IL-17E and ICAM-1, along with some other key cellular signaling points such as STAT3/5. ELISA results revealed a more than two-fold increase of NF-κB p65 (S536) in PKC-ι inhibited samples. This indicates elevated dimerization of NF-κB subunits prior to its activation in order to accelerate NF-κB activation as a result of downstream depletion. Our Western and RT-qPCR data demonstrated that PKC-ι inhibition downregulates NF-κB translocation to the nucleus therefore phospho NF-κB levels increase in order to diminish the effect of PKC-ι inhibition. However, elevated FOXO1 does not allow NF-κB to annex the control since it is missing the essential assistance needed from PKC-ι due to its inhibition from ICA-1T and ICA-1S inhibitors.

106

Elevated STAT3/5 activity is connected to multiple types of cancer (238–241). IL-6 and IL-5 are known to upregulate STAT signaling, thereby providing survival features in many types of cancers. Importantly, upregulated STAT3 increases the transcription of c-Jun. Our ELISA results indicated that STAT3 and STAT5 activities were retarded due to PKC-ι inhibition, leading to c-Jun diminution. Hornsveld *et al.* showed that the JNK pathway and FOXO1 cross talk where FOXO1 provides tumor suppressing features by weakening JNK activity (246). JNK activates c-Jun by phosphorylation. Western blot and RT-qPCR analysis demonstrated that c-Jun depletion lessened PKC-ι expression, which suggested that c-Jun acts as an activator of PKC-ι expression. This confirms that in addition to FOXO1, c-Jun is involved in regulating PKC-ι expression, but in a promoting manner. These results suggest that FOXO1 plays a dominant role over c-Jun upon PKC-ι inhibition, possibly through multiple mechanisms, such as the reduction of JNK signaling, retarding PKC-ι expression and cell cycle arrest. This also explains why apoptosis was stimulated in melanoma cells as a result of inhibition of PKC-ι in addition to downregulation of the PI3K/AKT and NF-κB pathways. Overall, FOXO1 is very important in enhancing anti-tumor activities upon PKC-ι inhibition and it plays the central role of oncogenic PKC-ι depletion.

In conclusion, our overall data suggest that PKC-ι is a major regulatory component responsible for inducing cell growth, differentiation, survival, migration and invasion while PKC-ζ is mainly involved in NF-κB signaling to promote cell growth and survival in human melanoma cells. In addition, PKC-ι is critical for the elevated Vimentin activity thereby driving major cytoskeletal changes essential for EMT facilitating migration and invasion. Our results also suggest that ICA-1T, ICA-1S and ζ-Stat are effective aPKC inhibitors in melanoma cells and do not affect normal melanocytes at the optimal working concentrations for melanoma cells *in-vitro*. In addition, ACPD and DNDA are effective as aPKC inhibitors wherever specific inhibition between PKC-ι and PKC-

ζ is not essential. These five inhibitors can reduce cell proliferation, migration and invasion, while inducing apoptosis in SK-MEL-2 and MeWo malignant cell lines. Finally, the evidence we collected based on the malignant cell lines, indicates PKC-ι and PKC-ζ are potential therapeutic targets for metastatic melanoma *in-vitro*.

7.2 Future Directions

The proposed research will address the overarching challenge to revolutionize treatment regimens by replacing interventions that have life-threatening toxicities with ones that are safe and effective such as our PKC-ι specific inhibitors. Positive outcomes of *in-vivo* research will support the *in-vitro* data reported here and provide evidence that PKC-ι is a potential novel target for the treatment of melanoma. The novel concept that PKC-ι may influence melanoma cell proliferation, survival and motility through discussed pathways is important because it addresses a relationship between melanoma progression and an oncogene PKC-ι.

(1) Determining the *in-vivo* effects of ICA-1T, ICA-1S and ζ-Stat on SK-MEL-2-Luc and MeWo-Luc xenograft tumors in mice, including tumor growth, cell cycle progression, metastasis, apoptosis, PKC activity, pathological status and evaluation of pathways in which PKC-ι involves such as AKT/NF-κB and Par6/RhoA/Smad. These *in-vivo* results will be helpful to support the *in-vitro* data reported in this dissertation.

(2) Establishing the pharmacokinetics, toxicology, structure-activity relationship, off-target effects of selected inhibitors using *in-vivo* models. These parameters are essential tools in the pre-clinical

108

research setup and therefore need to be performed in order to forward the research from the benchtop to the clinics.

(3) Studying the effects of combination therapy with these inhibitors using some established melanoma therapeutics such as BRAF inhibitors. This will be helpful to optimize the effects and concentrations, dose, etc. in order to achieve best possible outcomes of anti-aPKC therapeutics.

(4) Studying the impact of aPKC inhibition of other cancer types such as prostate, breast, lung, glioblastoma, kidney etc. both *in-vitro* and *in-vivo* to investigate the role of aPKCs in cancer progression and to develop a generalize concept of aPKC activities in cancer thereby promoting the importance of aPKC inhibition in cancer research.

(5) Studying the regulatory mechanism of PKC-ζ in melanoma cells both *in-vitro* and *in-vivo* in order to gain better knowledge of how these two similar proteins transcriptionally regulate at different conditions.

CHAPTER 8

MATERIALS AND METHODS

8.1 Materials

ICA-1 nucleotide (ICA-1T) and nucleoside (ICA-1S) were synthesized by Therachem (Jaipur, India). ACPD (Product # R426911) was purchased from Sigma Aldrich (St. Louis, MO, USA). DNDA (NSC6082) and ζ-Stat (NSC37044) were obtained from the National Institutes of Health, (NIH) (Bethesda, MD, USA). They were dissolved in sterile distilled water (vehicle) prior to use. Antibodies were purchased as follows with the applied concentrations: PKC-ι (610175, 1:2000) and Bcl-2 (610538, 1:500) from BD Biosciences (San Jose, CA, USA) and PKC-ζ (sc-17781, 1:1000), NF-kB p65 (sc-372-G, 1:1000), IκBα (sc-1643, 1:500), phospho IκBα (sc-8404, 1:400) and Caspase-3 (sc-7272, 1:1000), from Santa Cruz Biotechnology (Santa Cruz, CA, USA); phospho PKC-ζ (PA5-17837, 1:500), E-Cadherin (701134, 1:1000), Vimentin (MA3-745, 1:1000), Myelin basic protein (MBP) (PA1-10008, 1:500) and phospho PKC-ι (44-968G, 1:500) from Thermo Fisher Scientific (Waltham, MA, USA); early growth response protein 1 (EGR1; 4153S, 1:500), c-Jun (9165S, 1:400), phospho c-Jun (3270S, 1:250), FOXO1 (2880S, 1:500), phospho FOXO1 (9464S, 1:400), phospho AKT (4059S, 1:500), phospho Vimentin (13614S, 1:500), SNAIL1 (3879S, 1:400), phospho PTEN (9551, 1:1000), phospho IκKα/β (2697, 1:500), PARP (9532, 1:1000) and cleaved-PARP (9185, 1:1000) from Cell Signaling Technology (Danvers, MA, USA); and β-actin peroxidase (A3854, 1:4000) from Sigma-Aldrich (St. Louis,

110

MO, USA); CD44 (ab97478, 1:2000), RhoA (ab54835, 1:1000), PRRX1 (ab211292, 1:500) and β-catenin (ab16051, 1:2000) from Abcam (Cambridge, UK). Phospho MBP (Thr 125, 1:400) (Catalog # 05-429) from EMD Millipore (Billerica, MA). Enhanced chemiluminescence solution (34080) was purchased from Pierce (Rockford, IL, USA). Dulbecco's phosphate-buffered saline without Mg^{2+} and Ca^{2+} (D8537) and Trypsin–EDTA (ethylenediaminetetraacetic acid) solution (T4049) were purchased from Sigma-Aldrich. Human small interfering RNA (*si*RNA) for PKC-ι (SR303741), PKC-ζ (303747), EGR1 (SR301358), c-Jun (SR302499), FOXO1 (SR301618) paired box gene 3 (PAX3; SR303360), interferon regulatory factor 9 (IRF9; SR307030), SNAIL (SR304489), and NF-κB p65 (SR321602) were purchased from Origene Technologies Inc. (Rockville, MD, USA) and *si*RNA for PRRX1 (AM16708) was purchased from Thermo Fisher Scientific. The NF-κB specific inhibitor, 4-methyl-N1-(3-phenylpropyl)-1,2-benzenediamine (JSH-23) (J4455) was purchased from Sigma-Aldrich. 4-[3-(4-iodophenyl)-2-(4-nitropheny))-2H-5-tetrazolio]-1,3-benzene disulfonate (WST-1) reagent for cell proliferation (11644807001) was purchased from Roche Diagnostics (Mannhelm, Germany). Basement membrane extraction (BME) (3455-096-02) was purchased from Trevigen (Gaithersburg, MD, USA). Human recombinant proteins PKC-ι (PV3183), PKC-ζ (P2273), TNFα (10602HNAE25), TGFβ1 (PHG9204) and MBP (MBS717422) were purchased from Thermo Fisher Scientific and MyBioSource (San Diego, CA, USA) respectively.

8.2 Molecular docking

ICA-1T, ICA-1S, and ζ-Stat were docked on solved crystal structures of PKC-ι with and without bound ATP (PDB 3A8W, 3A8X) using the molecular docking program AutoDock Vina (264). The three dimensional compound structures were translated from SMILES string to protein data

111

bank (PDB) file using the NCI/CADD translator (https://cactus.nci.nih.gov/translate/) (265). SWISS-MODELs of PKC-ζ were generated using the human PKC-ζ sequence (UniProt Q05513) and the crystallized PKC-ι structures as templates. Modeled PKC-ζ structures were processed for geometric minimization using Phenix (v 1.11.1-2575). Ligands and PKC structures were prepared for docking using AutoDockTools 1.5.6 (9_17_14 build). Molecular docking was performed using AutoDock Vina 1.1.2 (May 11, 2011 build). Top scoring docked ligand conformations, ranked by lowest kcal/mol scores coupled with visual inspections, were then selected for localized Vina screening. Docking output files were visualized with, and molecular images generated using Pymol (v 1.7.2.1). All molecular docking tasks were performed on a high performance workstation running Linux. Molecular docking for ACPD and DNDA was performed using homologous models for PKC-ι and PKC-ζ as described in Pillai, *et al.* (99).

8.3 Cells and cell culture

The SK-MEL-2 (ATCC® HTB-68™), MeWo (ATCC® HTB-65™) melanoma cell lines and primary epidermal normal melanocyte cell line (ATCC® PCS-200-013™) were purchased from the American Type Tissue Culture Collection (ATCC; Rockville, MD, USA). MEL-F-NEO normal melanocyte cell line was purchased from Zen-Bio, Inc. (Research Triangle Park, NC, USA). All cells were frozen in liquid nitrogen immediately with early passages with "Gibco Recovery" cell culture freezing medium from Thermo Fisher Scientific (12648010). The cells of passages 2 to 5 were resuscitated from liquid nitrogen and cultured for <3 months before re-initiating culture from the same passage for each tested experiment. The ATCC and Zen-Bio Inc. authenticated the cell lines using morphology, karyotyping and PCR-based approaches (266). All cell lines were cultured at 37 °C and 5% CO_2. Dermal cell basal medium (PCS-200-030) with melanocyte growth kit (PCS-

112

200-042) were used for PCS-200-013 and melanocyte growth medium (MEL-2) was used for MEL-F-NEO cell culturing according to the respective instruction manual. Eagle's minimum essential media- EMEM (90% v/v) with fetal bovine serum-FBS (10% v/v) and Penicillin (5 µg/mL) were used for SK-MEL-2 and MeWo cell culturing. All cell lines were seeded and grown as monolayers in T25 or T75 flasks.

8.4 Western blot analysis

The Bradford protein assay was used to measure the protein concentrations of extracted cell lysates in each experiment (inhibitor treatments or *si*RNA treatments). Total protein (40-80 µg) was loaded into each well measuring the equivalent volumes of the cell lysates, separated by 10% SDS-PAGE and electro-blotted onto supported nitrocellulose membranes. Western blot separation and Transferring processes were carried out in an ice cold environment in a chamber filled with ice. At the same time, both running buffer and transfer buffer were kept in 4°C to maintain the low temperature prior to use. Each blot was blocked for 1 h with 4.5% bovine serum albumin (BP1600-100, Thermo Fischer Scientific) in TBST solution (0.1% V/V Tween in 1X TBS) at room temperature (approximately 25°C). Protein bands were probed with each targeted primary antibody at 4°C overnight followed by horseradish-peroxidase-conjugate anti-mouse or anti-rabbit secondary antibody for 2 h at room temperature. Immuno-reactive bands were visualized with enhanced chemiluminescence solution (34080) according to the manufacturer's instructions (Pierce Inc., Rockford, IL, USA). Goat anti-mouse IgG (170-6516) and goat anti-rabbit IgG (170-6515) secondary antibodies were used from Bio-Rad Laboratories (Hercules, CA, USA). Manufacturer's recommended concentrations were used for all tested primary and secondary antibodies. β-actin was used as the internal control in each Western blot.

113

8.5 PKC activity assay

PKC activity assay was conducted by monitoring the phosphorylation of MBP (0.025 mg/ml), a known substrate for PKCs. The detailed procedure was performed as described in Pillai, *et al.* for all five inhibitors (0.1 to 10/20 µM) on recombinant PKC-ι and PKC-ζ (0.01 µg/µl) (99). Samples then fractionated by SDS-PAGE and immunoblotted for phosphorylated MBP. Kinase activity was calculated based on the densitometry values of Western blots.

8.6 Inhibitor dose response curves and WST-1 assay for cell viability and cytotoxicity

PCS-200-013, MEL-F-NEO, SK-MEL-2 and MeWo cells (4×10^4) were cultured in T25 flasks and treated with either an equal volume of sterile water (vehicle control) or inhibitors using a series of concentrations (0.1-10 µM). The detailed procedure was performed as described in Pillai, *et al*. for all five inhibitors on recombinant PKC-ι and PKC-ζ (0.01 µg/µL) using a series of inhibitor concentrations (0-10 µM) (99).

WST-1 assay was performed by culturing approximately 4×10^3 cells/well (PCS-200-013, MEL-F-NEO, SK-MEL-2 and MeWo) in a 96 well plate. After 24 h post plating time, fresh media were supplied (200 µl/well) and treated with either an equal volume of sterile water (vehicle control) or with the IC_{50} concentrations of ACPD (2.5 µM), DNDA (2.5 µM), ICA-1T (1 µM) or ICA-1S (2.5 µM) or ζ-Stat (5 µM). These IC_{50} values were obtained based on the dose response curves. Additional doses were supplied every 24 h during a 3 day incubation period. At the end of 3 day treatment, media were removed and fresh media (100 µL) were added with WST-1 reagent (10 µL) to each well. The absorbance was measured at 450 nm for every 1 h up to 10 hours using the Synergy HT microplate reader from Biotek (Winooski, VT, USA).

114

8.7 Wound healing assay cell migration

The detailed procedure was performed for SK-MEL-2 and MeWo cells as described in Justus, *et al.* (267). Cells were treated with either sterile water or inhibitors to achieve respective IC_{50} concentrations and plates were incubated at 37°C and 5% CO_2. Photographs of wound closure were taken utilizing a Motic AE31E microscope with Moticam BTU8 Tablet (40× magnification) at 24 h intervals for 3 days and analyzed using "ImageJ" image processing program (National Institutes of Health, Rockville, MD, USA).

8.8 Basement membrane extract (BME) assay for cell invasion

This *in-vitro* invasion assay was performed for SK-MEL-2 and MeWo cells as described in Feoktistova, *et al.* using BME (0.2×) as the inner coating of transwell plate (268). Cells were treated with either sterile water or inhibitors to achieve respective IC_{50} concentrations and plates were incubated at 37°C and 5% CO_2 for 3 days. At the end of the 3rd day, crystal violet (0.5%) was used to stain the cells adhered to the bottom surface of the membrane in transwell insert to visualize the inhibition of invasion. Photographs of the stained cells were taken from Motic AE31E microscope with Moticam BTU8 Tablet (100× magnification) after washing the extra stains remained in the transwell plate. Subsequently, 70% Ethanol (200 μl) was added to dissolve crystal violet and absorbance was measured at 590 nm.

8.9 Immunofluorescence microscopy

SK-MEL-2 and MeWo cells were plated in chamber slides (154461, Thermo Fisher Scientifics) and treated with either sterile water or inhibitors to achieve respective IC_{50} concentration of ICA-1T. Slides were incubated at 37°C and 5% CO_2 for 3 days. At the end of the 3rd day, cells were prepared as described in El Bassit, *et al.* (269) and stained for PKC-ι (ab5282 anti-rabbit polyclonal primary antibody 1:200 and A21206 anti-rabbit secondary antibody at 1:1000; green) and for Vimentin (MA3-745 anti-mouse monoclonal primary antibody at 1:40 and A32727 anti-mouse secondary antibody at 1:1000; red) to visualize under the Nikon Mirco-FX fluorescence microscope with Jenoptik D-07739 Jena camera (200× magnification). 4′,6-diamidino-2-phenylindole (DAPI) in Gold Antifade Mountant (S36938; blue) was used to visualize the nucleus.

8.10 Identification of possible transcription factors (TFs) which bind to the PRKCI gene

The PRKCI gene sequence was obtained from ensemble.org (ENSG00000163558) which locates in chromosome 3 from bp170222365-170305981 (3q26.2) (270,271). The forward strand sequence was used and compared with EPD/Eukaryotic Promoter Database (https://epd.vital-it.ch/index.php) for its promoter sequence. A specific sequence was then selected (chromosome 3; 170220768-170225128); the sequence contains the promoter, promoter flank, enhancer and a motif feature. This sequence predicted possible TFs that can bind within a dissimilarity margin ≤10% using PROMO, which is a virtual laboratory for studying transcription factor binding sites in DNA sequences (http://alggen.lsi.upc.es/). TF targets were then compared with the Genomatix Matinspector results to generate the final TF list for the following experiments.

116

8.11 Knockdown of TFs, PKC-ι and NF-κB gene expression by *si*RNA

Each *si*RNA contained a pool of three combined RNA sequences for the targeted gene and respective control *si*RNA contained a scrambled sequence, which did not lead to specific degradation of any known cellular messenger RNA and whose sequence is a proprietary of Origene Technologies Inc. The experiments performed with *si*RNA are as follows: Approximately 1×10^5 cells (SK-MEL-2 and MeWo) were cultured in T25 flasks and at 24 h post-plating, fresh medium was supplied and the cells were treated with a 20 nM concentration of one of the transcription factor *si*RNAs or scrambled *si*RNA as a control using '*si*Tran' *si*RNA transfection reagent (TT300002) from Origene Technologies, Inc. according to the manufacturer's recommended ratios. After 48 h of the post-treatment period, cells were subsequently lifted and cell lysates were collected with cell lysis buffer (C7027, Invitrogen/Thermo Fisher Scientific). Western blot analysis was performed as previously described in the study by Win, *et al.* (80).

8.12 Immunoprecipitation and Western blot analysis

Approximately 1×10^5 cells (SK-MEL-2 and MeWo) were cultured in T75 flasks and 24 h post plating, fresh media were supplied and cells were treated with either an equal volume of sterile water or IC_{50} concentration of the tested inhibitor. Additional doses were supplied every 24 h during a 3 day incubation period. Cells were then lifted using Trypsin and the cell lysates were collected either with cell lysis buffer (Catalog # C7027, Invitrogen) or IP lysis buffer (Catalog # 87788, Thermo Fisher). For the IP, the cell lysates were collected in the same way and 200 μg of total protein from each lysate was immunoprecipitated using primary antibody of interest (either

117

PKC-ι or Vimentin) and analyzed using Western blots after separated by SDS-PAGE. The Western blots were performed as described in 8.4.

8.13 Densitometry

The intensity of western blot bands was measured using 'Image Studio Lite 5.x' software developed by LI-COR Biosciences (Lincoln, NE, USA) in which the background intensity was subtracted from the intensity of each band to obtain the corrected intensity of the proteins.

8. 14 Analysis of cytokine expression using enzyme-linked immunosorbent assay (ELISA)

An ELISA containing a cytokine array (Cat. no. ARY005B) was obtained from R&D Systems (Minneapolis, MN, USA). Approximately $1x10^5$ cells (SK-MEL-2 and MeWo) were cultured in T25 flasks and at 24 h post-plating, fresh medium was supplied and the cells were treated with a 20 nM concentration of PKC-ι *si*RNA or scrambled siRNA as a control. After 48 h of the post-treatment period, the cells were subsequently lifted, lysed, processed and analyzed according to manufacturer's instructions using cytokine array kit reagents. Total protein (100 μg) from each sample was used to expose the membranes and chemoluminescence photographs as Western blots were taken to analyze the cytokine expression profiles of the melanoma cells upon PKC-ι *si*RNA knockdown.

8.15 Immunopaired antibody detection assay (IPAD)

Approximately $1x10^5$ cells were cultured in T25 flasks and at 24 h post-plating, fresh medium was supplied and the cells were treated with either volume of sterile water (control) or the IC_{50} concentration of ICA-1T (1 μM). Additional doses were supplied every 24 h during a 3-day incubation period at 37°C. The cells were then lysed and lysates were prepared with the final total protein concentration being >2 μg/ml and then delivered to ActivSignal, LLC (Natick, MA, USA) for further processing and analyzing. The ActivSignal IPAD platform is a multiplex ELISA-based proprietary technology for analyzing the activity of multiple signaling pathways in one reaction with high sensitivity and specificity. The activities of >20 signaling pathways were monitored simultaneously in a single well through assessing the expression or protein phosphorylation of 70 target human proteins.

8.16 Reverse transcription-quantitative PCR (RT-qPCR)

qPCR was performed on RNA isolated from SK-MEL-2 and MeWo cell lysates collected after *si*RNA treatments for PKC-ι, c-Jun and FOXO1 against scrambled *si*RNA as the control. Total RNA was isolated from the cell pellets using RNA lysis buffer which comes with the RNeasy mini kit (74104) from Qiagen (Germantown, MD, USA). RNA was reverse transcribed into cDNA with You-Prime First Strand Beads (27-9264-01) form GE healthcare UK Ltd. (Buckinghamshire, UK). qPCR was performed on cDNA using the QuantStudio3 Real-Time PCR system (Thermo Fisher Scientific). Gene expression was observed for PKC-ι (primers: Forward, CACACTTTCCAAGCCAAGCG and reverse, GGCGTCCAAGTCCCCATATT), c-Jun (primers: Forward, GTGCCGAAAAAGGAAGCTGG and reverse,

119

CTGCGTTAGCATGAGTTGGC), FOXO1 (primers: Forward, ATGGCTTGGTGTCTTTCTTTTCT and reverse, TGTGGCTGACAAGACTTAACTCAA), IL-17E (primers: Forward, GCCACCACTCCTGTCTCTTC and reverse, CCAGGGGCTCTTTCTTCTCC), IL-6 (primers: Forward, GCTCCCTACACACATGCCTT and reverse, CCTTCCCTGTGCATGGTGAT), IL-8 (primers: Forward, CAGAGACAGCAGAGCACAC and reverse, ATCAGGAAGGCTGCCAAGAG) and ICAM-1 (primers: Forward, GGGAACAACCGGAAGGTGTA and reverse, CAGTTCCACCCGTTCTGGAG). β-actin (primers: Forward, AGAGCTACGAGCTGCCTGAC and reverse, AGCACTGTGTTGGCGTACAG) was used as an internal control. PCR reactions used SYBR-Green PCR Mix (Applied Biosystems, Foster City, CA, USA). cDNA was denatured at at 95°C for 10 min, followed by 40 cycles of denaturing at 95°C for 20 sec and an annealing stage of 65°C for 40 sec. QuantStudio Software 2.0 was used to quantify gene expression using $2^{-\Delta\Delta CT}$ (Thermo Fisher Scientific) as explained by Livak and Schmittgen (272).

8.17 Statistical analysis

All data are presented as the means ± SD. Statistical analysis was performed with one- or two-way ANOVA followed by Tukey's HSD test as a multiple comparisons test using the 'VassarStats' web tool for statistical analysis. *P*-values ≤0.05 or ≤0.01 were considered to indicate statistically significant differences.

120

CHAPTER 9

REFERENCES

1. Inoue M, Kishimoto A, Takai Y, Nishizuka Y. Studies on a cyclic nucleotide-independent protein kinase and its proenzyme in mammalian tissues. II. Proenzyme and its activation by calcium-dependent protease from rat brain. J Biol Chem. 1977;252:7610–6.

2. Kishimoto A, Takai Y, Mori T, Kikkawa U, Nishizuka Y. Activation of calcium and phospholipid-dependent protein kinase by diacylglycerol, its possible relation to phosphatidylinositol turnover. J Biol Chem. 1980;255:2273–6.

3. Newton AC. Protein Kinase C: Structure, Function, and Regulation. J Biol Chem. 1995;270:28495–8.

4. Castagna M, Takai Y, Kaibuchi K, Sano K, Kikkawa U, Nishizuka Y. Direct activation of calcium-activated, phospholipid-dependent protein kinase by tumor-promoting phorbol esters. J Biol Chem. 1982;257:7847–51.

5. Mellor H, Parker PJ. The extended protein kinase C superfamily. Biochem J. 1998;332:281–92.

6. Sturany S, Lint JV, Gilchrist A, Vandenheede JR, Adler G, Seufferlein T. Mechanism of Activation of Protein Kinase D2(PKD2) by the CCKB/Gastrin Receptor. J Biol Chem. 2002;277:29431–6.

7. Bartsch JW, Mukai H, Takahashi N, Ronsiek M, Fuchs S, Jockusch H, et al. The Protein Kinase N (PKN) GenePRKCL1/Prkcl1Maps to Human Chromosome 19p12–p13.1 and Mouse Chromosome 8 with Close Linkage to the Myodystrophy (myd) Mutation. Genomics. 1998;49:129–32.

8. Palmer RH, Ridden J, Parker PJ. Cloning and expression patterns of two members of a novel protein-kinase-C-related kinase family. Eur J Biochem. 1995;227:344–51.

9. Hurley JH, Newton AC, Parker PJ, Blumberg PM, Nishizuka Y. Taxonomy and function of C1 protein kinase C homology domains. Protein Sci Publ Protein Soc. 1997;6:477–80.

10. Parker PJ, Coussens L, Totty N, Rhee L, Young S, Chen E, et al. The complete primary structure of protein kinase C--the major phorbol ester receptor. Science. 1986;233:853–9.

121

11. Burns DJ, Bell RM. Protein kinase C contains two phorbol ester binding domains. J Biol Chem. 1991;266:18330–8.

12. Johnson JE, Giorgione J, Newton AC. The C1 and C2 domains of protein kinase C are independent membrane targeting modules, with specificity for phosphatidylserine conferred by the C1 domain. Biochemistry. 2000;39:11360–9.

13. Newton AC. Protein kinase C. Seeing two domains. Curr Biol CB. 1995;5:973–6.

14. Hirano Y, Yoshinaga S, Ogura K, Yokochi M, Noda Y, Sumimoto H, et al. Solution structure of atypical protein kinase C PB1 domain and its mode of interaction with ZIP/p62 and MEK5. J Biol Chem. 2004;279:31883–90.

15. Selbie L, Schmitzpeiffer C, Sheng Y, Biden T. Molecular-Cloning and Characterization of Pkc(iota), an Atypical Isoform. J Biol Chem. 1993;268:24296–302.

16. Balendran A, Biondi RM, Cheung PC, Casamayor A, Deak M, Alessi DR. A 3-phosphoinositide-dependent protein kinase-1 (PDK1) docking site is required for the phosphorylation of protein kinase Czeta (PKCzeta) and PKC-related kinase 2 by PDK1. J Biol Chem. 2000;275:20806–13.

17. Tsutakawa SE, Medzihradszky KF, Flint AJ, Burlingame AL, Koshland DE. Determination of in Vivo Phosphorylation Sites in Protein Kinase C. J Biol Chem. 1995;270:26807–12.

18. Keranen LM, Dutil EM, Newton AC. Protein kinase C is regulated in vivo by three functionally distinct phosphorylations. Curr Biol CB. 1995;5:1394–403.

19. Gao T, Toker A, Newton AC. The carboxyl terminus of protein kinase c provides a switch to regulate its interaction with the phosphoinositide-dependent kinase, PDK-1. J Biol Chem. 2001;276:19588–96.

20. Yaffe MB, Rittinger K, Volinia S, Caron PR, Aitken A, Leffers H, et al. The structural basis for 14-3-3:phosphopeptide binding specificity. Cell. 1997;91:961–71.

21. Dutil EM, Toker A, Newton AC. Regulation of conventional protein kinase C isozymes by phosphoinositide-dependent kinase 1 (PDK-1). Curr Biol. 1998;8:1366–75.

22. Behn-Krappa A, Newton AC. The hydrophobic phosphorylation motif of conventional protein kinase C is regulated by autophosphorylation. Curr Biol CB. 1999;9:728–37.

23. Balendran A, Hare GR, Kieloch A, Williams MR, Alessi DR. Further evidence that 3-phosphoinositide-dependent protein kinase-1 (PDK1) is required for the stability and phosphorylation of protein kinase C (PKC) isoforms. FEBS Lett. 2000;484:217–23.

24. Rodriguez MM, Ron D, Touhara K, Chen C-H, Mochly-Rosen D. RACK1, a Protein Kinase C Anchoring Protein, Coordinates the Binding of Activated Protein Kinase C and Select Pleckstrin Homology Domains in Vitro. Biochemistry. 1999;38:13787–94.

122

25. Jaken S. Protein kinase C isozymes and substrates. Curr Opin Cell Biol. 1996;8:168–73.

26. Hansra G, Garcia-Paramio P, Prevostel C, Whelan RD, Bornancin F, Parker PJ. Multisite dephosphorylation and desensitization of conventional protein kinase C isotypes. Biochem J. 1999;342:337–44.

27. Rumsby MG, Drew L, Warr JR. Protein kinases and multidrug resistance. Cytotechnology. 1998;27:203–24.

28. Lu Z, Liu D, Hornia A, Devonish W, Pagano M, Foster DA. Activation of protein kinase C triggers its ubiquitination and degradation. Mol Cell Biol. 1998;18:839–45.

29. Chou MM, Hou W, Johnson J, Graham LK, Lee MH, Chen C-S, et al. Regulation of protein kinase C ζ by PI 3-kinase and PDK-1. Curr Biol. 1998;8:1069–78.

30. Griner EM, Kazanietz MG. Protein kinase C and other diacylglycerol effectors in cancer. Nat Rev Cancer. 2007;7:281–94.

31. Garg R, Benedetti LG, Abera MB, Wang H, Abba M, Kazanietz MG. Protein kinase C and cancer: what we know and what we do not. Oncogene. 2014;33:5225–37.

32. Cameron AJ, Procyk KJ, Leitges M, Parker PJ. PKC alpha protein but not kinase activity is critical for glioma cell proliferation and survival. Int J Cancer. 2008;123:769–79.

33. Haughian JM, Reno EM, Thorne AM, Bradford AP. Protein Kinase C alpha (PKCα) dependent signaling mediates endometrial cancer cell growth and tumorigenesis. Int J Cancer J Int Cancer. 2009;125:2556–64.

34. Nakagawa S, Fujii T, Yokoyama G, Kazanietz MG, Yamana H, Shirouzu K. Cell growth inhibition by all-trans retinoic acid in SKBR-3 breast cancer cells: involvement of protein kinase Calpha and extracellular signal-regulated kinase mitogen-activated protein kinase. Mol Carcinog. 2003;38:106–16.

35. Kong C, Zhu Y, Liu D, Yu M, Li S, Li Z, et al. Role of protein kinase C-alpha in superficial bladder carcinoma recurrence. Urology. 2005;65:1228–32.

36. Stewart JR, O'Brian CA. Resveratrol antagonizes EGFR-dependent Erk1/2 activation in human androgen-independent prostate cancer cells with associated isozyme-selective PKC alpha inhibition. Invest New Drugs. 2004;22:107–17.

37. Suga K, Sugimoto I, Ito H, Hashimoto E. Down-regulation of protein kinase C-alpha detected in human colorectal cancer. Biochem Mol Biol Int. 1998;44:523–8.

38. von Brandenstein M, Pandarakalam JJ, Kroon L, Loeser H, Herden J, Braun G, et al. MicroRNA 15a, inversely correlated to PKCα, is a potential marker to differentiate between benign and malignant renal tumors in biopsy and urine samples. Am J Pathol. 2012;180:1787–97.

123

39. Hill K, Erdogan E, Khoor A, Walsh M, Leitges M, Murray N, et al. Protein kinase Cα suppresses Kras-mediated lung tumor formation through activation of a p38 MAPK-TGFβ signaling axis. Oncogene. 2014;33:2134–44.

40. Yu W, Murray NR, Weems C, Chen L, Guo H, Ethridge R, et al. Role of cyclooxygenase 2 in protein kinase C beta II-mediated colon carcinogenesis. J Biol Chem. 2003;278:11167–74.

41. Kim J, Choi Y-L, Vallentin A, Hunrichs BS, Hellerstein MK, Peehl DM, et al. Centrosomal PKCβII and pericentrin are critical for human prostate cancer growth and angiogenesis. Cancer Res. 2008;68:6831–9.

42. Espinosa I, Briones J, Bordes R, Brunet S, Martino R, Sureda A, et al. Membrane PKC-beta 2 protein expression predicts for poor response to chemotherapy and survival in patients with diffuse large B-cell lymphoma. Ann Hematol. 2006;85:597–603.

43. Teicher BA, Menon K, Alvarez E, Shih C, Faul MM. Antiangiogenic and antitumor effects of a protein kinase Cbeta inhibitor in human breast cancer and ovarian cancer xenografts. Invest New Drugs. 2002;20:241–51.

44. Teicher BA, Menon K, Alvarez E, Galbreath E, Shih C, Faul M. Antiangiogenic and antitumor effects of a protein kinase Cbeta inhibitor in human T98G glioblastoma multiforme xenografts. Clin Cancer Res Off J Am Assoc Cancer Res. 2001;7:634–40.

45. Irie K, Yanagita RC, Nakagawa Y. Challenges to the development of bryostatin-type anticancer drugs based on the activation mechanism of protein kinase Cδ. Med Res Rev. 2012;32:518–35.

46. Yonezawa T, Kurata R, Kimura M, Inoko H. PKC delta and epsilon in drug targeting and therapeutics. Recent Pat DNA Gene Seq. 2009;3:96–101.

47. Gonelli A, Mischiati C, Guerrini R, Voltan R, Salvadori S, Zauli G. Perspectives of protein kinase C (PKC) inhibitors as anti-cancer agents. Mini Rev Med Chem. 2009;9:498–509.

48. Zhao M, Xia L, Chen G-Q. Protein kinase cδ in apoptosis: a brief overview. Arch Immunol Ther Exp (Warsz). 2012;60:361–72.

49. Basu A, Pal D. Two faces of protein kinase Cδ: the contrasting roles of PKCδ in cell survival and cell death. ScientificWorldJournal. 2010;10:2272–84.

50. Mischak H, Goodnight JA, Kolch W, Martiny-Baron G, Schaechtle C, Kazanietz MG, et al. Overexpression of protein kinase C-delta and -epsilon in NIH 3T3 cells induces opposite effects on growth, morphology, anchorage dependence, and tumorigenicity. J Biol Chem. 1993;268:6090–6.

51. Cacace AM, Guadagno SN, Krauss RS, Fabbro D, Weinstein IB. The epsilon isoform of protein kinase C is an oncogene when overexpressed in rat fibroblasts. Oncogene. 1993;8:2095–104.

52. Perletti GP, Folini M, Lin HC, Mischak H, Piccinini F, Tashjian AH. Overexpression of protein kinase C epsilon is oncogenic in rat colonic epithelial cells. Oncogene. 1996;12:847–54.

53. Cai H, Smola U, Wixler V, Eisenmann-Tappe I, Diaz-Meco MT, Moscat J, et al. Role of diacylglycerol-regulated protein kinase C isotypes in growth factor activation of the Raf-1 protein kinase. Mol Cell Biol. 1997;17:732–41.

54. Cacace AM, Ueffing M, Philipp A, Han EK, Kolch W, Weinstein IB. PKC epsilon functions as an oncogene by enhancing activation of the Raf kinase. Oncogene. 1996;13:2517–26.

55. Perletti GP, Concari P, Brusaferri S, Marras E, Piccinini F, Tashjian AH. Protein kinase Cepsilon is oncogenic in colon epithelial cells by interaction with the ras signal transduction pathway. Oncogene. 1998;16:3345–8.

56. Hamilton M, Liao J, Cathcart MK, Wolfman A. Constitutive association of c-N-Ras with c-Raf-1 and protein kinase C epsilon in latent signaling modules. J Biol Chem. 2001;276:29079–90.

57. Cacace AM, Ueffing M, Han EK, Marmè D, Weinstein IB. Overexpression of PKCepsilon in R6 fibroblasts causes increased production of active TGFbeta. J Cell Physiol. 1998;175:314–22.

58. Cadoret A, Baron-Delage S, Bertrand F, Kornprost M, Groyer A, Gespach C, et al. Oncogene-induced up-regulation of Caco-2 cell proliferation involves IGF-II gene activation through a protein kinase C-mediated pathway. Oncogene. 1998;17:877–87.

59. Pan Q, Bao LW, Kleer CG, Sabel MS, Griffith KA, Teknos TN, et al. Protein kinase C epsilon is a predictive biomarker of aggressive breast cancer and a validated target for RNA interference anticancer therapy. Cancer Res. 2005;65:8366–71.

60. Brenner W, Färber G, Herget T, Wiesner C, Hengstler JG, Thüroff JW. Protein kinase C eta is associated with progression of renal cell carcinoma (RCC). Anticancer Res. 2003;23:4001–6.

61. Krasnitsky E, Baumfeld Y, Freedman J, Sion-Vardy N, Ariad S, Novack V, et al. PKCη is a novel prognostic marker in non-small cell lung cancer. Anticancer Res. 2012;32:1507–13.

62. Lu H-C, Chou F-P, Yeh K-T, Chang Y-S, Hsu NC, Chang J-G. Expression of protein kinase C family in human hepatocellular carcinoma. Pathol Oncol Res POR. 2010;16:385–91.

63. Rhodes DR, Kalyana-Sundaram S, Tomlins SA, Mahavisno V, Kasper N, Varambally R, et al. Molecular concepts analysis links tumors, pathways, mechanisms, and drugs. Neoplasia N Y N. 2007;9:443–54.

64. Dhanasekaran SM, Dash A, Yu J, Maine IP, Laxman B, Tomlins SA, et al. Molecular profiling of human prostate tissues: insights into gene expression patterns of prostate development during puberty. FASEB J Off Publ Fed Am Soc Exp Biol. 2005;19:243–5.

65. Dyrskjøt L, Kruhøffer M, Thykjaer T, Marcussen N, Jensen JL, Møller K, et al. Gene expression in the urinary bladder: a common carcinoma in situ gene expression signature exists disregarding histopathological classification. Cancer Res. 2004;64:4040–8.

66. Sanchez-Carbayo M, Socci ND, Lozano J, Saint F, Cordon-Cardo C. Defining molecular profiles of poor outcome in patients with invasive bladder cancer using oligonucleotide microarrays. J Clin Oncol Off J Am Soc Clin Oncol. 2006;24:778–89.

67. Basso K, Margolin AA, Stolovitzky G, Klein U, Dalla-Favera R, Califano A. Reverse engineering of regulatory networks in human B cells. Nat Genet. 2005;37:382–90.

68. Sun L, Hui A-M, Su Q, Vortmeyer A, Kotliarov Y, Pastorino S, et al. Neuronal and glioma-derived stem cell factor induces angiogenesis within the brain. Cancer Cell. 2006;9:287–300.

69. French PJ, Swagemakers SMA, Nagel JHA, Kouwenhoven MCM, Brouwer E, van der Spek P, et al. Gene expression profiles associated with treatment response in oligodendrogliomas. Cancer Res. 2005;65:11335–44.

70. Rickman DS, Bobek MP, Misek DE, Kuick R, Blaivas M, Kurnit DM, et al. Distinctive molecular profiles of high-grade and low-grade gliomas based on oligonucleotide microarray analysis. Cancer Res. 2001;61:6885–91.

71. Bredel M, Bredel C, Juric D, Harsh GR, Vogel H, Recht LD, et al. Functional network analysis reveals extended gliomagenesis pathway maps and three novel MYC-interacting genes in human gliomas. Cancer Res. 2005;65:8679–89.

72. Stearman RS, Dwyer-Nield L, Zerbe L, Blaine SA, Chan Z, Bunn PA, et al. Analysis of Orthologous Gene Expression between Human Pulmonary Adenocarcinoma and a Carcinogen-Induced Murine Model. Am J Pathol. 2005;167:1763–75.

73. Galvez AS, Duran A, Linares JF, Pathrose P, Castilla EA, Abu-Baker S, et al. Protein Kinase Cζ Represses the Interleukin-6 Promoter and Impairs Tumorigenesis In Vivo. Mol Cell Biol. 2009;29:104–15.

74. Lenburg ME, Liou LS, Gerry NP, Frampton GM, Cohen HT, Christman MF. Previously unidentified changes in renal cell carcinoma gene expression identified by parametric analysis of microarray data. BMC Cancer. 2003;3:31.

75. Talantov D, Mazumder A, Yu JX, Briggs T, Jiang Y, Backus J, et al. Novel genes associated with malignant melanoma but not benign melanocytic lesions. Clin Cancer Res Off J Am Assoc Cancer Res. 2005;11:7234–42.

76. Buchholz M, Braun M, Heidenblut A, Kestler HA, Klöppel G, Schmiegel W, et al. Transcriptome analysis of microdissected pancreatic intraepithelial neoplastic lesions. Oncogene. 2005;24:6626–36.

126

77. Mustafi R, Cerda S, Chumsangsri A, Fichera A, Bissonnette M. Protein Kinase-zeta inhibits collagen I-dependent and anchorage-independent growth and enhances apoptosis of human Caco-2 cells. Mol Cancer Res MCR. 2006;4:683–94.

78. Nazarenko I, Jenny M, Keil J, Gieseler C, Weisshaupt K, Sehouli J, et al. Atypical protein kinase C zeta exhibits a proapoptotic function in ovarian cancer. Mol Cancer Res MCR. 2010;8:919–34.

79. Ma L, Tao Y, Duran A, Llado V, Galvez A, Barger JF, et al. Control of Nutrient Stress-Induced Metabolic Reprogramming by PKCζ in Tumorigenesis. Cell. 2013;152:599–611.

80. Win HY, Acevedo-Duncan M. Atypical protein kinase C phosphorylates IKK alpha beta in transformed non-malignant and malignant prostate cell survival. Cancer Lett. 2008;270:302–11.

81. Filomenko R, Poirson-Bichat F, Billerey C, Belon J-P, Garrido C, Solary E, et al. Atypical protein kinase C zeta as a target for chemosensitization of tumor cells. Cancer Res. 2002;62:1815–21.

82. Bezombes C, de Thonel A, Apostolou A, Louat T, Jaffrézou J-P, Laurent G, et al. Overexpression of protein kinase Czeta confers protection against antileukemic drugs by inhibiting the redox-dependent sphingomyelinase activation. Mol Pharmacol. 2002;62:1446–55.

83. Cataldi A, Centurione L, Di Pietro R, Rapino M, Bosco D, Grifone G, et al. Protein kinase C zeta nuclear translocation mediates the occurrence of radioresistance in friend erythroleukemia cells. J Cell Biochem. 2003;88:144–51.

84. Xin M, Gao F, May WS, Flagg T, Deng X. Protein kinase Czeta abrogates the proapoptotic function of Bax through phosphorylation. J Biol Chem. 2007;282:21268–77.

85. Rimessi A, Zecchini E, Siviero R, Giorgi C, Leo S, Rizzuto R, et al. The selective inhibition of nuclear PKCζ restores the effectiveness of chemotherapeutic agents in chemoresistant cells. Cell Cycle Georget Tex. 2012;11:1040–8.

86. Zhang L, Huang J, Yang N, Liang S, Barchetti A, Giannakakis A, et al. Integrative genomic analysis of protein kinase C (PKC) family identifies PKCiota as a biomarker and potential oncogene in ovarian carcinoma. Cancer Res. 2006;66:4627–35.

87. Eder AM, Sui X, Rosen DG, Nolden LK, Cheng KW, Lahad JP, et al. Atypical PKCι contributes to poor prognosis through loss of apical-basal polarity and Cyclin E overexpression in ovarian cancer. Proc Natl Acad Sci U S A. 2005;102:12519–24.

88. Nanjundan M, Nakayama Y, Cheng KW, Lahad J, Liu J, Lu K, et al. Amplification of MDS1/EVI1 and EVI1, located in the 3q26.2 amplicon, is associated with favorable patient prognosis in ovarian cancer. Cancer Res. 2007;67:3074–84.

89. Gustafson WC, Ray S, Jamieson L, Thompson EA, Brasier AR, Fields AP. Bcr-Abl regulates protein kinase Ciota (PKCiota) transcription via an Elk1 site in the PKCiota promoter. J Biol Chem. 2004;279:9400–8.

90. Murray NR, Jamieson L, Yu W, Zhang J, Gökmen-Polar Y, Sier D, et al. Protein kinase Cι is required for Ras transformation and colon carcinogenesis in vivo. J Cell Biol. 2004;164:797–802.

91. Scotti ML, Bamlet WR, Smyrk TC, Fields AP, Murray NR. Protein Kinase C Iota is Required for Pancreatic Cancer Cell Transformed Growth and Tumorigenesis. Cancer Res. 2010;70:2064–74.

92. Murray NR, Kalari KR, Fields AP. Protein kinase Cι expression and oncogenic signaling mechanisms in cancer. J Cell Physiol. 2011;226:879–87.

93. Frederick L, Matthews J, Jamieson L, Justilien V, Thompson E, Radisky D, et al. Matrix metalloproteinase-10 is a critical effector of protein kinase Cι-Par6α-mediated lung cancer. Oncogene. 2008;27:4841–53.

94. Regala RP, Davis RK, Kunz A, Khoor A, Leitges M, Fields AP. Atypical Protein Kinase Cι is Required for Bronchioalveolar Stem Cell Expansion and Lung Tumorigenesis. Cancer Res. 2009;69:7603–11.

95. Regala RP, Weems C, Jamieson L, Copland JA, Thompson EA, Fields AP. Atypical protein kinase Ciota plays a critical role in human lung cancer cell growth and tumorigenicity. J Biol Chem. 2005;280:31109–15.

96. Regala RP, Weems C, Jamieson L, Khoor A, Edell ES, Lohse CM, et al. Atypical protein kinase C iota is an oncogene in human non-small cell lung cancer. Cancer Res. 2005;65:8905–11.

97. Justilien V, Jameison L, Der CJ, Rossman KL, Fields AP. Oncogenic Activity of Ect2 Is Regulated through Protein Kinase Cι-mediated Phosphorylation. J Biol Chem. 2011;286:8149–57.

98. Regala RP, Thompson EA, Fields AP. Atypical protein kinase C-L expression and aurothiomalate sensitivity in human lung cancer cells. Cancer Res. 2008;68:5888–95.

99. Pillai P, Desai S, Patel R, Sajan M, Farese R, Ostrov D, et al. A novel PKC-iota inhibitor abrogates cell proliferation and induces apoptosis in neuroblastoma. Int J Biochem Cell Biol. 2011;43:784–94.

100. Desai SR, Pillai PP, Patel RS, McCray AN, Win-Piazza HY, Acevedo-Duncan ME. Regulation of Cdk7 activity through a phosphatidylinositol (3)-kinase/PKC-ι-mediated signaling cascade in glioblastoma. Carcinogenesis. 2012;33:10–9.

101. Acevedo-Duncan M, Patel R, Whelan S, Bicaku E. Human glioma PKC-iota, and PKC-beta II phosphorylate cyclin-dependent kinase activating kinase during the cell cycle. Cell Prolif. 2002;35:23–36.

102. Atwood SX, Li M, Lee A, Tang JY, Oro AE. Gli activation by aPKC iota/lambda regulates basal cell carcinoma growth. Nature. 2013;494:484–8.

103. Baldwin RM, Parolin D a. E, Lorimer I a. J. Regulation of glioblastoma cell invasion by PKC iota and RhoB. Oncogene. 2008;27:3587–95.

104. Ishiguro H, Akimoto K, Nagashima Y, Kojima Y, Sasaki T, Ishiguro-Imagawa Y, et al. aPKCλ/ι promotes growth of prostate cancer cells in an autocrine manner through transcriptional activation of interleukin-6. Proc Natl Acad Sci. 2009;106:16369–74.

105. Cronin KA, Lake AJ, Scott S, Sherman RL, Noone A-M, Howlader N, et al. Annual Report to the Nation on the Status of Cancer, part I: National cancer statistics. Cancer. 2018;124:2785–800.

106. Rastrelli M, Tropea S, Rossi CR, Alaibac M. Melanoma: epidemiology, risk factors, pathogenesis, diagnosis and classification. Vivo Athens Greece. 2014;28:1005–11.

107. Duncan LM. The Classification of Cutaneous Melanoma. Hematol Oncol Clin North Am. 2009;23:501–13.

108. Meyle KD, Guldberg P. Genetic risk factors for melanoma. Hum Genet. 2009;126:499–510.

109. Caini S, Gandini S, Sera F, Raimondi S, Fargnoli MC, Boniol M, et al. Meta-analysis of risk factors for cutaneous melanoma according to anatomical site and clinico-pathological variant. Eur J Cancer. 2009;45:3054–63.

110. MacKie RM, Hauschild A, Eggermont AMM. Epidemiology of invasive cutaneous melanoma. Ann Oncol Off J Eur Soc Med Oncol. 2009;20 Suppl 6:vi1-7.

111. Lasithiotakis K, Leiter U, Krüger-Krasagakis S, Tosca A, Garbe C. Comparative analysis of incidence and clinical features of cutaneous malignant melanoma in Crete (Greece) and southern Germany (central Baden-Württemberg). Br J Dermatol. 2006;154:1123–7.

112. Rigel DS. Epidemiology of melanoma. Semin Cutan Med Surg. 2010;29:204–9.

113. Markovic SN, Erickson LA, Rao RD, McWilliams RR, Kottschade LA, Creagan ET, et al. Malignant Melanoma in the 21st Century, Part 1: Epidemiology, Risk Factors, Screening, Prevention, and Diagnosis. Mayo Clin Proc. 2007;82:364–80.

114. Stern RS. The risk of melanoma in association with long-term exposure to PUVA. J Am Acad Dermatol. 2001;44:755–61.

115. Bevona C, Goggins W, Quinn T, Fullerton J, Tsao H. Cutaneous Melanomas Associated With Nevi. Arch Dermatol. 2003;139:1620–4.

129

116. Gandini S, Sera F, Cattaruzza MS, Pasquini P, Abeni D, Boyle P, et al. Meta-analysis of risk factors for cutaneous melanoma: I. Common and atypical naevi. Eur J Cancer. 2005;41:28–44.

117. Watt AJ, Kotsis SV, Chung KC. Risk of melanoma arising in large congenital melanocytic nevi: a systematic review. Plast Reconstr Surg. 2004;113:1968–74.

118. Stam-Posthuma JJ, Duinen C van, Scheffer E, Vink J, Bergman W. Multiple primary melanomas. J Am Acad Dermatol. 2001;44:22–7.

119. Titus-Ernstoff L, Perry AE, Spencer SK, Gibson JJ, Cole BF, Ernstoff MS. Pigmentary characteristics and moles in relation to melanoma risk. Int J Cancer. 2005;116:144–9.

120. Rigel DS, Russak J, Friedman R. The Evolution of Melanoma Diagnosis: 25 Years Beyond the ABCDs. CA Cancer J Clin. 2010;60:301–16.

121. Neila J, Soyer HP. Key points in dermoscopy for diagnosis of melanomas, including difficult to diagnose melanomas, on the trunk and extremities. J Dermatol. 2011;38:3–9.

122. Carlos G, Anforth R, Clements A, Menzies AM, Carlino MS, Chou S, et al. Cutaneous Toxic Effects of BRAF Inhibitors Alone and in Combination With MEK Inhibitors for Metastatic Melanoma. JAMA Dermatol. 2015;151:1103–9.

123. Ascierto PA, McArthur GA, Dréno B, Atkinson V, Liszkay G, Di Giacomo AM, et al. Cobimetinib combined with vemurafenib in advanced BRAFV600-mutant melanoma (coBRIM): updated efficacy results from a randomised, double-blind, phase 3 trial. Lancet Oncol. 2016;17:1248–60.

124. Chapman PB, Hauschild A, Robert C, Haanen JB, Ascierto P, Larkin J, et al. Improved Survival with Vemurafenib in Melanoma with BRAF V600E Mutation. N Engl J Med. 2011;364:2507–16.

125. Maverakis E, Cornelius LA, Bowen GM, Phan T, Patel FB, Fitzmaurice S, et al. Metastatic Melanoma – A Review of Current and Future Treatment Options [Internet]. 2015 [cited 2019 Feb 11]. Available from: https://www.ingentaconnect.com/content/mjl/adv/2015/00000095/00000005/art00002

126. John HE, Mahaffey PJ. Laser ablation and cryotherapy of melanoma metastases. J Surg Oncol. 2014;109:296–300.

127. Bouchlaka MN, Sckisel GD, Wilkins D, Maverakis E, Monjazeb AM, Fung M, et al. Mechanical disruption of tumors by iron particles and magnetic field application results in increased anti-tumor immune responses. PloS One. 2012;7:e48049.

128. Delaney G, Barton M, Jacob S. Estimation of an optimal radiotherapy utilization rate for melanoma: a review of the evidence. Cancer. 2004;100:1293–301.

129. Yamamoto T, Ueta E, Osaki T. Apoptosis induction by interleukin-2-activated cytotoxic lymphocytes in a squamous cell carcinoma cell line and Daudi cells - involvement of reactive oxygen species-dependent cytochrome c and reactive oxygen species-independent apoptosis-inducing factors. Immunology. 2003;110:217–24.

130. Atkins MB, Lotze MT, Dutcher JP, Fisher RI, Weiss G, Margolin K, et al. High-dose recombinant interleukin 2 therapy for patients with metastatic melanoma: analysis of 270 patients treated between 1985 and 1993. J Clin Oncol Off J Am Soc Clin Oncol. 1999;17:2105–16.

131. Moff SL, Corey GR, Gottfredsson M. Distant Cutaneous Granulomas after Bacille Calmette-Guérin Immunotherapy for Malignant Melanoma: Case for Direct Infection. Clin Infect Dis. 1999;29:1569–70.

132. Theofilopoulos AN, Baccala R, Beutler B, Kono DH. Type I interferons (alpha/beta) in immunity and autoimmunity. Annu Rev Immunol. 2005;23:307–36.

133. Werdin F, Tennenhaus M, Schaller H-E, Rennekampff H-O. Evidence-based Management Strategies for Treatment of Chronic Wounds. Eplasty [Internet]. 2009 [cited 2019 Feb 18];9. Available from: https://www.ncbi.nlm.nih.gov/pmc/articles/PMC2691645/

134. Wolchok JD, Kluger H, Callahan MK, Postow MA, Rizvi NA, Lesokhin AM, et al. Nivolumab plus ipilimumab in advanced melanoma. N Engl J Med. 2013;369:122–33.

135. Selzer E, Okamoto I, Lucas T, Kodym R, Pehamberger H, Jansen B. Protein kinase C isoforms in normal and transformed cells of the melanocytic lineage. Melanoma Res. 2002;12:201–9.

136. Eisinger M, Marko O. Selective proliferation of normal human melanocytes in vitro in the presence of phorbol ester and cholera toxin. Proc Natl Acad Sci U S A. 1982;79:2018–22.

137. Baird WM, Boutwell RK. Tumor-promoting Activity of Phorbol and Four Diesters of Phorbol in Mouse Skin. Cancer Res. 1971;31:1074–9.

138. Philip PA, Rea D, Thavasu P, Carmichael J, Stuart NS, Rockett H, et al. Phase I study of bryostatin 1: assessment of interleukin 6 and tumor necrosis factor alpha induction in vivo. The Cancer Research Campaign Phase I Committee. J Natl Cancer Inst. 1993;85:1812–8.

139. Gonzalez R, Ebbinghaus S, Henthorn TK, Miller D, Kraft AS. Treatment of patients with metastatic melanoma with bryostatin-1--a phase II study. Melanoma Res. 1999;9:599–606.

140. Propper DJ, Macaulay V, O'Byrne KJ, Braybrooke JP, Wilner SM, Ganesan TS, et al. A phase II study of bryostatin 1 in metastatic malignant melanoma. Br J Cancer. 1998;78:1337–41.

141. Weitman SD, Langevin AR, Berkow RL, Thomas PJ, Hurwitz CA, Kraft AS, et al. A phase I trial of bryostatin-1 in children with refractory solid tumors: A Pediatric Oncology Group Study. Clin Cancer Res. 1999;5:2344–8.

131

142. Ratnayake WS, Apostolatos CA, Apostolatos AH, Schutte RJ, Huynh MA, Ostrov DA, et al. Oncogenic PKC-ι activates Vimentin during epithelial-mesenchymal transition in melanoma; a study based on PKC-ι and PKC-ζ specific inhibitors. Cell Adhes Migr. 2018;0:1–17.

143. Ratnayake WS, Apostolatos AH, Ostrov DA, Acevedo-Duncan M. Two novel atypical PKC inhibitors; ACPD and DNDA effectively mitigate cell proliferation and epithelial to mesenchymal transition of metastatic melanoma while inducing apoptosis. Int J Oncol. 2017;51:1370–82.

144. Ratnayke WS, Apostolatos CA, Breedy S, Apostolatos AH, Acevedo-Duncan M. FOXO1 regulates oncogenic PKC-ι expression in melanoma inversely to c-Jun in an autocrine manner via IL-17E and ICAM-1 activation. World Acad Sci J. 2019;1:25–38.

145. Ratnayake WS, Apostolatos CA, Acevedo-Duncan M. Atypical Protein Kinase Cs in Melanoma Progression. Cutan Melanoma [Internet]. 2019 [cited 2019 Mar 22]; Available from: https://www.intechopen.com/online-first/atypical-protein-kinase-cs-in-melanoma-progression

146. Stallings-Mann M, Jamieson L, Regala RP, Weems C, Murray NR, Fields AP. A Novel Small-Molecule Inhibitor of Protein Kinase Cι Blocks Transformed Growth of Non–Small-Cell Lung Cancer Cells. Cancer Res. 2006;66:1767–74.

147. Bensen WG, Moore N, Tugwell P, D'Souza M, Singal DP. HLA antigens and toxic reactions to sodium aurothiomalate in patients with rheumatoid arthritis. J Rheumatol. 1984;11:358–61.

148. Sajan MP, Acevedo-Duncan ME, Standaert ML, Ivey RA, Lee M, Farese RV. Akt-Dependent Phosphorylation of Hepatic FoxO1 Is Compartmentalized on a WD40/ProF Scaffold and Is Selectively Inhibited by aPKC in Early Phases of Diet-Induced Obesity. Diabetes. 2014;63:2690–701.

149. Sajan MP, Ivey RA, Farese RV. Metformin action in human hepatocytes: coactivation of atypical protein kinase C alters 5 '-AMP-activated protein kinase effects on lipogenic and gluconeogenic enzyme expression. Diabetologia. 2013;56:2507–16.

150. Sajan MP, Ivey RA, Lee MC, Farese RV. Hepatic insulin resistance in ob/ob mice involves increases in ceramide, aPKC activity, and selective impairment of Akt-dependent FoxO1 phosphorylation. J Lipid Res. 2015;56:70–80.

151. Wooten MW, Seibenhener ML, Zhou GS, Vandenplas ML, Tan TH. Overexpression of atypical PKC in PC12 cells enhances NGF-responsiveness and survival through an NF-kappa B dependent pathway. Cell Death Differ. 1999;6:753–64.

152. Barnes PJ, Karin M. Nuclear Factor-κB — A Pivotal Transcription Factor in Chronic Inflammatory Diseases [Internet]. http://dx.doi.org/10.1056/NEJM199704103361506. 2009 [cited 2019 Feb 19]. Available from: https://www.nejm.org/doi/10.1056/NEJM199704103361506

153. Sen R, Baltimore D. Inducibility of κ immunoglobulin enhancer-binding protein NF-κB by a posttranslational mechanism. Cell. 1986;47:921–8.

154. Tilborghs S, Corthouts J, Verhoeven Y, Arias D, Rolfo C, Trinh XB, et al. The role of Nuclear Factor-kappa B signaling in human cervical cancer. Crit Rev Oncol Hematol. 2017;120:141–50.

155. Baldwin AS. Series Introduction: The transcription factor NF-κB and human disease. J Clin Invest. 2001;107:3–6.

156. Caamaño J, Hunter CA. NF-κB Family of Transcription Factors: Central Regulators of Innate and Adaptive Immune Functions. Clin Microbiol Rev. 2002;15:414–29.

157. Hoesel B, Schmid JA. The complexity of NF-κB signaling in inflammation and cancer. Mol Cancer. 2013;12:86.

158. Perkins ND. NF-κB: tumor promoter or suppressor? Trends Cell Biol. 2004;14:64–9.

159. Xia Y, Shen S, Verma IM. NF-κB, an Active Player in Human Cancers. Cancer Immunol Res. 2014;2:823–30.

160. Chaturvedi MM, Sung B, Yadav VR, Kannappan R, Aggarwal BB. NF-κB addiction and its role in cancer: 'one size does not fit all.' Oncogene. 2011;30:1615–30.

161. Kucharczak J, Simmons MJ, Fan Y, Gélinas C. To be, or not to be: NF-κB is the answer – role of Rel/NF-κB in the regulation of apoptosis. Oncogene. 2003;22:8961–82.

162. Perkins ND, Gilmore TD. Good cop, bad cop: the different faces of NF-κB. Cell Death Differ. 2006;13:759–72.

163. Guttridge DC, Albanese C, Reuther JY, Pestell RG, Baldwin AS. NF-κB Controls Cell Growth and Differentiation through Transcriptional Regulation of Cyclin D1. Mol Cell Biol. 1999;19:5785–99.

164. Rosa FAL, Pierce JW, Sonenshein GE. Differential regulation of the c-myc oncogene promoter by the NF-kappa B rel family of transcription factors. Mol Cell Biol. 1994;14:1039–44.

165. Xie T-X, Xia Z, Zhang N, Gong W, Huang S. Constitutive NF-κB activity regulates the expression of VEGF and IL-8 and tumor angiogenesis of human glioblastoma. Oncol Rep. 2010;23:725–32.

166. Karin M, Cao Y, Greten FR, Li Z-W. NF-κB in cancer: from innocent bystander to major culprit. Nat Rev Cancer. 2002;2:301–10.

167. Toren P, Zoubeidi A. Targeting the PI3K/Akt pathway in prostate cancer: Challenges and opportunities (Review). Int J Oncol. 2014;45:1793–801.

133

168. Jia S, Liu Z, Zhang S, Liu P, Zhang L, Lee SH, et al. Essential roles of PI(3)K-p110beta in cell growth, metabolism and tumorigenesis. Nature. 2008;454:776–9.

169. Kremer CL, Klein RR, Mendelson J, Browne W, Samadzedeh LK, Vanpatten K, et al. Expression of mTOR signaling pathway markers in prostate cancer progression. The Prostate. 2006;66:1203–12.

170. Cantley LC. The phosphoinositide 3-kinase pathway. Science. 2002;296:1655–7.

171. Scott M, Fujita T, Liou H, Nolan G, Baltimore D. The P65-Subunit of Nf-Kappa-B Regulates I-Kappa-B by 2 Distinct Mechanisms. Genes Dev. 1993;7:1266–76.

172. Janicke RU, Sprengart ML, Wati MR, Porter AG. Caspase-3 is required for DNA fragmentation and morphological changes associated with apoptosis. J Biol Chem. 1998;273:9357–60.

173. Kroemer G. The proto-oncogene Bcl-2 and its role in regulating apoptosis. Nat Med. 1997;3:614–20.

174. Watson A, Askew J, Benson R. Poly(adenosine Diphosphate Ribose) Polymerase Inhibition Prevents Necrosis Induced by H2o2 but Not Apoptosis. Gastroenterology. 1995;109:472–82.

175. Soldani C, Scovassi AI. Poly(ADP-ribose) polymerase-1 cleavage during apoptosis: An update. Apoptosis. 2002;7:321–8.

176. van Raam BJ, Drewniak A, Groenewold V, van den Berg TK, Kuijpers TW. Granulocyte colony-stimulating factor delays neutrophil apoptosis by inhibition of calpains upstream of caspase-3. Blood. 2008;112:2046–54.

177. Cohen GM. Caspases: the executioners of apoptosis. Biochem J. 1997;326:1–16.

178. Kasof GM, Lu JJ, Liu DR, Speer B, Mongan KN, Gomes BC, et al. Tumor necrosis factor-alpha induces the expression of DR6, a member of the TNF receptor family, through activation of NF-kappa B. Oncogene. 2001;20:7965–75.

179. Kiesslich T, Pichler M, Neureiter D. Epigenetic control of epithelial-mesenchymal-transition in human cancer (Review). Mol Clin Oncol. 2013;1:3–11.

180. Thiery JP, Sleeman JP. Complex networks orchestrate epithelial-mesenchymal transitions. Nat Rev Mol Cell Biol. 2006;7:131–42.

181. Thiery JP, Acloque H, Huang RYJ, Nieto MA. Epithelial-mesenchymal transitions in development and disease. Cell. 2009;139:871–90.

182. Choi SS, Diehl AM. Epithelial-to-mesenchymal transitions in the liver. Hepatol Baltim Md. 2009;50:2007–13.

183. Kirchner T, Brabletz T. Patterning and Nuclear β-Catenin Expression in the Colonic Adenoma-Carcinoma Sequence. Am J Pathol. 2000;157:1113–21.

184. Nakaya Y, Sheng G. Epithelial to mesenchymal transition during gastrulation: an embryological view. Dev Growth Differ. 2008;50:755–66.

185. Qin Q, Xu Y, He T, Qin C, Xu J. Normal and disease-related biological functions of Twist1 and underlying molecular mechanisms. Cell Res. 2012;22:90–106.

186. Piera-Velazquez S, Li Z, Jimenez SA. Role of endothelial-mesenchymal transition (EndoMT) in the pathogenesis of fibrotic disorders. Am J Pathol. 2011;179:1074–80.

187. Hanahan D, Weinberg RA. Hallmarks of cancer: the next generation. Cell. 2011;144:646–74.

188. Hanahan D, Weinberg RA. The hallmarks of cancer. Cell. 2000;100:57–70.

189. Hong S-M, Li A, Olino K, Wolfgang CL, Herman JM, Schulick RD, et al. Loss of E-Cadherin Expression and Outcome among Patients with Resectable Pancreatic Adenocarcinomas. Mod Pathol Off J U S Can Acad Pathol Inc. 2011;24:1237–47.

190. Jouppila-Mättö A, Tuhkanen H, Soini Y, Pukkila M, Närkiö-Mäkelä M, Sironen R, et al. Transcription factor snail1 expression and poor survival in pharyngeal squamous cell carcinoma. Histol Histopathol. 2011;26:443–9.

191. Lamouille S, Xu J, Derynck R. Molecular mechanisms of epithelial–mesenchymal transition. Nat Rev Mol Cell Biol. 2014;15:178–96.

192. Lai Y-K, Lee W-C, Chen K-D. Vimentin serves as a phosphate sink during the apparent activation of protein kinases by okadaic acid in mammalian cells. J Cell Biochem. 53:161–8.

193. Goto H, Yasui Y, Kawajiri A, Nigg EA, Terada Y, Tatsuka M, et al. Aurora-B Regulates the Cleavage Furrow-specific Vimentin Phosphorylation in the Cytokinetic Process. J Biol Chem. 2003;278:8526–30.

194. Snider NT, Omary MB. Post-translational modifications of intermediate filament proteins: mechanisms and functions. Nat Rev Mol Cell Biol. 2014;15:163–77.

195. Ivaska J, Vuoriluoto K, Huovinen T, Izawa I, Inagaki M, Parker PJ. PKCε-mediated phosphorylation of vimentin controls integrin recycling and motility. EMBO J. 2005;24:3834–45.

196. Yasui Y, Goto H, Matsui S, Manser E, Lim L, Nagata Ki null, et al. Protein kinases required for segregation of vimentin filaments in mitotic process. Oncogene. 2001;20:2868–76.

197. Eriksson JE, He T, Trejo-Skalli AV, Härmälä-Braskén A-S, Hellman J, Chou Y-H, et al. Specific in vivo phosphorylation sites determine the assembly dynamics of vimentin intermediate filaments. J Cell Sci. 2004;117:919–32.

198. Goto H, Kosako H, Tanabe K, Yanagida M, Sakurai M, Amano M, et al. Phosphorylation of Vimentin by Rho-associated Kinase at a Unique Amino-terminal Site That Is Specifically Phosphorylated during Cytokinesis. J Biol Chem. 1998;273:11728–36.

199. Zhu Q-S, Rosenblatt K, Huang K-L, Lahat G, Brobey R, Bolshakov S, et al. Vimentin is a novel AKT1 target mediating motility and invasion. Oncogene. 2011;30:457–70.

200. Cheng T-J, Tseng Y-F, Chang W-M, Chang MD-T, Lai Y-K. Retaining of the assembly capability of vimentin phosphorylated by mitogen-activated protein kinase-activated protein kinase-2. J Cell Biochem. 2003;89:589–602.

201. Yamaguchi T, Goto H, Yokoyama T, Silljé H, Hanisch A, Uldschmid A, et al. Phosphorylation by Cdk1 induces Plk1-mediated vimentin phosphorylation during mitosis. J Cell Biol. 2005;171:431–6.

202. Li Q-F, Spinelli AM, Wang R, Anfinogenova Y, Singer HA, Tang DD. Critical Role of Vimentin Phosphorylation at Ser-56 by p21-activated Kinase in Vimentin Cytoskeleton Signaling. J Biol Chem. 2006;281:34716–24.

203. Tsujimura K, Ogawara M, Takeuchi Y, Imajoh-Ohmi S, Ha MH, Inagaki M. Visualization and function of vimentin phosphorylation by cdc2 kinase during mitosis. J Biol Chem. 1994;269:31097–106.

204. Huang RY-J, Guilford P, Thiery JP. Early events in cell adhesion and polarity during epithelial-mesenchymal transition. J Cell Sci. 2012;125:4417–22.

205. Peinado H, Olmeda D, Cano A. Snail, Zeb and bHLH factors in tumour progression: an alliance against the epithelial phenotype? Nat Rev Cancer. 2007;7:415–28.

206. Ocaña OH, Córcoles R, Fabra Á, Moreno-Bueno G, Acloque H, Vega S, et al. Metastatic Colonization Requires the Repression of the Epithelial-Mesenchymal Transition Inducer Prrx1. Cancer Cell. 2012;22:709–24.

207. Xu S, Wang H, Pan H, Shi Y, Li T, Ge S, et al. ANRIL lncRNA triggers efficient therapeutic efficacy by reprogramming the aberrant INK4-hub in melanoma. Cancer Lett. 2016;381:41–8.

208. O'Connell MP, French AD, Leotlela PD, Weeraratna AT. Assaying Wnt5A-mediated invasion in melanoma cells. Methods Mol Biol Clifton NJ. 2008;468:243–53.

209. Apostolatos AH, Ratnayake WS, Smalley T, Islam A, Acevedo-Duncan M. Abstract 2369: Transcription activators that regulate PKC-iota expression and are downstream targets of PKC-iota. Cancer Res. 2017;77:2369–2369.

210. Inagaki M, Inagaki N, Takahashi T, Takai Y. Phosphorylation-Dependent Control of Structures of Intermediate Filaments: A Novel Approach Using Site- and Phosphorylation State-Specific Antibodies. J Biochem (Tokyo). 1997;121:407–14.

211. Xu J, Lamouille S, Derynck R. TGF-β-induced epithelial to mesenchymal transition. Cell Res. 2009;19:156–72.

212. Sahlgren C, Gustafsson MV, Jin S, Poellinger L, Lendahl U. Notch signaling mediates hypoxia-induced tumor cell migration and invasion. Proc Natl Acad Sci. 2008;105:6392–7.

213. Yang M-H, Hsu DS-S, Wang H-W, Wang H-J, Lan H-Y, Yang W-H, et al. Bmi1 is essential in Twist1-induced epithelial–mesenchymal transition. Nat Cell Biol. 2010;12:982–92.

214. Kim H-J, Litzenburger BC, Cui X, Delgado DA, Grabiner BC, Lin X, et al. Constitutively Active Type I Insulin-Like Growth Factor Receptor Causes Transformation and Xenograft Growth of Immortalized Mammary Epithelial Cells and Is Accompanied by an Epithelial-to-Mesenchymal Transition Mediated by NF-κB and Snail. Mol Cell Biol. 2007;27:3165–75.

215. Gunaratne A, Di Guglielmo GM. Par6 is phosphorylated by aPKC to facilitate EMT. Cell Adhes Migr. 2013;7:357–61.

216. Valcourt U, Kowanetz M, Niimi H, Heldin C-H, Moustakas A. TGF-beta and the Smad signaling pathway support transcriptomic reprogramming during epithelial-mesenchymal cell transition. Mol Biol Cell. 2005;16:1987–2002.

217. Nelson WJ. Remodeling Epithelial Cell Organization: Transitions Between Front–Rear and Apical–Basal Polarity. Cold Spring Harb Perspect Biol [Internet]. 2009 [cited 2017 Oct 3];1. Available from: https://www.ncbi.nlm.nih.gov/pmc/articles/PMC2742086/

218. Wu J, Lu M, Li Y, Shang Y-K, Wang S-J, Meng Y, et al. Regulation of a TGF-β1-CD147 self-sustaining network in the differentiation plasticity of hepatocellular carcinoma cells. Oncogene. 2016;35:5468–79.

219. Butler AM, Buzhardt MLS, Erdogan E, Li S, Inman KS, Fields AP, et al. A small molecule inhibitor of atypical protein kinase C signaling inhibits pancreatic cancer cell transformed growth and invasion. Oncotarget. 2015;6:15297–310.

220. Wisdom R, Johnson RS, Moore C. c-Jun regulates cell cycle progression and apoptosis by distinct mechanisms. EMBO J. 1999;18:188–97.

221. Angel P, Hattori K, Smeal T, Karin M. The jun proto-oncogene is positively autoregulated by its product, Jun/AP-1. Cell. 1988;55:875–85.

222. Lopez-Bergami P, Huang C, Goydos JS, Yip D, Bar-Eli M, Herlyn M, et al. Rewired ERK-JNK Signaling Pathways in Melanoma. Cancer Cell. 2007;11:447–60.

223. Vogt PK. Fortuitous convergences: the beginnings of JUN. Nat Rev Cancer. 2002;2:465–9.

137

224. Szabo E, Riffe ME, Steinberg SM, Birrer MJ, Linnoila RI. Altered cJUN expression: an early event in human lung carcinogenesis. Cancer Res. 1996;56:305–15.

225. Vleugel MM, Greijer AE, Bos R, van der Wall E, van Diest PJ. c-Jun activation is associated with proliferation and angiogenesis in invasive breast cancer. Hum Pathol. 2006;37:668–74.

226. Behrens A, Sibilia M, Wagner EF. Amino-terminal phosphorylation of c-Jun regulates stress-induced apoptosis and cellular proliferation. Nat Genet. 1999;21:326–9.

227. Nateri AS, Spencer-Dene B, Behrens A. Interaction of phosphorylated c-Jun with TCF4 regulates intestinal cancer development. Nature. 2005;437:281–5.

228. Rena G, Guo S, Cichy SC, Unterman TG, Cohen P. Phosphorylation of the Transcription Factor Forkhead Family Member FKHR by Protein Kinase B. J Biol Chem. 1999;274:17179–83.

229. Nakae J, Kitamura T, Kitamura Y, Biggs WH, Arden KC, Accili D. The Forkhead Transcription Factor Foxo1 Regulates Adipocyte Differentiation. Dev Cell. 2003;4:119–29.

230. Matsuzaki H, Daitoku H, Hatta M, Tanaka K, Fukamizu A. Insulin-induced phosphorylation of FKHR (Foxo1) targets to proteasomal degradation. Proc Natl Acad Sci. 2003;100:11285–90.

231. Huang HL and H. FOXO1: A Potential Target for Human Diseases [Internet]. Curr. Drug Targets. 2011 [cited 2018 Sep 15]. Available from: http://www.eurekaselect.com/74460/article

232. Borkhardt A, Repp R, Haas OA, Leis T, Harbott J, Kreuder J, et al. Cloning and characterization of AFX, the gene that fuses to MLL in acute leukemias with a t(X;11)(q13;q23). Oncogene. 1997;14:195–202.

233. Anderson MJ, Viars CS, Czekay S, Cavenee WK, Arden KC. Cloning and characterization of three human forkhead genes that comprise an FKHR-like gene subfamily. Genomics. 1998;47:187–99.

234. Zhang X, Tang N, Hadden TJ, Rishi AK. Akt, FoxO and regulation of apoptosis. Biochim Biophys Acta BBA - Mol Cell Res. 2011;1813:1978–86.

235. Farhan M, Wang H, Gaur U, Little PJ, Xu J, Zheng W. FOXO Signaling Pathways as Therapeutic Targets in Cancer. Int J Biol Sci. 2017;13:815–27.

236. Fu Z, Tindall D. FOXOs, cancer and regulation of apoptosis. Oncogene. 2008;27:2312.

237. Zhang Y, Zhang L, Sun H, Lv Q, Qiu C, Che X, et al. Forkhead transcription factor 1 inhibits endometrial cancer cell proliferation via sterol regulatory element-binding protein 1. Oncol Lett. 2017;13:731–7.

138

238. Hodge DR, Hurt EM, Farrar WL. The role of IL-6 and STAT3 in inflammation and cancer. Eur J Cancer. 2005;41:2502–12.

239. Yue P, Turkson J. Targeting STAT3 in cancer: how successful are we? Expert Opin Investig Drugs. 2009;18:45–56.

240. Page BDG, Khoury H, Laister RC, Fletcher S, Vellozo M, Manzoli A, et al. Small Molecule STAT5-SH2 Domain Inhibitors Exhibit Potent Antileukemia Activity. J Med Chem. 2012;55:1047–55.

241. Pardanani A, Lasho T, Smith G, Burns CJ, Fantino E, Tefferi A. CYT387, a selective JAK1/JAK2 inhibitor: *in vitro* assessment of kinase selectivity and preclinical studies using cell lines and primary cells from polycythemia vera patients. Leukemia. 2009;23:1441–5.

242. Jing N, Tweardy DJ. Targeting Stat3 in cancer therapy. Anticancer Drugs. 2005;16:601.

243. Rani A, Murphy JJ. STAT5 in Cancer and Immunity. J Interferon Cytokine Res Off J Int Soc Interferon Cytokine Res. 2016;36:226–37.

244. Korneev KV, Atretkhany K-SN, Drutskaya MS, Grivennikov SI, Kuprash DV, Nedospasov SA. TLR-signaling and proinflammatory cytokines as drivers of tumorigenesis. Cytokine. 2017;89:127–35.

245. Zhang X, Wrzeszczynska MH, Horvath CM, Darnell JE. Interacting Regions in Stat3 and c-Jun That Participate in Cooperative Transcriptional Activation. Mol Cell Biol. 1999;19:7138–46.

246. Hornsveld M, Dansen TB, Derksen PW, Burgering BMT. Re-evaluating the role of FOXOs in cancer. Semin Cancer Biol. 2018;50:90–100.

247. Sunters A, Madureira PA, Pomeranz KM, Aubert M, Brosens JJ, Cook SJ, et al. Paclitaxel-induced nuclear translocation of FOXO3a in breast cancer cells is mediated by c-Jun NH2-terminal kinase and Akt. Cancer Res. 2006;66:212–20.

248. Yuan Z, Guan Y, Wang L, Wei W, Kane AB, Chin YE. Central Role of the Threonine Residue within the p+1 Loop of Receptor Tyrosine Kinase in STAT3 Constitutive Phosphorylation in Metastatic Cancer Cells. Mol Cell Biol. 2004;24:9390–400.

249. Antonicelli F, Lorin J, Kurdykowski S, Gangloff SC, Naour RL, Sallenave JM, et al. CXCL10 reduces melanoma proliferation and invasiveness in vitro and in vivo. Br J Dermatol. 2011;164:720–8.

250. Zaynagetdinov R, Sherrill TP, Gleaves LA, McLoed AG, Saxon JA, Habermann AC, et al. Interleukin-5 Facilitates Lung Metastasis by Modulating the Immune Microenvironment. Cancer Res. 2015;75:1624–34.

251. Sun X, Cheng G, Hao M, Zheng J, Zhou X, Zhang J, et al. CXCL12 / CXCR4 / CXCR7 chemokine axis and cancer progression. Cancer Metastasis Rev. 2010;29:709–22.

139

252. Wightman SC, Uppal A, Pitroda SP, Ganai S, Burnette B, Stack M, et al. Oncogenic CXCL10 signalling drives metastasis development and poor clinical outcome. Br J Cancer. 2015;113:327–35.

253. Peng H, Chen P, Cai Y, Chen Y, Wu Q, Li Y, et al. Endothelin-1 increases expression of cyclooxygenase-2 and production of interlukin-8 in hunan pulmonary epithelial cells. Peptides. 2008;29:419–24.

254. Timani KA, Győrffy B, Liu Y, Mohammad KS, He JJ. Tip110/SART3 regulates IL-8 expression and predicts the clinical outcomes in melanoma. Mol Cancer [Internet]. 2018 [cited 2018 Sep 17];17. Available from: https://www.ncbi.nlm.nih.gov/pmc/articles/PMC6098614/

255. Yang M, Liu J, Piao C, Shao J, Du J. ICAM-1 suppresses tumor metastasis by inhibiting macrophage M2 polarization through blockade of efferocytosis. Cell Death Dis. 2015;6:e1780.

256. Groote ML de, Kazemier HG, Huisman C, Gun BTF van der, Faas MM, Rots MG. Upregulation of endogenous ICAM-1 reduces ovarian cancer cell growth in the absence of immune cells. Int J Cancer. 2014;134:280–90.

257. Benatar T, Cao MY, Lee Y, Lightfoot J, Feng N, Gu X, et al. IL-17E, a proinflammatory cytokine, has antitumor efficacy against several tumor types in vivo. Cancer Immunol Immunother. 2010;59:805–17.

258. Benatar T, Cao MY, Lee Y, Li H, Feng N, Gu X, et al. Virulizin induces production of IL-17E to enhance antitumor activity by recruitment of eosinophils into tumors. Cancer Immunol Immunother CII. 2008;57:1757–69.

259. Wei C, Sirikanjanapong S, Lieberman S, Delacure M, Martiniuk F, Levis W, et al. Primary mucosal melanoma arising from the eustachian tube with CTLA-4, IL-17A, IL-17C, and IL-17E upregulation. Ear Nose Throat J. 2013;92:36–40.

260. Blázquez AB, Vázquez-Calvo Á, Martín-Acebes MA, Saiz J-C. Pharmacological Inhibition of Protein Kinase C Reduces West Nile Virus Replication. Viruses. 2018;10:91.

261. Kim HK, Cho SW, Heo HJ, Jeong SH, Kim M, Ko KS, et al. A Novel Atypical PKC-Iota Inhibitor, Echinochrome A, Enhances Cardiomyocyte Differentiation from Mouse Embryonic Stem Cells. Mar Drugs. 2018;16:192.

262. Kwiatkowski J, Liu B, Tee DHY, Chen G, Ahmad NHB, Wong YX, et al. Fragment-Based Drug Discovery of Potent Protein Kinase C Iota Inhibitors. J Med Chem. 2018;61:4386–96.

263. Gan Z, Ding L, Burckhardt CJ, Lowery J, Zaritsky A, Sitterley K, et al. Vimentin Intermediate Filaments Template Microtubule Networks to Enhance Persistence in Cell Polarity and Directed Migration. Cell Syst. 2016;3:500–1.

264. Trott O, Olson AJ. AutoDock Vina: improving the speed and accuracy of docking with a new scoring function, efficient optimization and multithreading. J Comput Chem. 2010;31:455–61.

265. Weininger D. SMILES, a chemical language and information system. 1. Introduction to methodology and encoding rules. J Chem Inf Comput Sci. 1988;28:31–6.

266. Fogh J, Wright WC, Loveless JD. Absence of HeLa cell contamination in 169 cell lines derived from human tumors. J Natl Cancer Inst. 1977;58:209–14.

267. Justus CR, Leffler N, Ruiz-Echevarria M, Yang LV. In vitro Cell Migration and Invasion Assays. J Vis Exp JoVE [Internet]. 2014 [cited 2017 Nov 18]; Available from: https://www.ncbi.nlm.nih.gov/pmc/articles/PMC4186330/

268. Feoktistova M, Geserick P, Leverkus M. Crystal Violet Assay for Determining Viability of Cultured Cells. Cold Spring Harb Protoc. 2016;2016:pdb.prot087379.

269. El Bassit G, Patel RS, Carter G, Shibu V, Patel AA, Song S, et al. MALAT1 in Human Adipose Stem Cells Modulates Survival and Alternative Splicing of PKCδII in HT22 Cells. Endocrinology. 2017;158:183–95.

270. Venter JC, Adams MD, Myers EW, Li PW, Mural RJ, Sutton GG, et al. The Sequence of the Human Genome. Science. 2001;291:1304–51.

271. Fagerberg L, Hallström BM, Oksvold P, Kampf C, Djureinovic D, Odeberg J, et al. Analysis of the Human Tissue-specific Expression by Genome-wide Integration of Transcriptomics and Antibody-based Proteomics. Mol Cell Proteomics. 2014;13:397–406.

272. Livak KJ, Schmittgen TD. Analysis of relative gene expression data using real-time quantitative PCR and the 2(-Delta Delta C(T)) Method. Methods San Diego Calif. 2001;25:402–8.

APPENDIX A

The results demonstrated in this dissertation were published in the form of three full research articles and one book chapter. Publishers granted permissions to reproduce those contents and the emails, letters of permission granting are included in this section.

USF

Wishrawana Ratnayake <ratnayake@mail.usf.edu>

Permission to include images and content in a dissertation- Wishrawana S Ratnayake

2 messages

Wishrawana Ratnayake <ratnayake@mail.usf.edu>   Sun, Jan 20, 2019 at 8:34 PM
To: Spandidos Publication IJO <ijo@spandidos-publications.com>, support@spandidos-publications.com, contact@worldacademyofsciences.com
Cc: "Acevedo-Duncan, Mildred" <macevedo@usf.edu>

To Whom it may concern,

My name is Wishrawana S Ratnayake and I'm the 1st author/ co-1st author of the following papers published in the Spandidos journals; *International Journal of Oncology and World Academy of Sciences Journal*.

01)
Ratnayake WS, Apostolatos AH, Ostrov DA, Acevedo-Duncan M. Two novel atypical PKC inhibitors; ACPD and DNDA effectively mitigate cell proliferation and epithelial to mesenchymal transition of metastatic melanoma while inducing apoptosis. Int J Oncol. 2017;51: 1370–1382. doi:10.3892/ijo.2017.4131

02)
Ratnayake W, Apostolatos C, Breedy S, Apostolatos A, Acevedo-Duncan M. FOXO1 regulates oncogenic PKC-ι expression in melanoma inversely to c-Jun in an autocrine manner via IL-17E and ICAM-1 activation. World Acad Sci J. Vol. 1. Issue 1 25-38, 2019; doi:10.3892/wasj.2018.2

03)
Apostolatos AH, Ratnayake WS, Win-Piazza H, Apostolatos CA, Smalley T, Kang L, et al. Inhibition of atypical protein kinase C-ι effectively reduces the malignancy of prostate cancer cells by downregulating the NF-κB signaling cascade. Int J Oncol. 2018;53: 1836–1846. doi:10.3892/ijo.2018.4542

I am a doctoral candidate in the department of Chemistry, University of South Florida, Tampa, FL, USA and I need to include some of the information and images from these papers to my dissertation. Could you please let me know the way to get permission for this? Your immediate attention is highly appreciated.

P.S. I have copied this email to Dr. Mildred Acevedo-Duncan, who is the Corresponding Author of the said papers.

Thank you.

Sincerely,
Wishrawana S. Ratnayake
--

Wishrawana Sarathi Ratnayake
Doctoral Candidate,
Dr. Mildred Acevedo-Duncan's Lab,
Chemistry, USF.

International Journal of Oncology - Spandidos Publications <ijo@spandidos-publications.com>   Mon, Jan 21, 2019 at 5:48 AM
To: Wishrawana Ratnayake <ratnayake@mail.usf.edu>

Dear Authors,

142

www.manaraa.com

Thank you for contacting us. Please note that permission has been granted, so you can use the requested papers. Please do not hesitate to contact us if you have any more queries.

Yours sincerely,

Spandidos Publications
--

Spandidos Publications Ltd.
10, Vriaxidos Street
116 35 Greece
fax: +30 210 725 2922
tel: +30 210 722 2809
e-mail: ijo@spandidos-publications.com
web-site: www.spandidos-publications.com

[Quoted text hidden]

USF

Wishrawana Ratnayake <ratnayake@mail.usf.edu>

Permission to include images and content in a dissertation- Wishrawana S Ratnayake

3 messages

Wishrawana Ratnayake <ratnayake@mail.usf.edu> Sun, Jan 20, 2019 at 8:18 PM
To: support@tandfonline.com, permissionrequest@tandf.co.uk
Cc: "Acevedo-Duncan, Mildred" <macevedo@usf.edu>

To Whom it may concern,

My name is Wishrawana S Ratnayake and I'm the 1st author of the following paper published in the journal *Cell Adhesion and Migration*.

Ratnayake WS, Apostolatos CA, Apostolatos AH, Schutte RJ, Huynh MA, Ostrov DA, et al. Oncogenic PKC-ɪ activates Vimentin during epithelial-mesenchymal transition in melanoma; a study based on PKC-ɪ and PKC-ζ specific inhibitors. Cell Adhes Migr. 12(5), 2018;447-463. doi:10.1080/19336918.2018.1471323

I am a doctoral candidate in the department of Chemistry, University of South Florida, Tampa, FL, USA and I need to include some of the information and images from this paper to my dissertation. Could you please let me know the way to get permission for this? Your immediate attention is highly appreciated.

P.S. I have copied this email to Dr. Mildred Acevedo-Duncan, who is the Corresponding Author of the said paper.

Thank you.

Sincerely,
Wishrawana S. Ratnayake
--
Wishrawana Sarathi Ratnayake
Doctoral Candidate,
Dr. Mildred Acevedo-Duncan's Lab,
Chemistry, USF.

Academic UK Non Rightslink <permissionrequest@tandf.co.uk> Thu, Feb 28, 2019 at 5:07 AM
To: Wishrawana Ratnayake <ratnayake@mail.usf.edu>

Good Morning Wishrawana S. Ratnayake,

Thank you for your email.

Please find attached a copy of your licence granting you permission.

If you have any issues at all, please do let me know and I will be happy to help.

With kind regards,

Annabel

Annabel Flude – Permissions Administrator, Journals

Taylor & Francis Group

3 Park Square, Milton Park, Abingdon, Oxon, OX14 4RN, UK.

Tel: +44 (0)20 7017 7617

Fax: +44 (0)20 7017 6336

Web: www.tandfonline.com

e-mail: annabel.flude@tandf.co.uk

Taylor & Francis Group
an informa business

Taylor & Francis is a trading name of Informa UK Limited,

registered in England under no. 1072954

[Quoted text hidden]

📄 **P19 0432.pdf**
176K

144

28 February 2019

Dear Wishrawana S. Ratnayake,

Material requested: Wishrawana S. Ratnayake, Christopher A. Apostolatos, André H. Apostolatos, Ryan J. Schutte, Monica A. Huynh, David A. Ostrov & Mildred Acevedo-Duncan (2018) Oncogenic PKC-ι activates Vimentin during epithelial-mesenchymal transition in melanoma; a study based on PKC-ι and PKC-ζ specific inhibitors, Cell Adhesion & Migration, 12:5, 447-463, DOI: 10.1080/19336918.2018.1471323

Thank you for your correspondence requesting permission to reproduce the above mentioned material from our Journal in your printed Thesis and to be posted in the university's repository –Department of Chemistry, University of South Florida, Tampa, FL, USA.

We will be pleased to grant permission on the sole condition that you acknowledge the original source of publication and insert a reference to the article on the Journals website:

"This is the authors accepted manuscript of an article published as the version of record in 2018© Taylor & Francis- https://doi.org/10.1080/19336918.2018.1471323 ".

This permission does not cover any third party copyrighted work which may appear in the material requested.

Please note that this licence does not allow you to post our content on any third party websites or repositories.

This licence does not allow the use of the Publishers version/PDF (this is the version of record that is published on the publisher's website) to be posted online.

Thank you for your interest in our Journal.

Yours sincerely,

Annabel Flude – Permissions Administrator, Journals
Taylor & Francis Group
3 Park Square, Milton Park, Abingdon, Oxon, OX14 4RN, UK.
Tel: +44 (0)20 7017 7617
Fax: +44 (0)20 7017 6336
Web: www.tandfonline.com
e-mail: annabel.flude@tandf.co.uk

Taylor & Francis Group
an **informa** business

145

USF

Wishrawana Ratnayake <ratnayake@mail.usf.edu>

IntechOpen – Your Chapter is Published

3 messages

Rozmari Marijan <rozmari@intechopen.com>   Fri, Mar 8, 2019 at 8:00 AM
To: Wishrawana Ratnayake <ratnayake@mail.usf.edu>

Dear Dr. Ratnayake,

We are pleased to let you know that your chapter has now been published online. Congratulations!

Online First means chapters are published individually, after review and before the entire book is ready for publication, ensuring research is made available to the scientific community without delay.

Your chapter has been published in this way and is now searchable and citable by DOI, so you can start receiving citations and downloads immediately. Your open access chapter can be reused as you like, as the copyright remains yours and you gain impact immediately without being dependent on the last person to submit to the book.

Once the rest of the book is ready, it will become part of the broader publication.

You can view your chapter here: https://www.intechopen.com/online-first/atypical-protein-kinase-cs-in-melanoma-progression

Please check your publication promptly to ensure that it corresponds to the final version of your chapter.

Please feel free to share it with your colleagues and peers, and on social media.

Regards,

Rozmari Marijan
Author Service Manager
_____

IntechOpen
The Shard, 32 London Bridge Street, London SE1 9SG, United Kingdom

www.intechopen.com

INTECHOPEN LIMITED, Registered in England and Wales No. 11086078

We are IntechOpen, the world's leading publisher of Open Access books
Built by scientists, for scientists

Full Western blots of the bands in Figure 2.1.

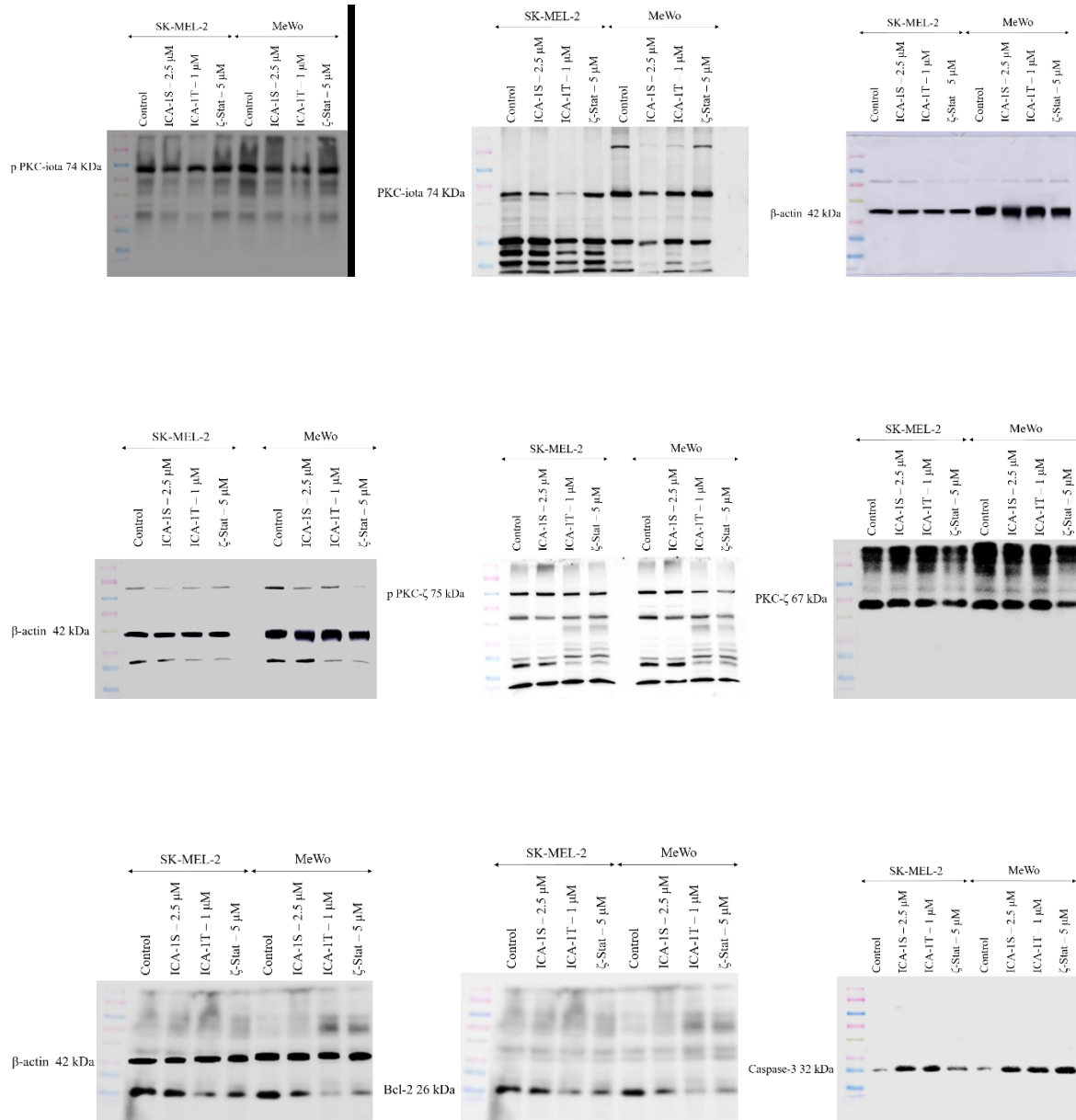147
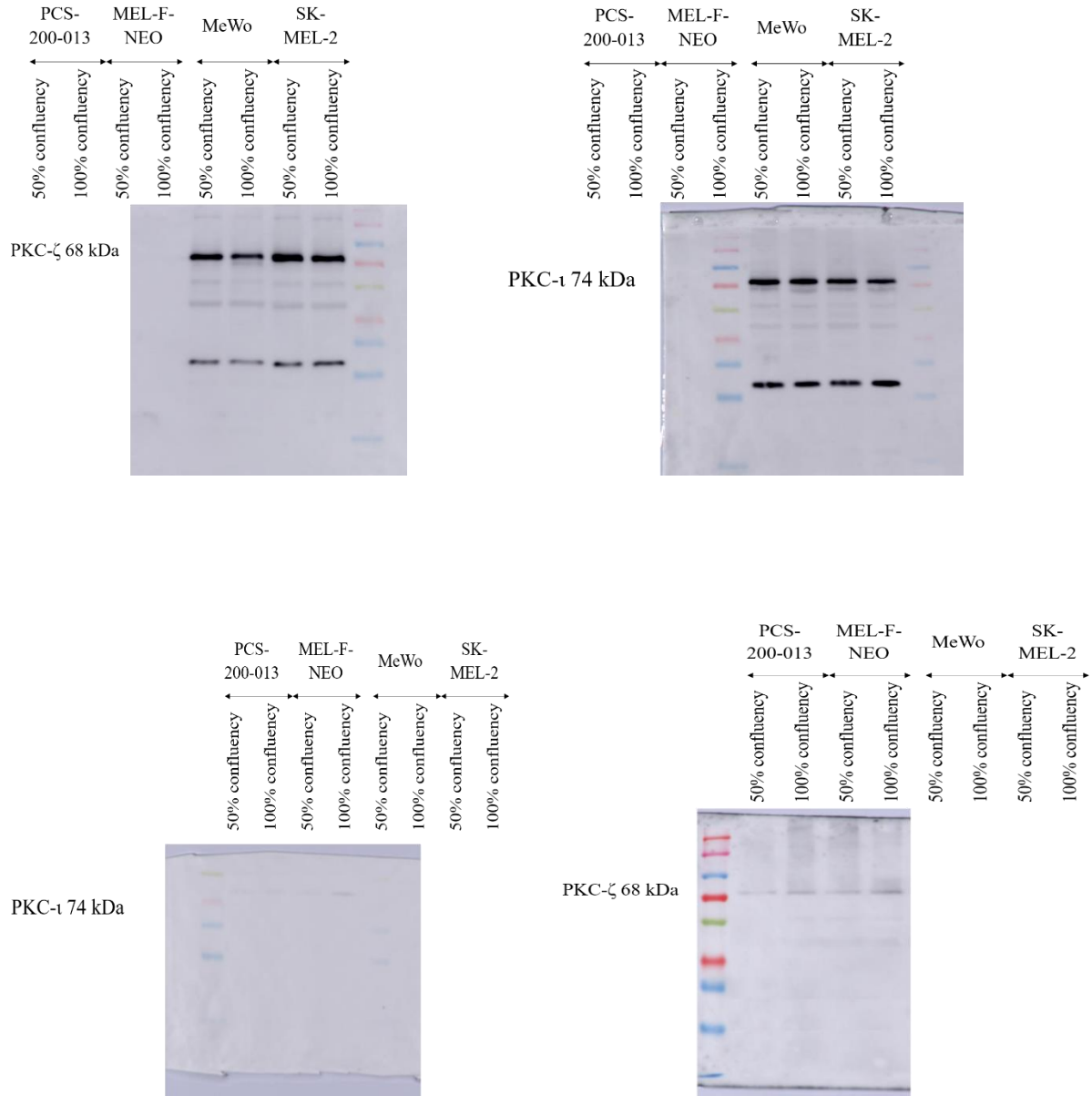
APPENDIX C

Full Western blots of the bands in Figure 4.1.

PTEN 54 kDa

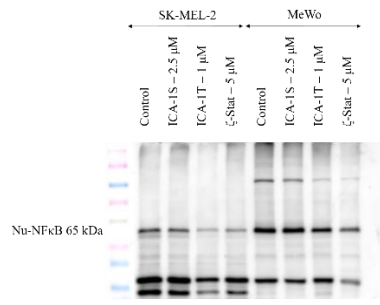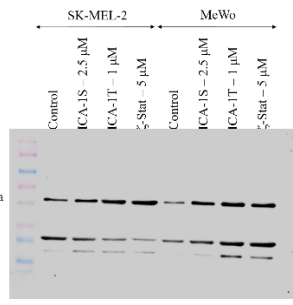p AKT (S473) 63 KDa
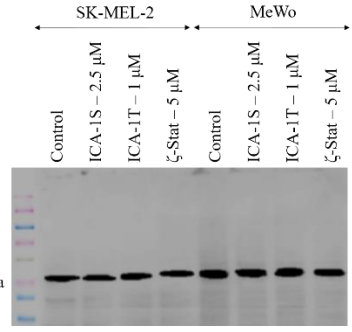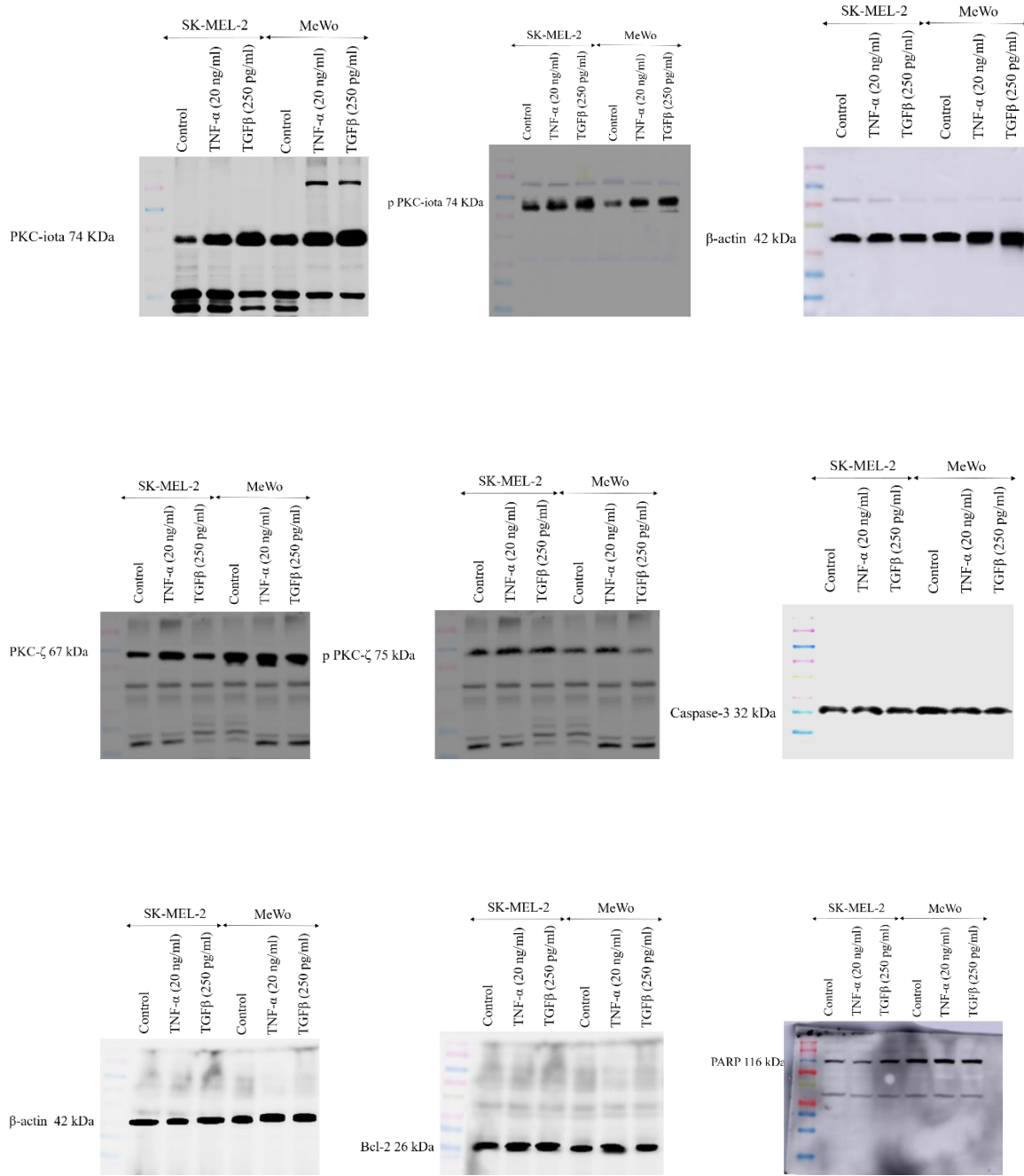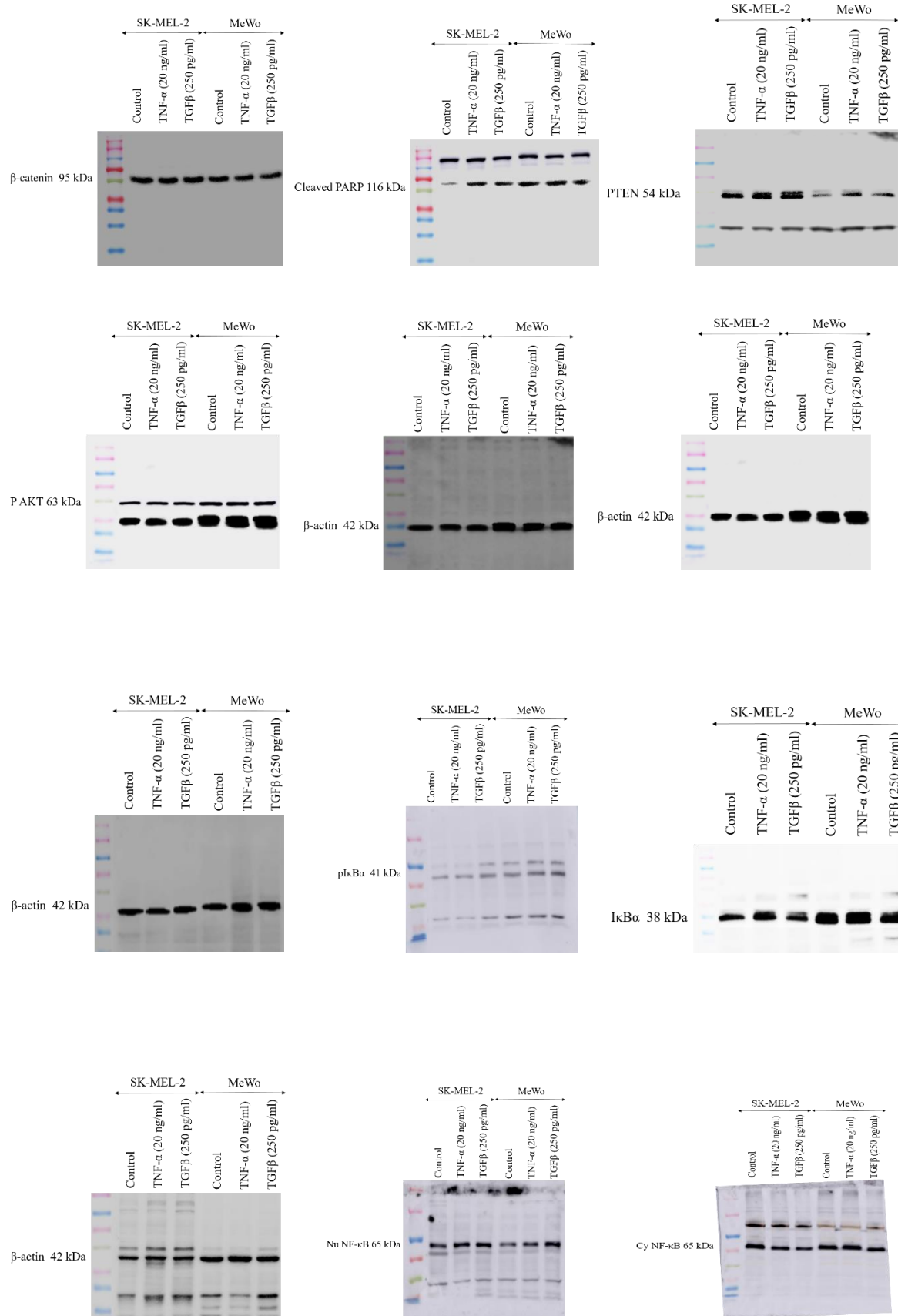
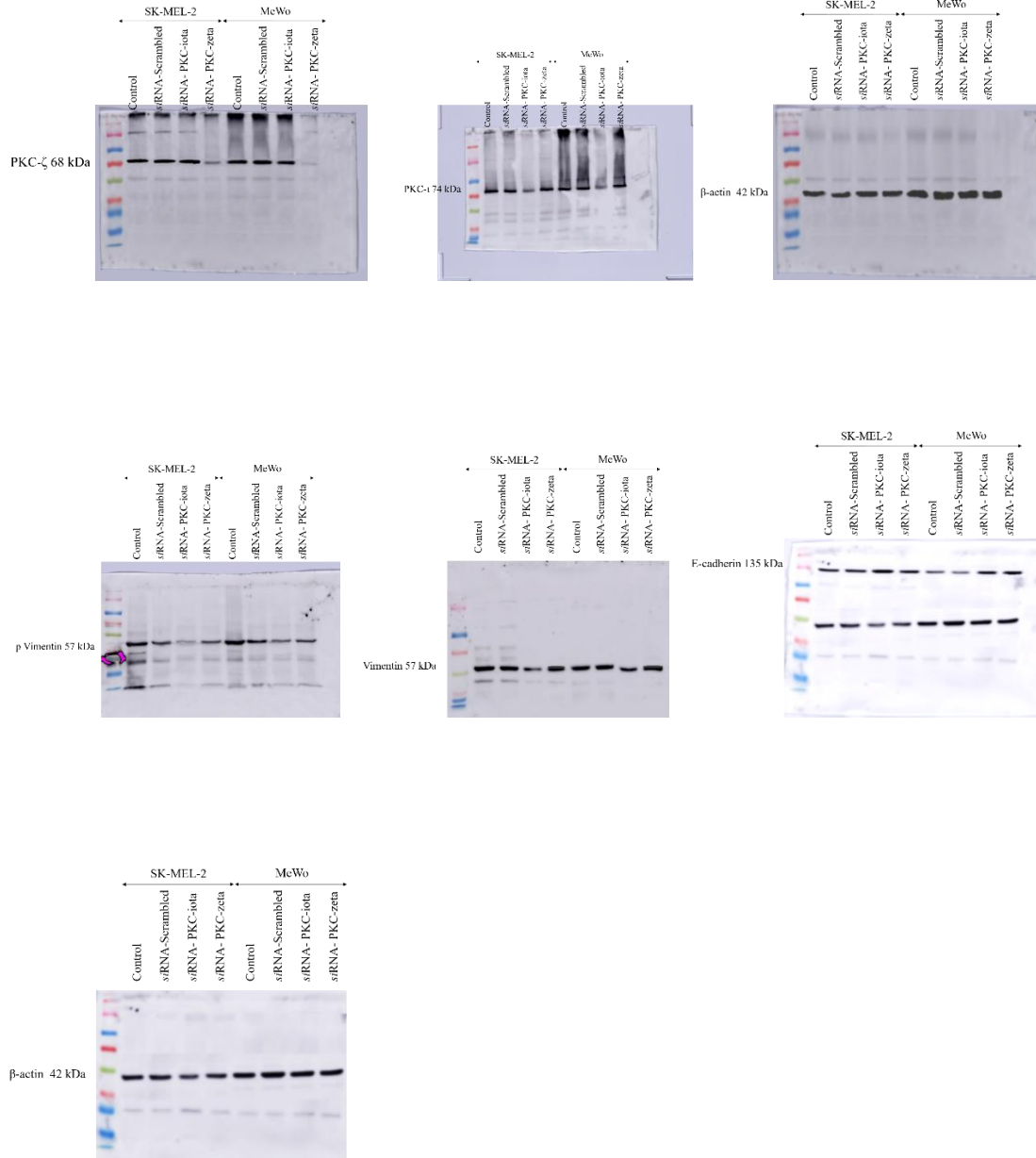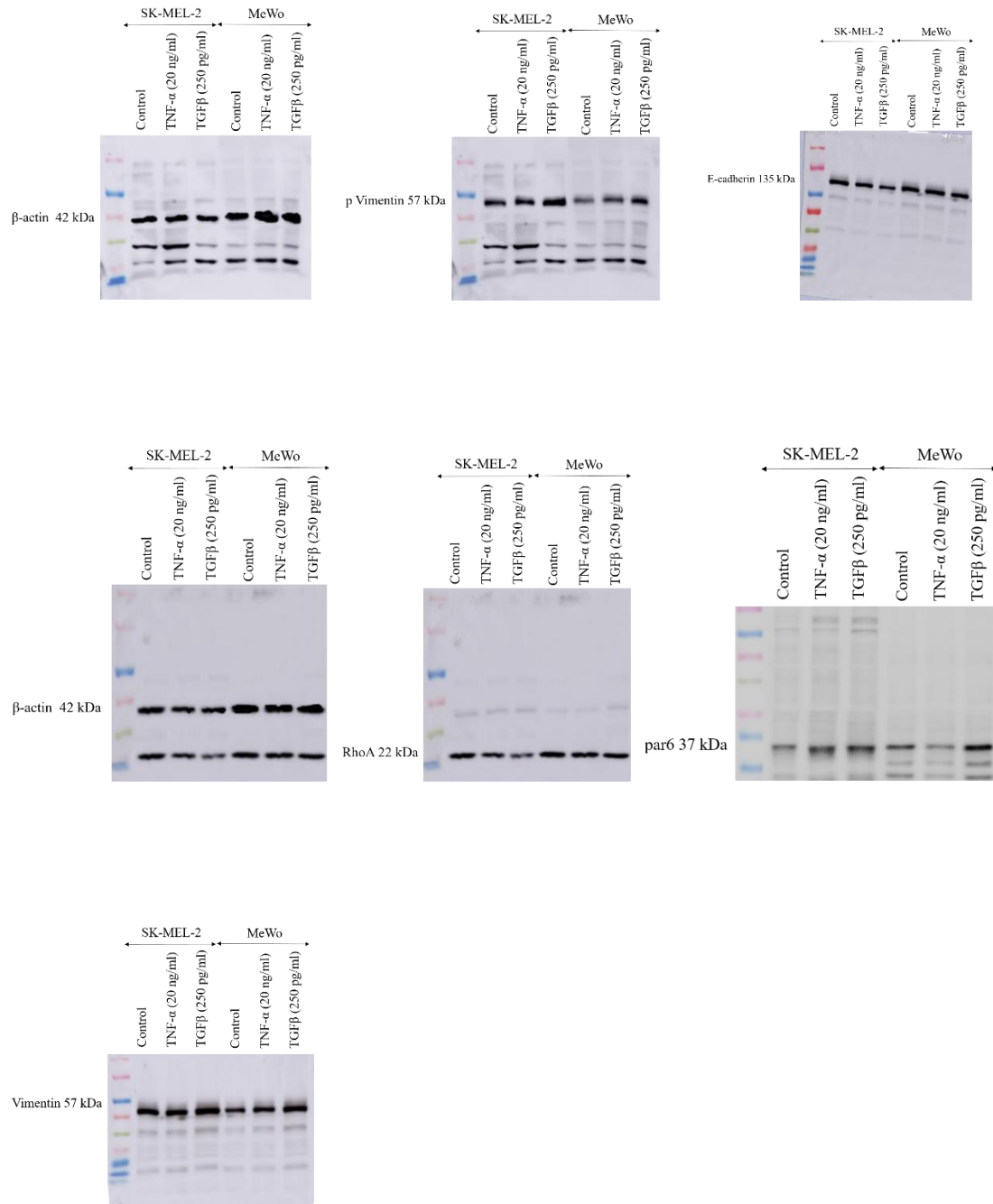β-actin 43 kDa

149

Full Western blots of the bands in Figure 4.3.

SK-MEL-2 MeWo

Control
ICA-1S – 2.5 µM
ICA-1T – 1 µM
ζ-Stat – 5 µM
Control
ICA-1S – 2.5 µM
ICA-1T – 1 µM
ζ-Stat – 5 µM

Nu-NFκB 65 kDa

SK-MEL-2 MeWo

Control
ICA-1S – 2.5 µM
ICA-1T – 1 µM
ζ-Stat – 5 µM
Control
ICA-1S – 2.5 µM
ICA-1T – 1 µM
ζ-Stat – 5 µM

Cy-NFκB 65 kDa

SK-MEL-2 MeWo

Control
ICA-1S – 2.5 µM
ICA-1T – 1 µM
ζ-Stat – 5 µM
Control
ICA-1S – 2.5 µM
ICA-1T – 1 µM
ζ-Stat – 5 µM

β-actin 42 kDa

SK-MEL-2 MeWo

Control
ICA-1S – 2.5 µM
ICA-1T – 1 µM
ζ-Stat – 5 µM
Control
ICA-1S – 2.5 µM
ICA-1T – 1 µM
ζ-Stat – 5 µM

β-actin 42 kDa
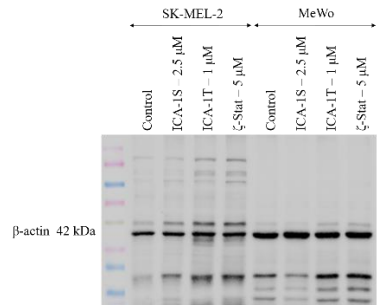
Full Western blots of the bands in Figure 4.5

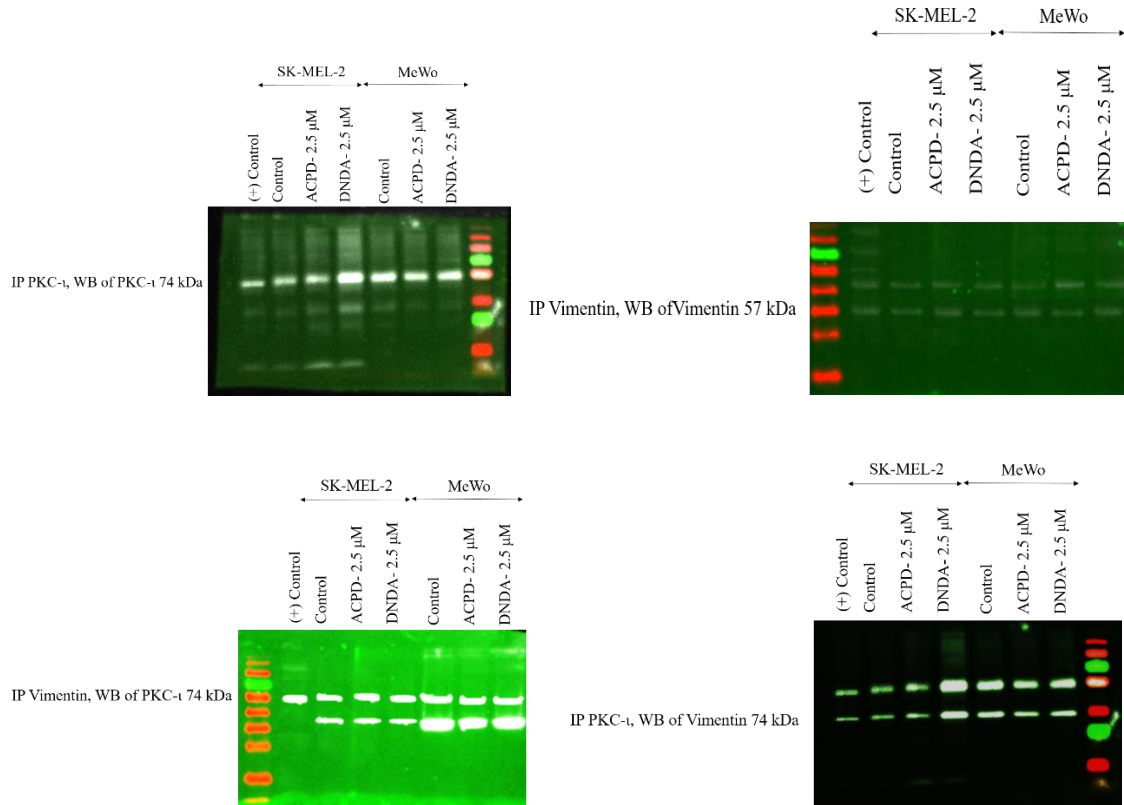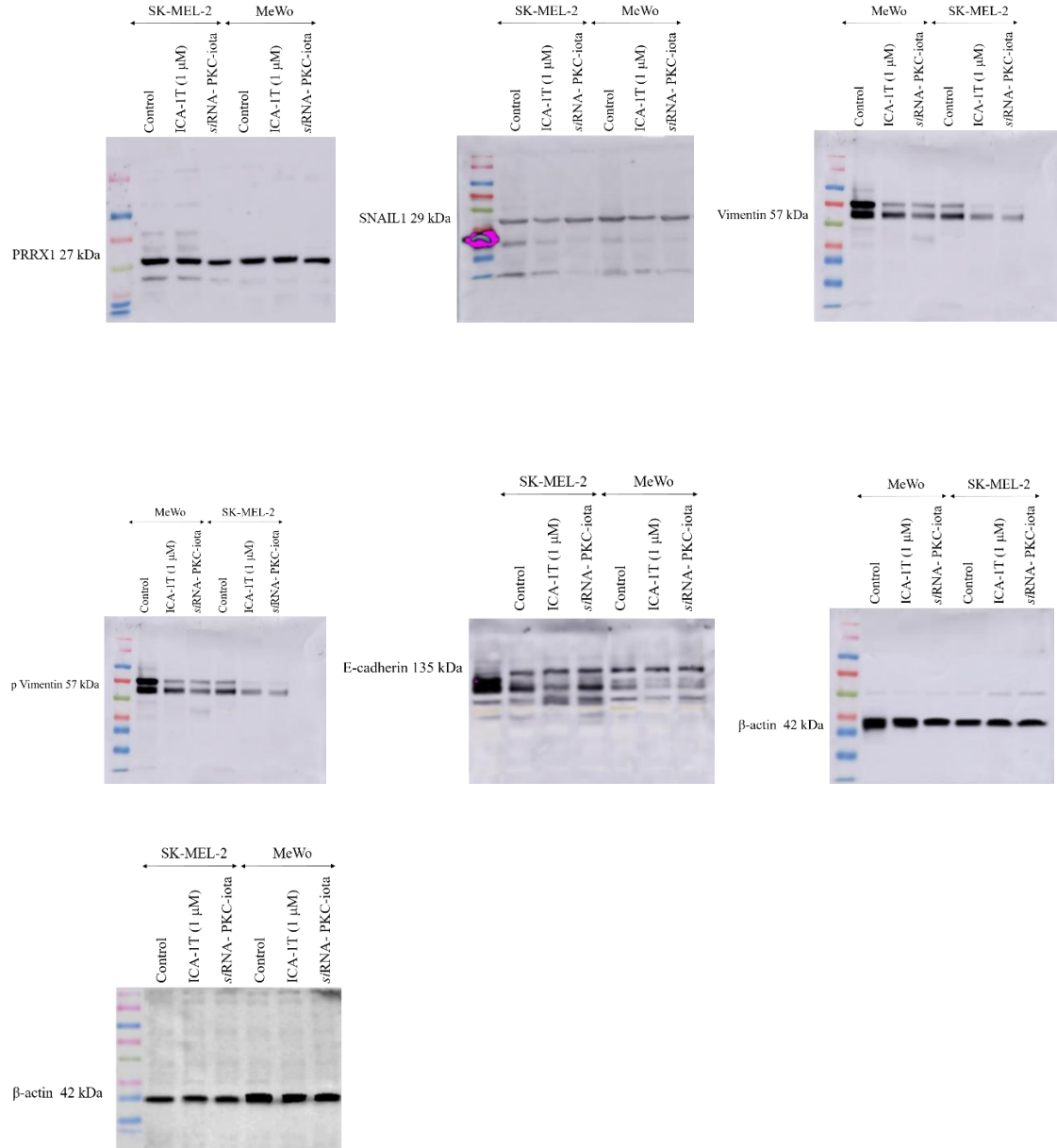## APPENDIX D

Full Western blots of the bands in Figure 5.9
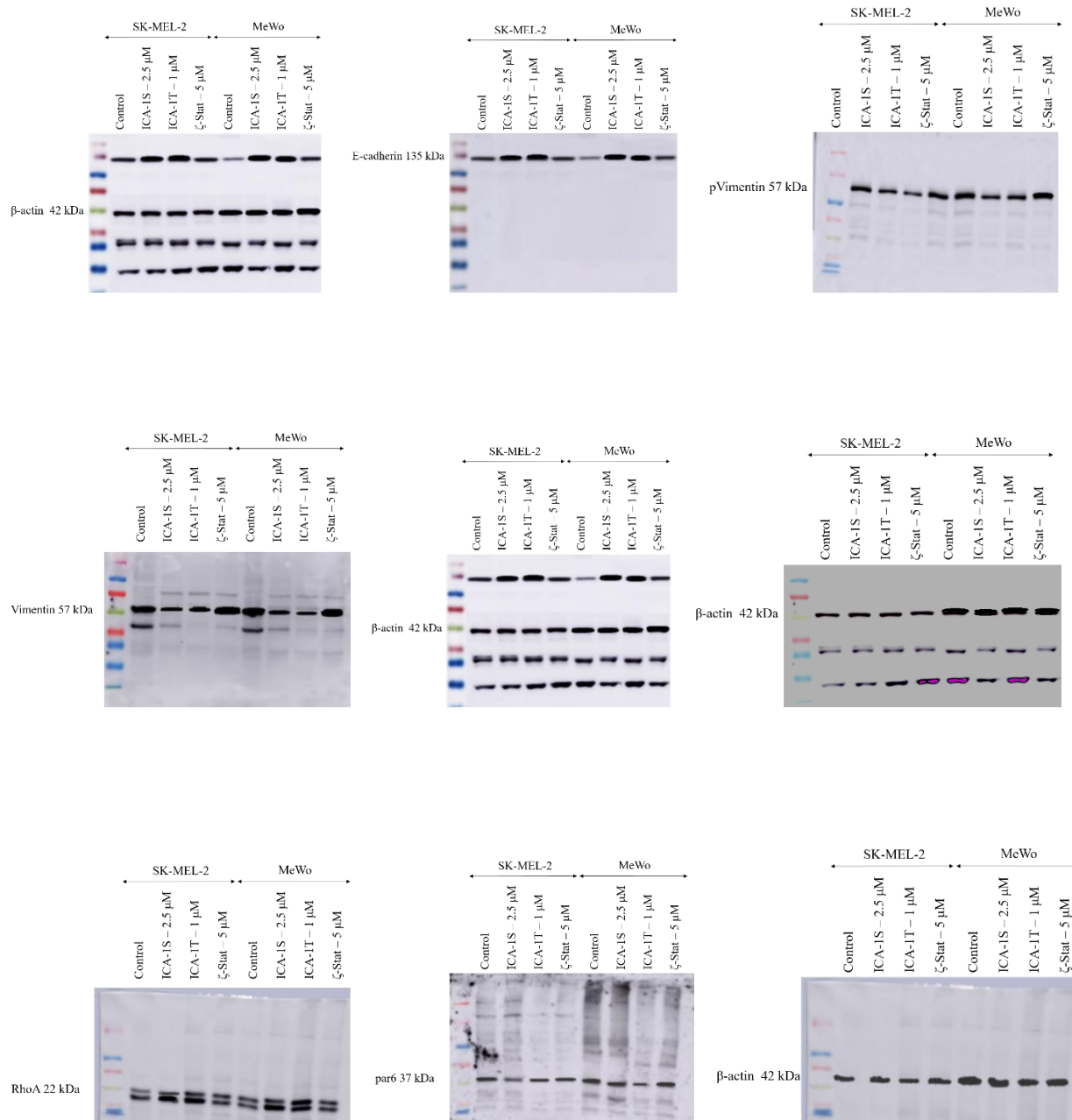
Full Western blots of the bands in Figure 5.11
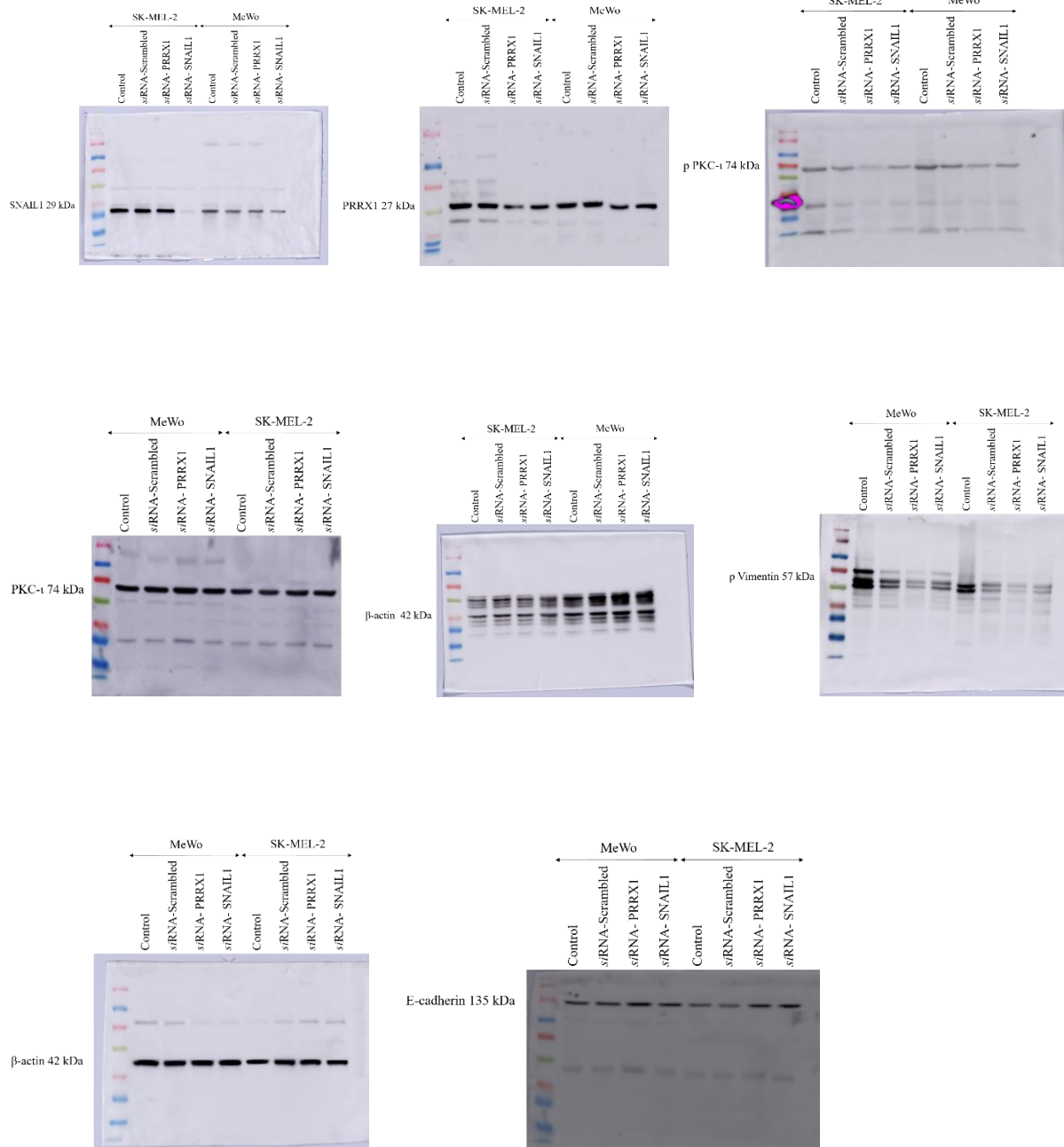
Full Western blots of the bands in Figure 5.13
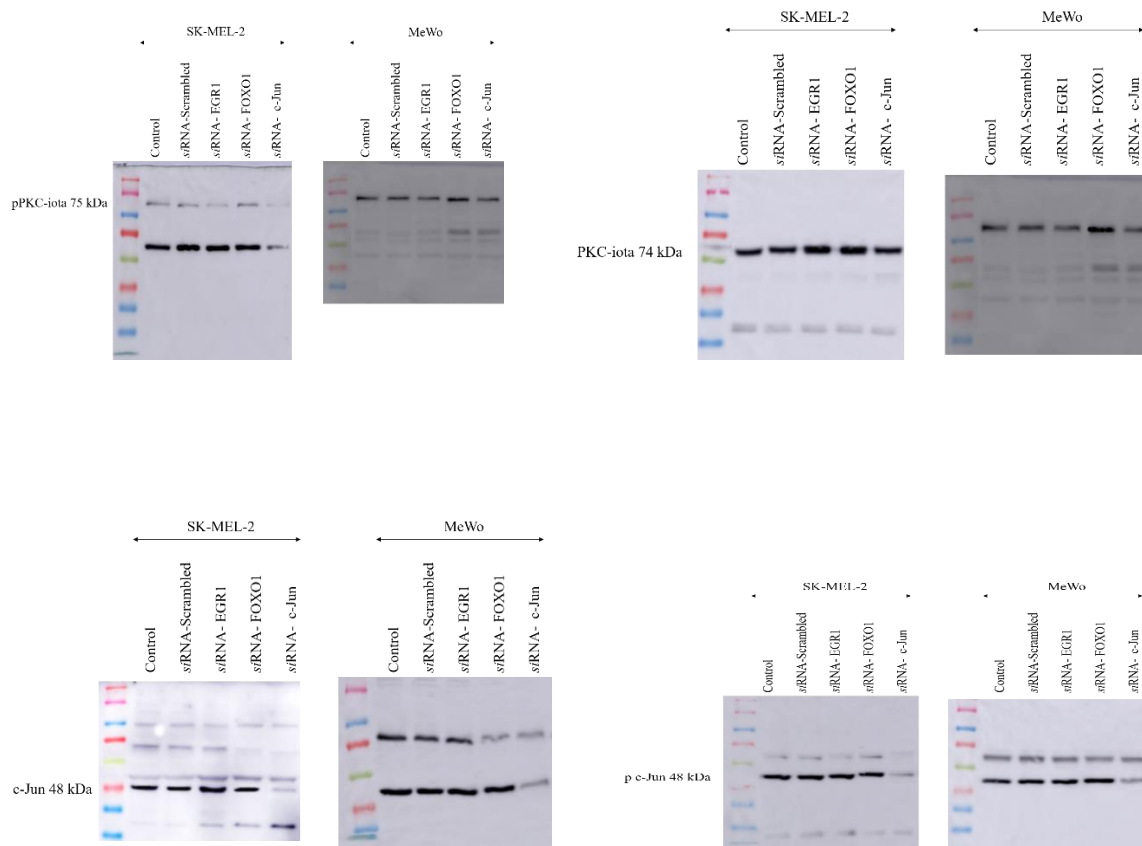
Full Western blots for the bands in Figure 5.15.

IP PKC-ι, WB of PKC-ι 74 kDa

IP Vimentin, WB ofVimentin 57 kDa

IP Vimentin, WB of PKC-ι 74 kDa

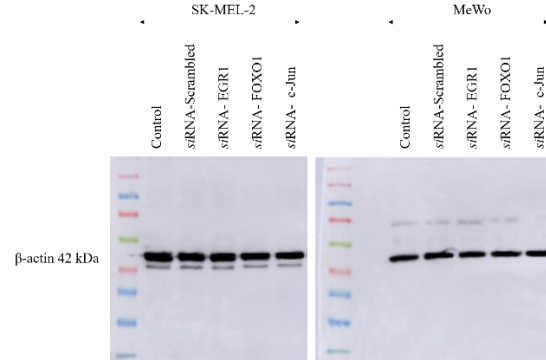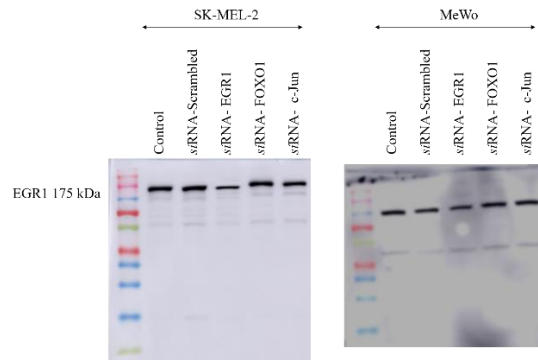IP PKC-ι, WB of Vimentin 74 kDa

Full Western blots for the bands in Figure 5.29.

Full Western blots for the bands in Figure 5.31.
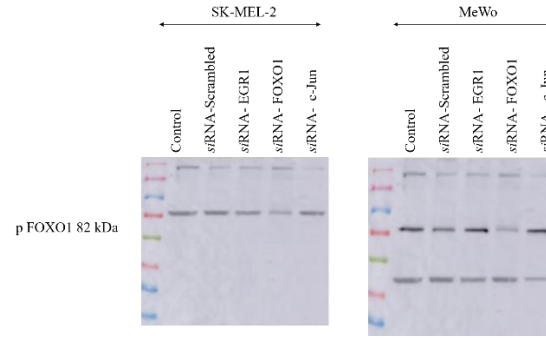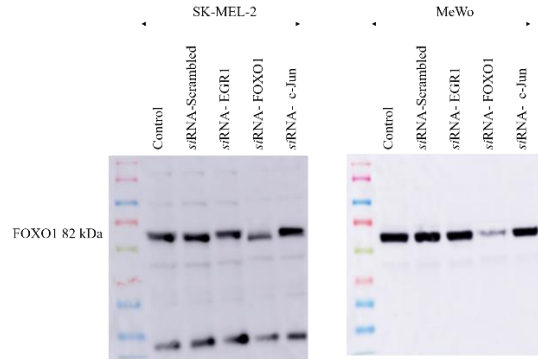
APPENDIX E

Full Western blots for the bands in Figure 6.1.

FOXO1 82 kDa

SK-MEL-2 — Control, siRNA-Scrambled, siRNA-EGR1, siRNA-FOXO1, siRNA-c-Jun

MeWo — Control, siRNA-Scrambled, siRNA-EGR1, siRNA-FOXO1, siRNA-c-Jun

p FOXO1 82 kDa

SK-MEL-2 — Control, siRNA-Scrambled, siRNA-EGR1, siRNA-FOXO1, siRNA-c-Jun

MeWo — Control, siRNA-Scrambled, siRNA-EGR1, siRNA-FOXO1, siRNA-c-Jun

EGR1 175 kDa

SK-MEL-2 — Control, siRNA-Scrambled, siRNA-EGR1, siRNA-FOXO1, siRNA-c-Jun

MeWo — Control, siRNA-Scrambled, siRNA-EGR1, siRNA-FOXO1, siRNA-c-Jun

β-actin 42 kDa

SK-MEL-2 — Control, siRNA-Scrambled, siRNA-EGR1, siRNA-FOXO1, siRNA-c-Jun

MeWo — Control, siRNA-Scrambled, siRNA-EGR1, siRNA-FOXO1, siRNA-c-Jun

Full Westerns blots for the Figure 6.7.